



Terms and Conditions of Use of Digitised Theses from Trinity College Library Dublin

Copyright statement

All material supplied by Trinity College Library is protected by copyright (under the Copyright and Related Rights Act, 2000 as amended) and other relevant Intellectual Property Rights. By accessing and using a Digitised Thesis from Trinity College Library you acknowledge that all Intellectual Property Rights in any Works supplied are the sole and exclusive property of the copyright and/or other IPR holder. Specific copyright holders may not be explicitly identified. Use of materials from other sources within a thesis should not be construed as a claim over them.

A non-exclusive, non-transferable licence is hereby granted to those using or reproducing, in whole or in part, the material for valid purposes, providing the copyright owners are acknowledged using the normal conventions. Where specific permission to use material is required, this is identified and such permission must be sought from the copyright holder or agency cited.

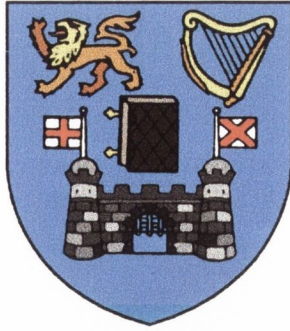
Liability statement

By using a Digitised Thesis, I accept that Trinity College Dublin bears no legal responsibility for the accuracy, legality or comprehensiveness of materials contained within the thesis, and that Trinity College Dublin accepts no liability for indirect, consequential, or incidental, damages or losses arising from use of the thesis for whatever reason. Information located in a thesis may be subject to specific use constraints, details of which may not be explicitly described. It is the responsibility of potential and actual users to be aware of such constraints and to abide by them. By making use of material from a digitised thesis, you accept these copyright and disclaimer provisions. Where it is brought to the attention of Trinity College Library that there may be a breach of copyright or other restraint, it is the policy to withdraw or take down access to a thesis while the issue is being resolved.

Access Agreement

By using a Digitised Thesis from Trinity College Library you are bound by the following Terms & Conditions. Please read them carefully.

I have read and I understand the following statement: All material supplied via a Digitised Thesis from Trinity College Library is protected by copyright and other intellectual property rights, and duplication or sale of all or part of any of a thesis is not permitted, except that material may be duplicated by you for your research use or for educational purposes in electronic or print form providing the copyright owners are acknowledged using the normal conventions. You must obtain permission for any other use. Electronic or print copies may not be offered, whether for sale or otherwise to anyone. This copy has been supplied on the understanding that it is copyright material and that no quotation from the thesis may be published without proper acknowledgement.



Mechanical Properties of Carbon Nanotube Polymer Composites

By

Bernd Lahr

A thesis submitted for the degree of

Doctor of Philosophy

to the

University of Dublin

Department of Physics

Trinity College Dublin

November 2001



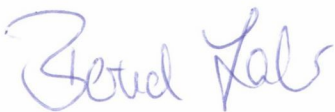
THESIS 6625

Declaration

I declare that the work in this thesis has not been previously submitted as an exercise for a degree at this or any other university.

The work described herein is entirely my own, except for the assistance mentioned in the acknowledgements and the collaborative work mentioned in the list of publications.

I agree that Trinity College Library may lend or copy this thesis on request.



Bernd Lahr

November 2001

To my parents and family.

„Don't tell me I'm still on that feekin' island? “

(Father Jack Hackett, in “Father Ted”, written by Dermot Morgan, Channel 4)

Acknowledgements

First of all I would like to thank Prof. Werner Blau for giving me the opportunity to carry out this research in his group. His help, advice and support was always greatly appreciated!

Numerous people have let me use their equipment or helped me with measurements, without which this work couldn't have been done: William Brennan, Denis Dowling, Hugh Byrne, Johnny Coleman, David John, Colin Reid, Manuel R  ther, Adrian Love, Keith Fortune, Cathal O'Domhnaill, Nick Randall, and surely much more which I can't remember at the moment...

I'd like to thank Anna Drury for the polymerisation of the PmPV.

A huge thanks to all the staff of the Physics Department, who were always there when help was needed: Tom Burke, Elaine, John Kelly, Pat, Jeanette, Michelle, Susan, Mick, Chris, Jemmer, and all the people who have been gone since.

Margaret and Brendan: thanks a lot for the proof reading and all...!!

I would like to thank all the members of 'Group Bu', past and present, who gave me help, advice, or kept me company while I was sippin' pints: Adam, Anna, Baptiste, Brian, Catriona, Christian, Colin, Connor, Gavin, Grace, Jean (again beside Grace; where else?), Johnny, Keith (hon.member), Kevin, Manuel, 2*Marc, Margaret, Marie-Laurence, Martin, Michael (and his friends Inky, Pinky, Blinky, and Clyde), Patrick mate, Rob, Sakina, Sandy, Sean, Stef, Stephanie, Stephen, Takeyuki, Valerie, and all others...

Stef a big thanks for being a perfect flatmate.

Thanks to my friends, here and abroad, Diarmuid, Don, Udo, Francois, Michael+Anja, Marie, Jens+Connie, Holli, Volker, Ralf, Gerd, Peter+Jutta, Trinity B's Killa Hoops, und alle anderen.

And to my parents, for all their love, help, support and belief.

“See you all in Mahaffy's...”

Abstract

In this study the production and optimisation of carbon nanotubes using the arc discharge method was investigated. The soot produced was analysed for the nanotube content. To remove the nanotubes from the soot a novel method of purification using PmPV was examined. Uniquely, the PmPV shows good interaction with carbon nanotubes. In contrast to other polymers, nanotubes are soluble in PmPV solutions, whereas the nanotube production by-products such as polyhedra and turbostratic graphite fall out. After purification a number of composites were made from the purified nanotubes with polymers such as PmPV, PMMA, and PS. Subsequently these nanotube based polymer composites have been characterised by a full range of thermal and mechanical techniques. The introduction of nanotubes is observed to substantially reinforce the PmPV composite systems, suggesting a new method to enhance mechanical properties of polymers without modification of the chemical and physical properties.

Table of contents

DECLARATION.....	II
ACKNOWLEDGEMENTS	V
ABSTRACT.....	VI
TABLE OF CONTENTS	VII
TABLE OF FIGURES	IX
CHAPTER 1 INTRODUCTION	12
1.1 SCIENTIFIC BACKGROUND.....	12
1.2 THESIS OUTLINE	15
CHAPTER 2 SCIENTIFIC BACKGROUND	18
2.1 INTRODUCTION TO POLYMERS.....	18
2.1.1 <i>Fibre reinforced polymers</i>	21
2.1.2 <i>Load transfer from matrix to fibre</i>	22
2.1.3 <i>Mechanical properties of polymers</i>	23
2.1.4 <i>Tensile strength of composites</i>	24
2.2 NANOTUBES	26
2.2.1 <i>Nanotube production methods</i>	28
CHAPTER 3 MATERIALS AND EXPERIMENTAL METHODS.....	32
3.1 MATERIALS	32
3.1.1 <i>Polymeric materials</i>	33
3.1.2 <i>Poly(phenylenevinylene)</i>	33
3.1.3 <i>Polystyrene and Polymethyl-methacrylate</i>	40
3.1.4 <i>Nanotube material</i>	41
3.2 SAMPLE PREPARATION	41
3.3 EXPERIMENTAL PROCEDURES	42
3.3.1 <i>General remarks</i>	42
3.3.2 <i>Characterisation of arc-discharge produced nanotubes</i>	42
3.3.3 <i>Thermogravimetric Analysis</i>	43
3.3.4 <i>Differential scanning calorimetry</i>	44
3.3.5 <i>Dynamic mechanical analysis</i>	45
3.3.6 <i>Transmission Electron Microscopy</i>	47
3.3.7 <i>Scanning Electron Microscopy SEM</i>	49
3.3.8 <i>Electron Paramagnetic Resonance spectroscopy</i>	50
3.4 MECHANICAL MEASUREMENTS	51
3.4.1 <i>Nanoindentation</i>	51
CHAPTER 4 NANOTUBE PRODUCTION.....	57
4.1 NANOTUBE PRODUCTION	57
4.1.1 <i>Variation of the voltage</i>	59
4.1.2 <i>Variation of the pressure</i>	66
4.1.3 <i>Variation of the current density</i>	69
4.2 RESULTS AND DISCUSSION	74
CHAPTER 5 THERMAL CHARACTERISATION.....	77
5.1 THERMOGRAVIMETRIC ANALYSIS OF PMPV	77
5.2 THERMOGRAVIMETRIC ANALYSIS OF NANOTUBE MATERIAL	82

5.3	THERMOGRAVIMETRIC ANALYSIS OF COMPOSITES	83
5.4	DIFFERENTIAL SCANNING CALORIMETRY OF COMPOSITES	87
5.5	DYNAMIC MECHANICAL ANALYSIS OF COMPOSITES.....	90
5.6	RESULTS AND DISCUSSION	93
CHAPTER 6 MECHANICAL PROPERTIES OF COMPOSITE MATERIALS		95
6.1	SAMPLE PREPARATION	95
6.2	NANOINDENTATION	97
6.2.1	<i>Hardness</i>	99
6.2.2	<i>Young's modulus</i>	101
6.3	RESULTS AND DISCUSSION	106
CHAPTER 7 CONCLUSIONS.....		109
PUBLICATION LIST		112

Table of figures

Figure 2.1 a) Polyethylene, b) Polypropylene, c) Polyvinylchloride, and d) Polystyrene ...	19
Figure 2.2 a) Polyacetal, and b) Polycarbonate	20
Figure 2.3 Stress-strain behaviour of polymer composites.....	22
Figure 2.4 General structure of silane.	23
Figure 2.5 Stress strain behaviour of different polymers.....	23
Figure 2.6 a) diamond b) graphite and c) C ₆₀	26
Figure 2.7 a) C ₆₀ b) C ₇₀ c) C ₆₀ Cl ₆	27
Figure 2.8: (a) armchair; (b) zigzag; (c) chiral single walled nanotubes	28
Figure 2.9 Krätschmer-Huffman generator	29
Figure 2.10 Arc discharge produced deposit.....	30
Figure 3.1 Poly(m-phenylenevinylene-2,5-di-n-octyloxy-1,4-phenylenevinylene) PmPV .	34
Figure 3.2 Wittig mechanism	35
Figure 3.3 Horner mechanism	36
Figure 3.4 Wittig mechanism yielding either trans or cis alkene.....	37
Figure 3.5 Preparation pathway of the starting materials	38
Figure 3.6 Polymerisation of PmPV	39
Figure 3.7 Structure formula of a) PS and b) PMMA	40
Figure 3.8 TGA plot of polymeric material.....	43
Figure 3.9 DSC plot	45
Figure 3.10 DMA plot.....	46
Figure 3.11 Hitachi 7000 TEM	47
Figure 3.12 Schematic of TEM	48
Figure 3.13 TEM grid, diameter 3mm.....	48
Figure 3.14 Schematic of SEM	49
Figure 3.15 Schematic of nanoindenter	51
Figure 3.16 Load vs. displacement plot.....	52
Table 3.17 Constants depending on indenter geometry	54
Figure 4.1 a) to d) SEM images of nanotube soot	58
Figure 4.2 SEM image of nanotube soot produced at 22.6V	60
Figure 4.3 SEM image of nanotube soot produced at 22.7V	61
Figure 4.4 SEM image of nanotube soot produced at 22.8V	62
Figure 4.5 SEM image of nanotube soot produced at 22.9V	63

Figure 4.6 SEM image of nanotube soot produced at 23.0V	63
Figure 4.7 TEM picture of soot produced at 22.9V.....	64
Figure 4.8 TEM picture of soot produced at 23.0V.....	65
Figure 4.9 TEM picture of soot produced at 23.0V.....	66
Figure 4.10 SEM image of nanotube soot produced at 300Torr.....	67
Figure 4.11 SEM image of nanotube soot produced at 350Torr.....	67
Figure 4.12 SEM image of nanotube soot produced at 400Torr.....	68
Figure 4.13 SEM image of nanotube soot produced at 450Torr.....	68
Figure 4.14 SEM image of nanotube soot produced at 32A	70
Figure 4.15 SEM image of nanotube soot produced at 34A	70
Figure 4.16 SEM image of nanotube soot produced at 36A	71
Figure 4.17 SEM image of nanotube soot produced at 38A	71
Figure 4.18 SEM image of nanotube soot produced at 39A	72
Figure 4.19 SEM image of nanotube soot produced at 40A	72
Table 4.20 EPR results.....	73
Figure 4.21 SEM image of nanotube soot produced at 45A	74
Figure 5.1 Comparison of TGA in air and in nitrogen.....	78
Figure 5.2 TGA of PmPV with impurities.....	78
Table 5.3 Elemental analysis of the residue	79
Figure 5.4 TGA of PmPV polymerised at different temperatures	80
Figure 5.5 First derivatives ($\Delta m/\Delta T$)	80
Figure 5.6 TGA and 1 st derivative of a different PmPV batch.....	81
Figure 5.7 TGA graph of nanotube soot (produced at 37A).....	82
Figure 5.8 TGA graph of pristine graphite	83
Figure 5.9 1 st derivative of nanotube PmPV composite.....	84
Figure 5.10 TGA graph of nanotube PmPV composite.....	85
Figure 5.11 TGA graph of nanotube PmPV composites	86
Figure 5.12 DSC of PMMA	87
Figure 5.13 DSC of PMMA composites	88
Figure 5.14 DSC of PS.....	89
Figure 5.15 DSC of PS composite with 50 % nanotubes	89
Figure 5.16 FT-IR interference pattern for PmPV composite with 50% nanotubes	90
Figure 5.17 DMA of PmPV composite with 50% nanotubes	92
Picture 6.1 AFM micrograph of an indentation in PmPV	97
Figure 6.2 Topographic information from an AFM micrograph	98
Table 6.3 Hardness of PmPV-nanotube composite films	99

Table 6.4	Hardness of PMMA-nanotube composite films	100
Table 6.5	Hardness of PS-nanotube composite films	100
Table 6.6	Young's moduli of PmPV-nanotube composites.....	102
Figure 6.7	Young's moduli of PmPV-nanotube composites.....	103
Table 6.8	Young's moduli of PMMA-nanotube composites	103
Table 6.9	Young's moduli of PS-nanotube composites.....	104
Figure 6.10	Young's moduli of PMMA-nanotube composites.....	104
Figure 6.11	Young's moduli of PS-nanotube composites	105
Figure 6.12	Young's moduli of PMMA-nanotube composites.....	106

Chapter 1

Introduction

1.1 Scientific background

In the past 50 years plastics or polymers have found their way into every aspect of our lives. Polymers have replaced traditional materials such as metal, wood, or ceramics for one or more of the following reasons: ease of processing, low cost, light weight, outstanding mechanical properties, and chemical inertness. Over 100 years ago natural rubber was extracted to produce tires and wellingtons. Today life seems impossible without the extensive use of polymers and they can be found in many applications from toys to car components. Modern medical care would be unfeasible without use of polymers in products such as pacemakers, artificial limbs or clean room-produced surgery equipment. Cars could not drive without tires, drive belts, plastic fuel tanks, all the plastic pipes and hoses. Electric current would not flow through conductors without plastic used as insulation, household appliances need their insulating housings. Plastic films revolutionised food packaging. Air travel is

now more economical because of the use of a vast range of ultra light but strong plastic parts in aircraft.

Regarding their mechanical properties, the introduction of fibre-reinforced polymers represents a significant development. Glass fibre has been used for a long time in materials engineering because of the high strength to weight ratio. From first applications in aeronautical and space industry, fibre reinforced materials have become available in everyday products such as tennis rackets, skis, and car body parts. The fibres on their own are very fragile and brittle, however when being incorporated in a polymeric matrix they show enormous potential. One of the main disadvantages of such composites lies in the processing methods, such as injection moulding or extrusion, as the fibres can break during production. For optimum load transfer from the matrix to the fibre a high aspect ratio (the ratio of diameter to length of a fibre) is necessary, however such long fibres tend to break when being processed. A high aspect ratio is required to achieve the highest load transfer, hence the fibres have to be short and strong, so that low cost production processes can be applied.

In 1991 S. Iijima discovered long cylindrical forms of carbon molecules, the so-called carbon nanotubes¹. His first initial observations were on multi layered concentric cylinders, i.e. multiwalled nanotubes (MWNTs). Later on single walled nanotubes (SWNTs) were observed as well². Nanotubes are a special form of fullerenes. The first observed form of the fullerenes, the C₆₀, was discovered in 1985 by Kroto, Curl and Smalley³, a discovery which was awarded the Nobel Prize in Chemistry in 1996. In a C₆₀ molecule 60 carbon atoms are arranged like the

pattern of a soccer ball, with pentagons and hexagons, to build a spherical molecule. Nanotubes in general consist of one or more layers of concentrically wrapped sheets of graphite. Single walled nanotubes consist of a single 'rolled-up' layer of graphite comprising of carbon hexagons whereas multi walled nanotubes consists of several layers. The diameter of nanotubes is between 1 and 3nm for SWNTs². Their length cannot be determined with precision as they appear in bundles, where the beginning and the end of an individual nanotube cannot be distinguished. MWNTs have diameters usually between 2 and 50 nm and a length between 0.2 and 2 μ m¹.

Nanotubes were first observed in soot generated in a Krätschmer generator⁴, an arc discharge apparatus, which was previously used for the production of fullerenes. In this generator an arc is created between two graphite electrodes, where one is consumed and forms a deposit at the other electrode. In this deposit, beneath an outer shell of sintered graphite, is the soot which contains the nanotubes. Unfortunately the soot contains many other forms of carbon in large quantities, such as polyhedra, amorphous carbon or turbostratic graphite. Shortly after the discovery of nanotubes, theoretical calculations predicted unique properties. Depending on their chiralities, the angle by which the graphitic sheets are rolled up, they were expected to be either semi conducting or metallic⁵, and due to their unique structure they were expected to be stronger than steel⁶. First measurements confirmed their electrical properties^{7,8}, as this is the area of interest for most of researchers investigating nanotubes. Other areas of interest are the use of nanotubes as field emitters⁹, single electron transistor¹⁰ or as mechanical actuators¹¹. Only recently has

research begun on the mechanical properties of nanotubes and nanotube containing composites.

Here in Trinity College, the group has vast experience in the area of conjugated polymers and their applications¹²⁻¹⁶. One polymer, which was used for optical applications, has shown unique interaction with nanotubes¹⁷. It was shown that by adding carbon nanotubes to the polymer, a novel composite material was produced. Electrical and optical properties were improved, however very little was known about the effect on mechanical properties.

This is the main motivation for the research described in this thesis. The nanotube production is investigated and optimised, and these nanotubes are used to create unique nanotube polymer composites. The mechanical properties of these composites are then investigated and characterised. A novel technique is used to carry out the mechanical testing and this is proven to be a valuable tool for composite characterisation.

1.2 Thesis outline

In this study two main areas were investigated. The objectives of this research was:

1. To improve production of carbon nanotubes using the Krätschmer generator.
2. To investigate the affect of adding various percentages of carbon nanotubes on the mechanical properties of these polymer composites.

Chapter 2 will have a closer look at the theory behind polymers and carbon nanotubes. It starts with a detailed look at polymers and their mechanical properties. This includes a review on fibre-reinforced materials. It also evaluates the different nanotube production methods and their pros and cons.

Chapter 3 is about the experimental methods used for the research of this thesis. Sample preparation will be discussed here as well, as the right sample preparation is crucial for the separation of nanotubes from the production by-products.

Chapter 4 deals with nanotube production in detail. Production parameters have been optimised to produce the best yield in the shortest time. The soot generated was evaluated, amongst other techniques, using electron microscopy and thermal analysis methods.

Chapter 5 is about thermal analysis of nanotube material and polymer-nanotube composites.

Chapter 6 describes mechanical analysis of polymers and carbon nanotube composites. The focus is on the Young's moduli of the composites, but the hardness of those materials used will also be discussed.

Finally, Chapter 7 contains the conclusions.

- ¹ S. Iijima, *Nature*, **354**, 56 (1991)
- ² D. S. Bethune, C. H. Kiang, M. S. Devries, G. Gorman, R. Savoy, J. Vazquez, and R. Beyers, *Nature*, **363**, 605 (1993)
- ³ H. W. Kroto, J. R. Heath, S. C. O'Brien, R. F. Curl, and R. E. Smalley, *Nature*, **318**, 162 (1985)
- ⁴ W. Krätschmer, L. D. Lamb, K. Fostiropoulos, and D. R. Huffman, *Nature*, **347**, 354 (1990)
- ⁵ J. W. Mintmire and C. T. White, *Carbon*, **33**, 893 (1995)
- ⁶ M. M. J. Treacy, T. W. Ebbesen, and J. M. Gibson, *Nature*, **381**, 678 (1996)
- ⁷ J. W. G. Wildoer, L. C. Venema, A. G. Rinzler, R. E. Smalley, and C. Dekker, *Nature*, **391**, 59 (1998)
- ⁸ T. W. Odom, J. L. Huang, P. Kim, and C. M. Lieber, *Nature*, **391**, 62 (1998)
- ⁹ Y. Saito, S. Uemura, and K. Hamaguchi, *Jpn. J. Appl. Phys. Part 2 - Lett.*, **37**, L346 (1998)
- ¹⁰ M. Ahlskog, R. Tarkiainen, L. Roschier, and P. Hakonen, *Appl. Phys. Lett.*, **77**, 4037 (2000)
- ¹¹ R. H. Baughman, C. X. Cui, A. A. Zakhidov, Z. Iqbal, J. N. Barisci, G. M. Spinks, G. G. Wallace, A. Mazzoldi, D. De Rossi, A. G. Rinzler, O. Jaschinski, S. Roth, and M. Kertesz, *Science*, **284**, 1340 (1999)
- ¹² A. P. Davey, A. Drury, S. Maier, H. J. Byrne, and W. J. Blau, *Synth. Met.*, **103**, 2478 (1999)
- ¹³ S. Maier, A. P. Davey, A. Drury, H. J. Byrne, and W. Blau, *Synth. Met.*, **101**, 31 (1999)
- ¹⁴ A. P. Davey, S. Elliott, O. Oconnor, and W. Blau, *J. Chem. Soc.-Chem. Commun.*, 1433 (1995)
- ¹⁵ S. J. Burbridge, H. Page, A. Drury, A. P. Davey, J. Callaghan, and W. Blau, *J. Mod. Opt.*, **41**, 1217 (1994)
- ¹⁶ W. J. Blau, H. J. Byrne, D. J. Cardin, and A. P. Davey, *J. Mater. Chem.*, **1**, 245 (1991)
- ¹⁷ S. A. Curran, P. M. Ajayan, W. J. Blau, D. L. Carroll, J. N. Coleman, A. B. Dalton, A. P. Davey, A. Drury, B. McCarthy, S. Maier, and A. Strevens, *Advanced Materials*, **10**, 1091 (1998)

Chapter 2

Scientific Background

2.1 Introduction to Polymers

Polymer chemistry is a significant area of materials science. Since the first polymers were made over 150 years ago, much has changed. Started with the polymerisation of epoxy resins by the Swedish chemist Berzelius in 1847, it took almost another 100 years for the first polymerisation of commercial quantities of polyethylene, one of the simplest polymer structures. Today's polymers have little or nothing in common with first polymeric products such as cellulose nitrate or phenol-formaldehyde, probably better known as Bakelite. Modern plastics are tailor made molecules, often specially developed and polymerised for specific applications. To understand the mechanical properties, such as hardness or modulus, it is necessary to have a closer look into the polymerisation and chemical structure of polymers in general.

Polymers can be divided into several groups. Initial polymeric products were made out of natural rubber. Rubber contains cross-linked molecules, and once polymerised they are insoluble or infusible. It was made first by South American natives out of the juice of a local tree. These juices (latex) form, when allowed to evaporate naturally, a film of rubber. The knowledge of the production of natural rubber, and the trees itself, was brought to Europe. This subsequently led to the development of “Mackintoshes” and waterproof fabrics. Around 1839 an American chemist called Charles Goodyear ‘accidentally’ developed the method of cross-linking or “vulcanisation”, when he dropped some rubber, mixed it with sulphur, onto a hot stove. This method solved the problem of the main disadvantages of natural rubber, i.e. softness when heated or hardness when cooled.

Plastics are chain-like molecules, made up of many repeat units. Examples of different polymers are shown in Figure 2.1.

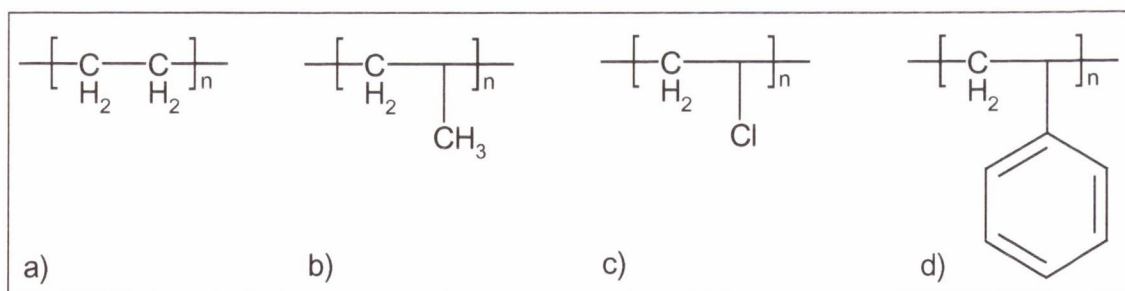


Figure 2.1 a) Polyethylene, b) Polypropylene, c) Polyvinylchloride, and d) Polystyrene

Polymers consist of a main carbon chain, to which different side groups, or sometimes even side chains, are attached. In the simplest case of polyethylene, only

hydrogen atoms are bound to the carbon atoms, as shown in Figure 2.1 a). The name provides information about the monomer, e.g. here 'ethylene', for the polymer polyethylene. If the monomer was a chain of three carbon atoms with one carbon-carbon double bond, propylene, the resulting polymer is polypropylene. Other common side groups (and their resulting polymers) are chloride (polyvinyl chloride), styrene (polystyrene) or, if all hydrogens are substituted by fluoride, polytetrafluoride.

To obtain an even larger variety of properties, chemists developed polymers whose backbone does not consist of a simple chain of carbon atoms, but of structures that are more complex. Figure 2.2 shows two of the most common polymers made out of such monomers.

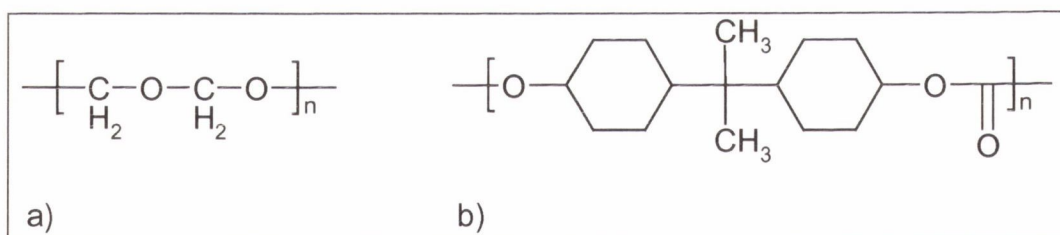


Figure 2.2 a) Polyacetal, and b) Polycarbonate

Sometimes the properties of crude polymers are not suitable as they are. There are many ways of altering polymer properties to tailor them for specific applications. To enhance the desirable properties of polymers, additives such as fillers, pigments, or fibres can be added to the polymer. The term 'additives' is generally used for other macromolecules such as plasticiser, stabiliser, or sometimes colorants. If solids are mixed into polymers usually the term compound is used. The range of solids can be

categorised in various ways, for instance into particulate or fibrous fillers. Particulate fillers are starch, glass beads, magnesia, silicates, or carbon black. Particulate fillers are often used to lower the price of the compound. Fibrous fillers are cellulose, wool, whiskers, or glass fibres. One of the main disadvantages of polymers is their low strength and low stiffness. To compensate for this, fibre reinforcement can be used.

2.1.1 Fibre reinforced polymers

Fibre reinforcement is used to improve the main disadvantage of polymeric matrixes, namely their low strength and stiffness. The measured strength of a polymer is usually even less than predicted, due to microscopic flaws and impurities. Embedding fibres helps to improve this main disadvantage.

Glass fibres were the first fibres used for polymer reinforcement and are still commonly used; due to their low cost and ease of production. Other advantages include their chemical stability and the fact that they are easy to handle.

In recent years, the development of organic fibres has shown vast improvements in the area of polymer composites. Carbon fibres are made by pyrolysing inexpensive precursors such as phenol hexamine or acrylics. Even though they are more expensive than glass fibres, they have, in general, better mechanical properties. Another big advantage, especially in the space and aeronautical industry is their lower density, strength to weight ratio and their stiffness to weight ratio.

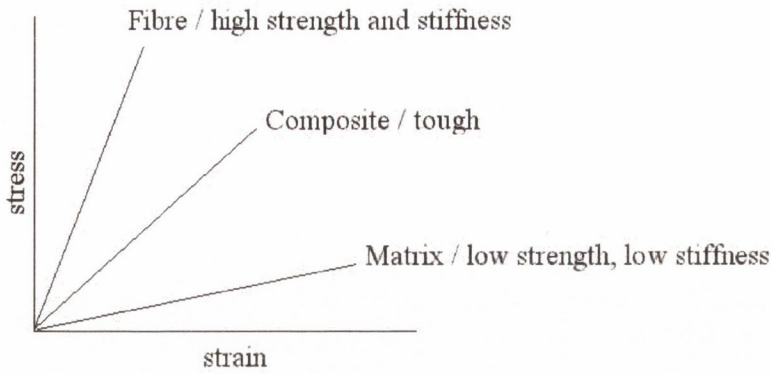


Figure 2.3 Stress-strain behaviour of polymer composites

Synthetic fibres are another type of filler used for composites. Fibres are spun from the melt, or out of solution, from polymers such as polyamides (Nylon), acrylics, polyethylene, or polyurethane. The melt spinning is the easiest and hence the cheapest way of producing fibres from thermoplastics. They are also made in so-called wet spinning, where the fibre is extruded into a coagulating liquid.

2.1.2 Load transfer from matrix to fibre

To obtain optimal mechanical properties in a composite, good interaction between matrix and fibre is necessary. If there is no natural interaction between the polymer and the fibre, the adhesion can be increased by the use of coupling agents. Otherwise, the fibres would simply be pulled-out of the matrix if under load. The basic concept of all coupling agents is the fact that they consist of a molecule with two different functional groups, one to interact with the matrix, the other one to bond to the fibre. Commonly used coupling agents are silanes. Their general structure is shown in figure 2.4.

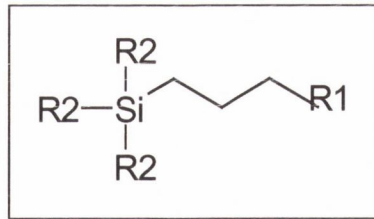


Figure 2.4 General structure of silane.
R1 is the functional group to bond with the fibre, R2 the group that interacts with the matrix.

2.1.3 Mechanical properties of polymers

The most common way to measure and describe the mechanical properties of a polymer is to examine its behaviour under load, especially under tensile load. The behaviour is best described in a stress-strain diagram. Figure 2.5 shows a range of stress-strain curves for different polymers of various strength, stiffness and toughness.

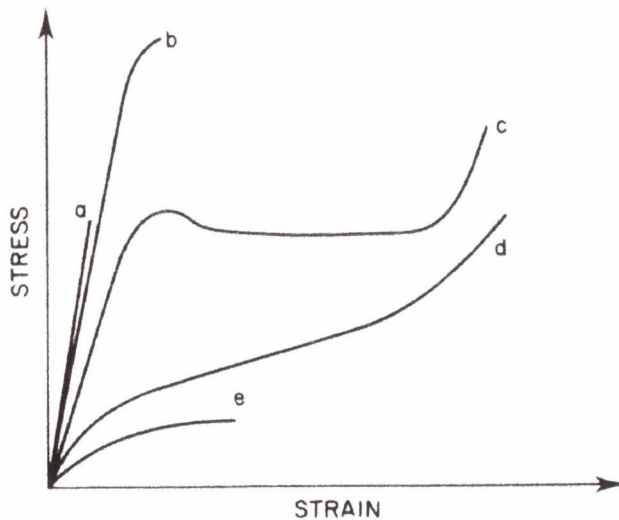


Figure 2.5 Stress strain behaviour of different polymers.
a) hard, brittle, b) hard, strong, c) hard, tough, d) soft, tough, e) soft, weak¹

The way in which a certain polymer reacts under stress is influenced by a huge number of different aspects, primarily its chemical structure, but including its average molecular chain length, its degree of polymerisation and its degree of crystallinity. As all polymers change their structure and morphology at different temperatures, the temperature has a major effect on the reaction to applied stress. Another important factor is the way in which the stress is applied. In general, an increase of the deformation rate leads to more brittle behaviour of polymers.

2.1.4 Tensile strength of composites

To understand the behaviour of reinforced composites, it seems to be most practical to look at continuous fibre reinforced composites first. With the ideal behaviour of a perfect load transfer between fibre and matrix, the following equation shows the stress on the composite,

$$\sigma_c = \sigma_f V_f + \sigma_m (1 - V_f)$$

where σ_f is the stress on the fibre, V_f is the volume fraction of the fibre, and σ_m is the stress on the matrix. This equation is valid until failure of one of the two phases. In fibre-reinforced plastics usually the fibre breaks first. However, in non-continuous fibre composites the mean fibre stress at failure is

$$\bar{\sigma}_f = (1 - l_c / 2l) \sigma_f$$

where l is the fibre length. Thus, the composite strength is given by

$$\sigma_c = \sigma_f V_f (1 - l_c / 2l) + \sigma_m (1 - V_f)$$

This expression is of course only valid for composites with a fibre length longer than the critical fibre length l_c . This critical fibre length describes the minimum length of a fibre, so that the load transfer from the matrix to the fibre is high enough above its mechanical limits, rather than pulling it out of the matrix. It can be determined by considering the force required to pull an embedded fibre with the length x and a diameter d out of a block of polymer. If a force P is applied to the free fibre end, it applies a tensile strength of

$$\sigma = 4P / \pi d^2$$

to this free end. In equilibrium this force is balanced by a shear force at the interface between the embedded fibre and the matrix which is equal to

$$P = \tau \pi x d$$

thus

$$\frac{\sigma \pi d^2}{4} = \tau \pi x d \quad \text{and}$$

$$\frac{x}{d} = \frac{\sigma}{4\tau}$$

If the fibre can just be pulled out of the matrix by a force marginally smaller than the fibre-breaking load, x must be equal to half the critical length $l_c / 2$ since only one end of the fibre is concerned. So the critical aspect ratio l_c / d can be written

$$\text{as } l_c / d = \sigma_f / 2\tau_i$$

where τ_i is the shear strength of the fibre-matrix interface.

2.2 Nanotubes

Up to 15 years ago it was thought, that carbon only existed in two forms or allotropes: graphite and diamond. However, in 1985 Kroto, Smalley and Curl discovered another stable allotrope of carbon²: the C_{60} or Buckminster fullerene as it was called later.

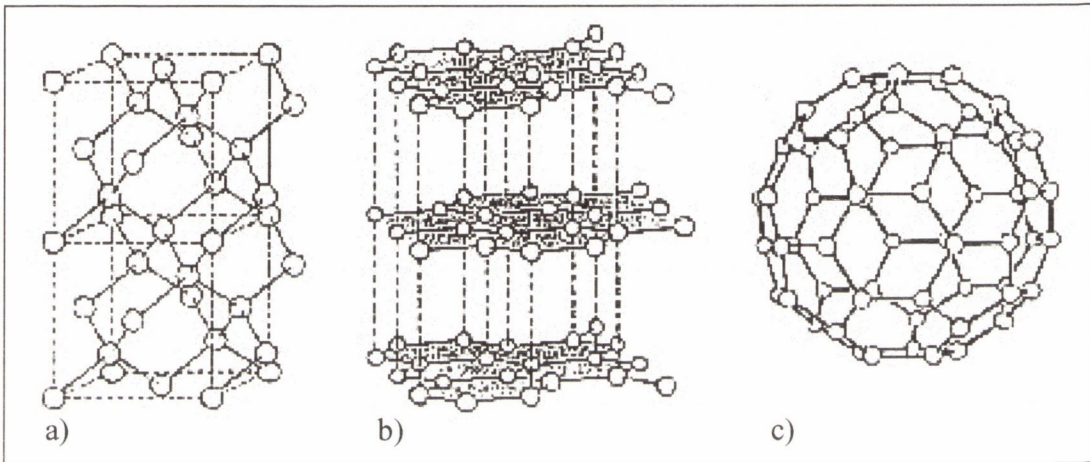


Figure 2.6 a) diamond b) graphite and c) C_{60}

This was to honour the architect Buckminster Fuller, who became famous for his domes built in similar way, as the carbon atoms are bond in a C_{60} molecule. Most scientists compare the structure of C_{60} with a soccer ball, consisting of 12 hexagons and 10 pentagons. Following this discovery, many more fullerenes were discovered, with different diameters and shapes. Figure 2.7 shows some different types of fullerenes.

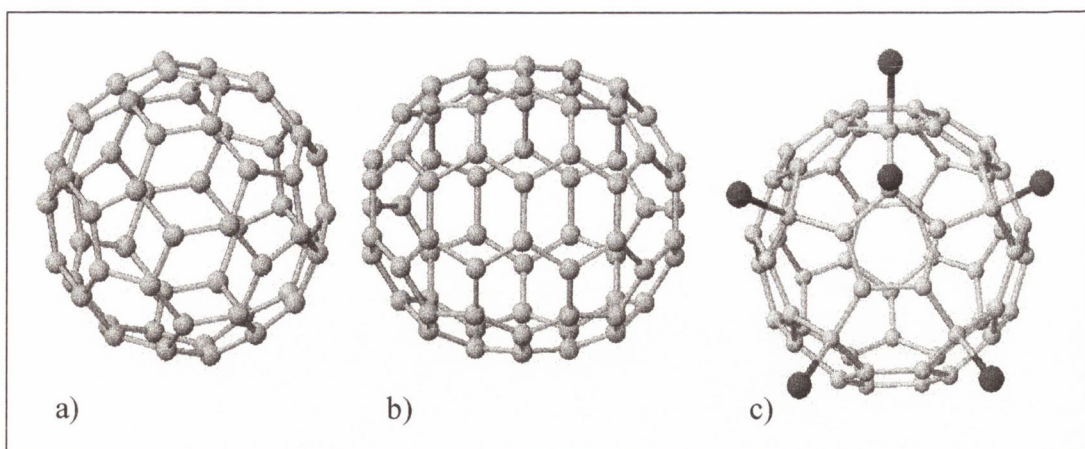


Figure 2.7 a) C_{60} b) C_{70} c) $C_{60}Cl_6$

Iijima discovered the most promising members of this family in 1991³. He was the first to report his observations of very long, tubular shaped fullerenes, structures that are now better known as carbon nanotubes. They are also described as hollow graphitic cylinders, with hemisphere shaped fullerenes capping the ends. Nanotubes are divided into two main groups, those consisting of a single layer of graphitic materials, so-called single walled nanotubes, and those with two or more layers, namely multiwalled nanotubes.

Depending on the way, in which the graphene is “rolled-up” to form a single walled nanotube, they are either semi conducting or metallic⁴. The two extremes, depending on the direction of the bonds in the carbon hexagons in relation to the tube axis, are called “armchair” and “zigzag” nanotubes; while the ones in-between are called “chiral”, as illustrated in Figure 2.8.

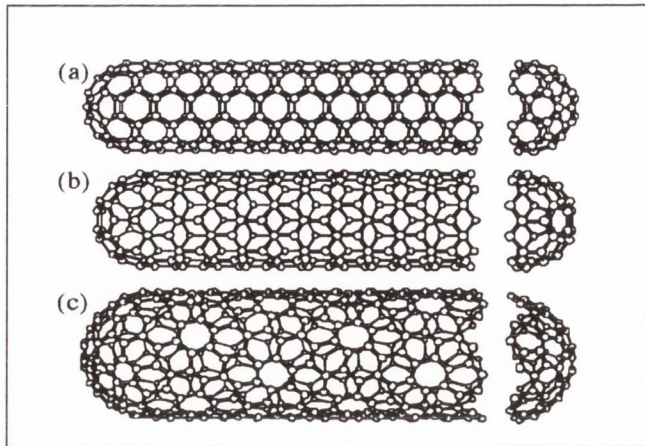


Figure 2.8 (a) armchair; (b) zigzag; (c) chiral single walled nanotubes

At present, there is much research into the electrical and optical properties of both, single- and multiwalled nanotubes. However very little is known about their mechanical properties and this is the main focus of this research.

2.2.1 Nanotube production methods

Nanotubes can be made in four different ways. One is the hydrocarbon pyrolysis⁵⁻⁷, where hydrocarbons (e.g. benzene, ethylene, acetylene) are pyrolysed in the presence of catalysts (e.g. cobalt, nickel, or iron), which are deposited on silicon or graphite substrates. Another production method is the high temperature laser ablation of graphite^{8, 9}, which is done in an inert atmosphere. In the gas phase created by the laser, the carbon forms some sort of a flake with at least one pentagon. More carbon atoms attach to the edge of the pentagon, and if the carbon density is high enough this reaction leads to the creation of tubular structures. The third and most recent discovered production method is the electrolysis of nanotubes^{10,11}. Here a graphite

electrode is immersed into molten LiCl, and under electrolytic conditions, fullerene related materials are formed.

However, the first observation of nanotubes was in arc-discharge produced soot, made in a so-called Krätschmer-Huffman generator, named after its inventors¹². This generator initially was made for the production of C₆₀ and similar structures, however by varying the parameters nanotubes can be produced as well. Figure 2.9 shows a sketch of such a generator.

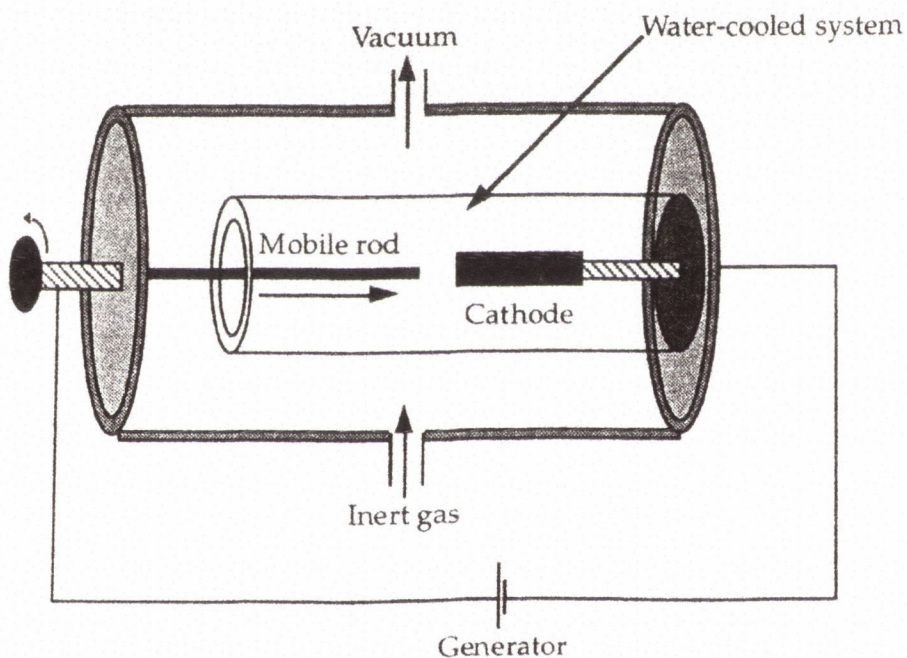


Figure 2.9 Krätschmer-Huffman generator

This generator is made of a metallic cylinder, cooled at the outside, and connected to a vacuum pump as shown in figure 2.9. In this chamber there are two graphite electrodes connected to a DC power supply. The chamber is filled with an inert gas, typically helium. The optimum conditions in the chamber, the applied current and

voltage are discussed later. The DC current passes through the electrodes, and creates a plasma arc in between consisting of carbon ions. During this arcing, a deposit forms on the negative electrode (cathode), while the positive electrode (anode) is consumed. The deposit formed (figure 2.10) has a tubular shape, with a hard, grey shell consisting of sintered graphite, and a soft core region, the so-called soot as shown in figure 2.10.

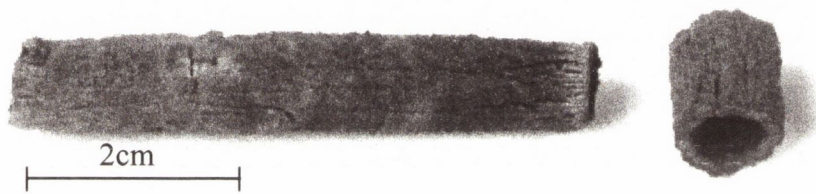


Figure 2.10 Arc discharge produced deposit

The soot comprises of polyhedral particles as well as nanotube material. The main accelerating force for the atoms is the ion current in the arc. As this force is parallel to the electrode axis and perpendicular to the electrode surface, the formation process proceeds with a higher rate along the axis. Hence, it is favourable for the formation of tubular structures.

- ¹ D. W. Clegg and A. A. Collyer, *Mechanical Properties of Reinforced Thermoplastics*, Elsevier Applied Science (1986), Ed.
- ² H. W. Kroto, J. R. Heath, S. C. O'Brien, R. F. Curl, and R. E. Smalley, *Nature*, **318**, 162 (1985)
- ³ S. Iijima, *Nature*, **354**, 56 (1991)
- ⁴ J. W. Mintmire and C. T. White, *Carbon*, **33**, 893 (1995)
- ⁵ M. Endo, K. Takeuchi, S. Igarashi, K. Kobori, M. Shiraishi, and H. W. Kroto, *J. Phys. Chem. Solids*, **54**, 1841 (1993)
- ⁶ S. Amelinckx, X. B. Zhang, D. Bernaerts, X. F. Zhang, V. Ivanov, and J. B. Nagy, *Science*, **265**, 635 (1994)
- ⁷ D. Bernaerts, X. B. Zhang, X. F. Zhang, S. Amelinckx, G. Vantendeloo, J. Vanlanduyt, V. Ivanov, and J. B. Nagy, *Philos. Mag. A-Phys. Condens. Matter Struct. Defect Mech. Prop.*, **71**, 605 (1995)
- ⁸ T. Guo, P. Nikolaev, A. G. Rinzler, D. Tomanek, D. T. Colbert, and R. E. Smalley, *J. Phys. Chem.*, **99**, 10694 (1995)
- ⁹ A. Thess, R. Lee, P. Nikolaev, H. J. Dai, P. Petit, J. Robert, C. H. Xu, Y. H. Lee, S. G. Kim, A. G. Rinzler, D. T. Colbert, G. E. Scuseria, D. Tomanek, J. E. Fischer, and R. E. Smalley, *Science*, **273**, 483 (1996)
- ¹⁰ W. K. Hsu, M. Terrones, J. P. Hare, H. Terrones, H. W. Kroto, and D. R. M. Walton, *Chem. Phys. Lett.*, **262**, 161 (1996)
- ¹¹ W. K. Hsu, J. P. Hare, M. Terrones, H. W. Kroto, D. R. M. Walton, and P. J. F. Harris, *Nature*, **377**, 687 (1995)
- ¹² W. Krätschmer, L. D. Lamb, K. Fostiropoulos, and D. R. Huffman, *Nature*, **347**, 354 (1990)

Chapter 3

Materials and Experimental Methods

This chapter describes the materials investigated and details the different experimental methods that were employed. In the first section, the materials are described. The second section deals with the methods of characterisation, which were used to analyse the crude as-produced nanotube material. The different mechanical measurements of the composites are discussed in the third section.

3.1 Materials

This chapter describes the materials used to carry out this research, namely the polymers and nanotubes used as discussed. In addition sample preparation of the composite films is also described.

3.1.1 Polymeric materials

Various different polymers have been used in this study. But in most cases, one polymer was always present: Poly(*m*-phenylenevinylene-2,5-di-*n*-octyloxy-1,4-phenylenevinylene) (PmPV). It has shown unique interaction with nanotubes¹⁻⁹, which have proven to be crucial for the preparation of nanotube-polymer composites. As the polymerisation route has a very big influence in the final structure of the polymer, and as this structure is very important for the interaction of the polymer with the nanotube material, the polymerisation route is described in greater detail.

3.1.2 Poly(phenylenevinylene)

Conjugated polymers have been of major interest in the recent years due to their electronic and photonic properties combined with the processing advantages of organic material¹⁰. Polyacetylene was the conductive polymer that launched the field of conductive polymer research¹¹. Other polymers studied extensively since the early 1980s include polypyrrole, polyfluorene, polythiophene, polyaniline and poly(phenylenevinylene).

The latter one poly(phenylenevinylene) (PPV) is of interest for the present work. Numerous applications have been published with PPV derived polymers as the key component e.g. LED's¹², photovoltaic cells¹³, FET's¹⁴, solid-state laser material¹⁵ etc.

The PPV derivative, Poly(*m*-phenylenevinylene-2,5-di-*n*-octyloxy-1,4-phenylenevinylene), shown in figure 3.1, has been intensely investigated in our research group

and also for the present thesis in connection with carbon nanotubes. This is due the fact that carbon nanotubes aggregate with PPV in solution and therefore PPV can be employed for the purification of carbon nanotubes.

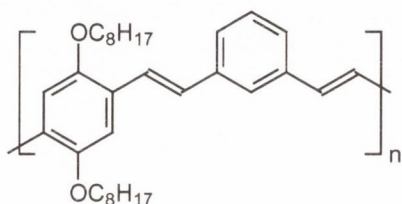


*Figure 3.1 Poly(m-phenylenevinylene-2,5-di-n-octyloxy-1,4-phenylenevinylene)
PmPV*

A number of synthetic approaches for soluble dialkoxy PPVs have been reported in the literature: Dehydrohalogenation¹⁶, elimination from sulfonium salts¹⁷ and aryl/ethylene coupling via Heck¹⁸ or Suzuki-reactions¹⁹, McMurray²⁰ and Wessling-Zimmermann route^{21, 22}.

Polymers synthesised by these methods contain small amounts of structural defects as a result of incomplete elimination, cross-linking or other side reactions during polymerisation. These reactions also have the disadvantage that alternating copolymers with different arylene vinylene units cannot be prepared.

Both Wittig and Horner are heterocoupling-processes and therefore these polycondensation routes are suitable for the synthesis of well-defined strictly alternating copolymers.

In the Wittig reaction, an aldehyde or ketone (II) is converted to an olefin by reaction with a phosphorous ylide (I). The mechanism of this reaction is outlined in figure 3.2. Attack by the carbanionic centre of the ylide on the carbonyl carbon generates a labile diionic intermediate known as a *betaine* (III) which rapidly collapses to an oxaphosphetane (IV). Decomposition of the oxaphosphetane affords the alkene and a phosphine oxide.

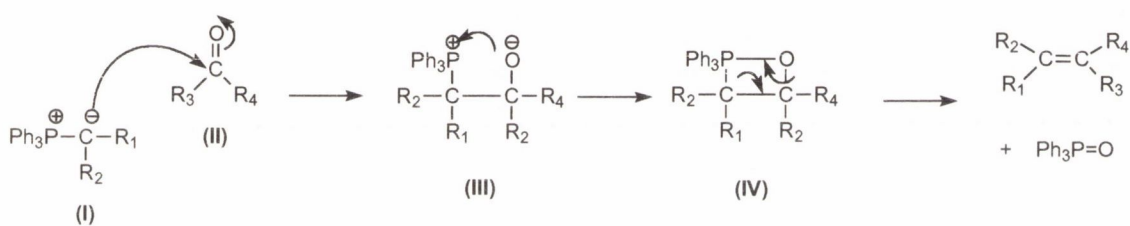


Figure 3.2 Wittig mechanism

The Wittig reaction has been modified by the use of ylides generated from other phosphorous compounds such as phosphine oxides and phosphonate esters.

Horner showed that phosphine oxides (V) react with aldehydes or ketones (VI) to give a β -alkoxyphosphine oxide (VII) which liberates the alkene (VIII) when treated with base.

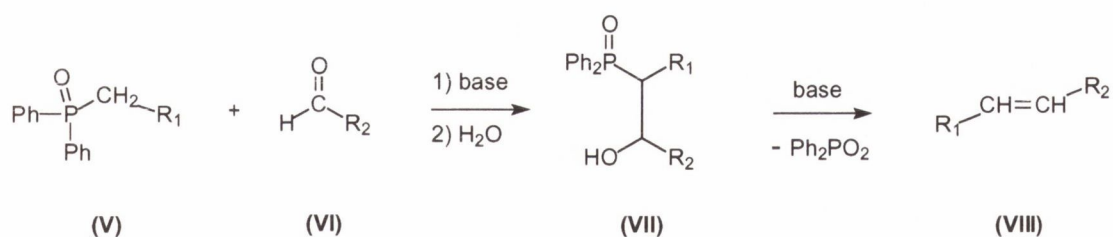


Figure 3.3 Horner mechanism

Both routes have been employed for the synthesis of poly(*m*-phenylenevinylene-2,5-di-*n*-octyloxy-1,4-phenylenevinylene).

Investigation in our group²³ has shown that the preparation method and also the employed reaction conditions influence the polymers final structure. The formation of the C=C bond results in two different isomers. Additionally, the molecular weights vary. It was found that the binding abilities of the polymer on the nanotube are greatly influenced by the polymerisation conditions²⁴.

Figure 3.4 shows the formation of both *cis* and *trans* alkene on the example of the Wittig mechanism.

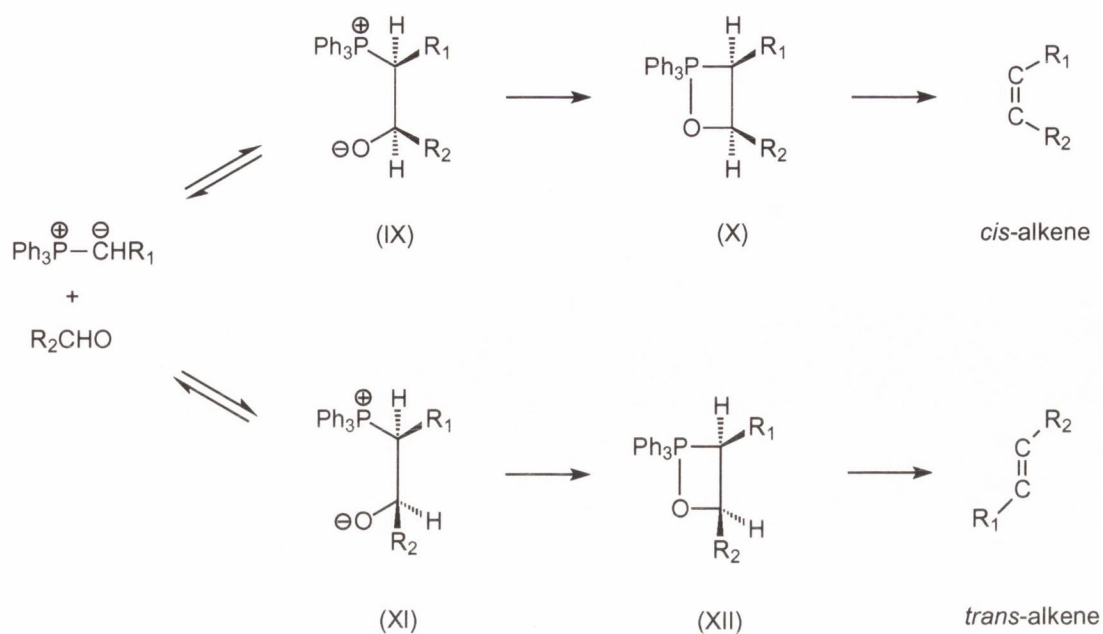


Figure 3.4 Wittig mechanism yielding either *trans* or *cis* alkene

In this process, a phosphorane adds to a ketone or aldehyde yielding two different betaine intermediates which in turn determine the formation of the either *cis* or *trans* isomer. The so-called *erythro* betaine (IX) leads to the formation of the *cis*-alkene whereas the *threo* betaine (XI) gives rise to the formation of the *trans*-alkene. The terms *erythro*- and *threo* betaine have their origin in proteine chemistry²⁵. Generally a mixture of *trans* and *cis* moieties is obtained. The percentage of either conformation depends on the reaction conditions, i.e. temperature, the choice of polar or nonpolar solvents, the addition of salts and base and finally the choice of starting materials.

Generally, Horner-ylides are more reactive than the corresponding Wittig-ylides which frequently do not react with ketones²⁶.

Furthermore the Horner reaction resulted in better yields in previous investigations and higher molecular weights²⁷.

The following scheme presents the synthesis route to obtain the suitable starting material for the Wittig and Horner condensation polymerisation.

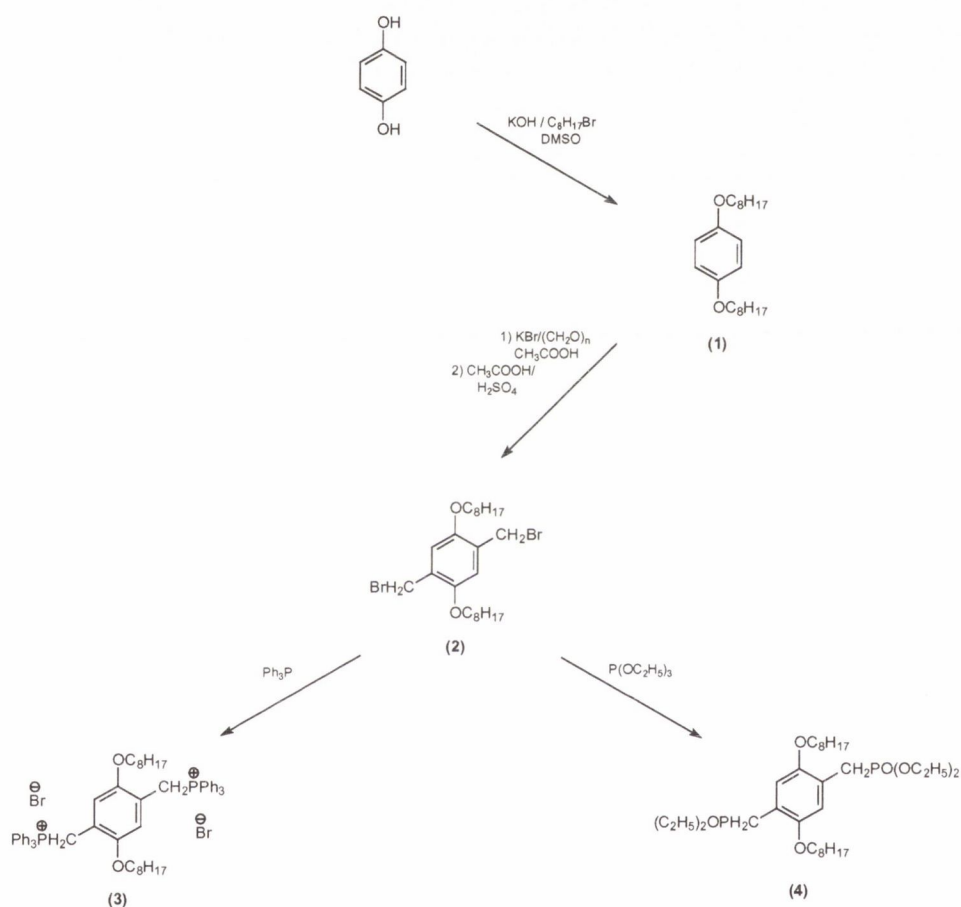


Figure 3.5 Preparation pathway of the starting materials

The first step is a mild alkylation of hydroquinone with bromo-octane. This octyloxy side chain is introduced for solubility reasons. The basic poly (phenylenevinylene) is not soluble in organic solvents.

1,4-Di-*n*-octyloxybenzene (1) was then bromomethylated using paraformaldehyde and potassium bromide to give 1,4-bis(2,5-di-*n*-octyloxy)bromomethyl benzene.

From the final step, depending on the reaction condition and the reagent, either the Wittig type phosphonium salt or the Horner type phosphonate ester is obtained: 1,4-bis(bromomethyl)-2,5-di-n-octyloxybenzene (2) reacted with triphenylphosphine yields 2,5-di-n-octyloxy-1,4-xylyl-bis-phosphonium bromide (3), while the so called *Arbuzov* reaction of (2) with triethylphosphite gives 2,5-di-n-octyloxy-1,4-xylyl-diethylphosphonate-ester (4).

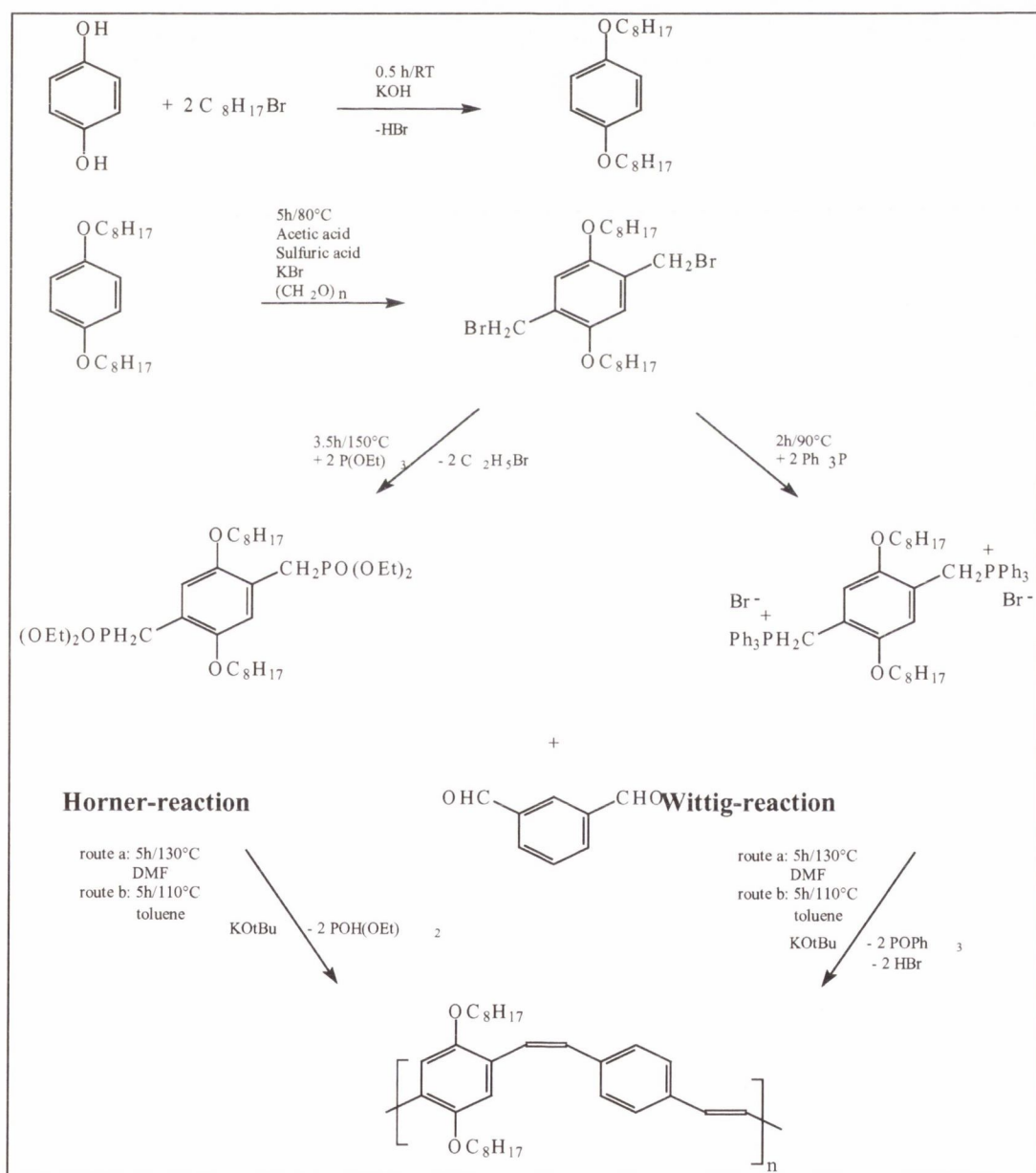


Figure 3.6 Polymerisation of PmPV

Figure 3.6 shows the final polymerisation reaction.

A range of polymers have been synthesised by varying reaction conditions, i.e. reaction temperature in different solvents, in order to investigate the polymers' properties (molecular weights, *cis-trans* ratios, etc) and also the ability to bind nanotubes²⁴.

PmPV synthesised by Horner reaction at 80°C in toluene has been employed for the present work. PmPVs produced by the Wittig route or under different reaction conditions have been found to be of poorer quality regarding composite preparation properties.

3.1.3 Polystyrene and Polymethyl-methacrylate

Other polymers used in this research are standard Polymethyl-methacrylate (PMMA) and Polystyrene (PS) as shown in figure 3.7. Both polymers are standard materials and available from commercial suppliers. But as nanotubes do not disperse in PS or PMMA solutions, they had to be coated with PmPV. In this case the PmPV works as a coupling agent, similar to silanes with glass fibres, between fibre (here: the nanotubes) and the polymer (here: PS or PMMA).

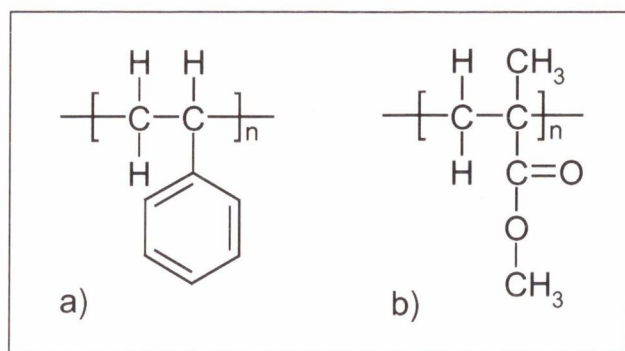


Figure 3.7 Structure formula of a) PS and b) PMMA

3.1.4 Nanotube material

The nanotubes used were produced in a Krätschmer-Huffman generator, thus are made in an arc discharge. This technique is best to obtain very long and very straight nanotubes, that means well graphitised nanotubes. The production method and the materials produced will be described in chapter 4.

Solely multi walled nanotubes were used. To produce single walled nanotubes using the arc discharge production method, it has to be significantly altered. Most single walled nanotubes produced with the arc-discharge method use Yttrium, Cobalt, Iron, or Nickel as a catalyst. These catalysts, pure or in a mixture, are put in a cylindrical hole in the cathode. Furthermore all parameters during arc-discharge production, such as current, voltage, and pressure, have to be adjusted.

Nanotubes in generally do not stay in solution. If they are dispersed in a solvent, for instance by ultrasonic power, they soon aggregate and fall out again. However if certain polymers such as PmPV are introduced, the nanotube–polymer interactions can be strong enough to form stable composite solutions.

3.2 Sample preparation

The nanotube material used was crude powder or soot, as produced from the Krätschmer generator. In a first step the PmPV was dissolved in toluene, in a concentration of 20g/l. The raw powder then was added to that solution and dispersed with a high power ultrasonic tip for 2 minutes. After that, the composite solution was placed in low power ultrasonic bath for two hours. Then the solution

was left 24 hours steady to settle. The nanotubes, now coated with the PmPV, stay in solution, whereas the nanotube production by-products such as polyhedra, turbostratic graphite, or amorphous carbon, precipitate out. The nanotube-PmPV solution is then decanted to separate it from the graphitic material.

3.3 Experimental procedures

3.3.1 General remarks

The following equipment was used:

TGA	Mettler System: TA 4000; Balance: TG 50; Processor: TC 11
DSC	Rheometric Scientific DSC SP Perkin-Elmer DSC 4, TA Microprocessor Controller System 4
SEM	Hitachi S-4300 elemental analysis: PGT Energy Dispersive X-ray Microanalysis Spectrometer (IMIX-PTS)
TEM	Hitachi H-7000
EPR	modified Bruker EPR
NHT	CSEM Nano Hardness Tester
DMA	TA Instruments DMA 2980
FT-IR	Nicolet NEXUS

3.3.2 Characterisation of arc-discharge produced nanotubes

The nanotubes described, characterised and measured in this thesis were produced as described in chapter 2. The average diameter and length of the tubes produced is important, but even more important is the purity of the soot. Since direct

measurement of the nanotube content is not available initially using the Krättschmer-generator method material is commonly investigated using electron microscopy. In addition, thermal analysis is also employed to characterise these polymer composites. One such method is the Thermogravimetric Analysis

3.3.3 Thermogravimetric Analysis

Thermogravimetric Analysis (TGA) is the study of the change of weight of a sample as a function of temperature. This method of characterisation provides valuable information about a material or a composite profile, namely the percentage of the components present, their decomposition, the temperature when this occurs or simply physical or chemical processes that occur within the material. Figure 3.8 shows a schematic TGA plot²⁸.

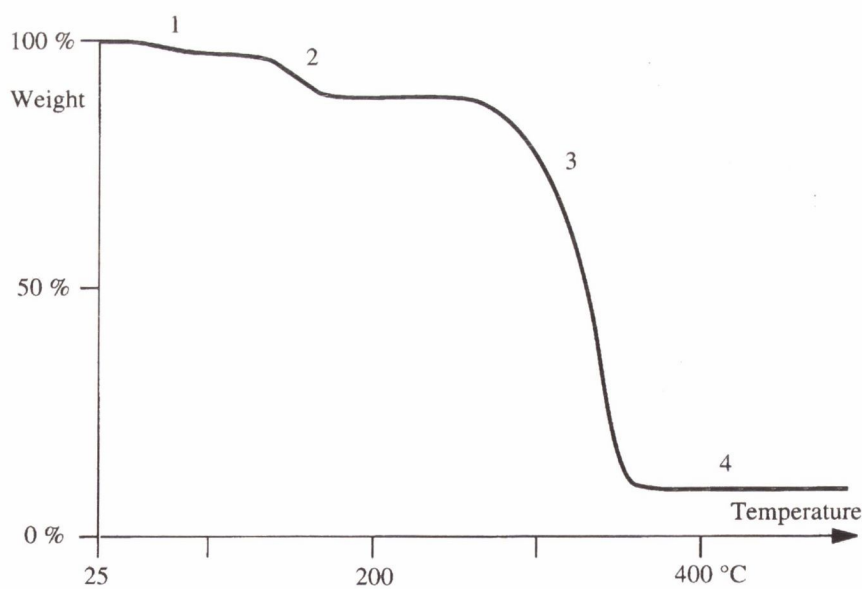


*Figure 3.8 TGA plot of polymeric material
1) volatile components (water, solvents), 2) loss of water of crystallisation, 3) decomposition, 4) residue*

The thermogravimetric analyser used in this thesis was a Mettler TC 11. It comprises of a microbalance (Mettler TG 50), which holds the crucible with the sample in a temperature-controlled furnace, and the control unit. Usually the sample weight is between 5 and 10mg, but the resolution of the microbalance allows the investigation of changes and transitions in samples of 1 or 2mg. All investigations are carried out in a controlled atmosphere. Depending on the purpose of the measurement usually dry nitrogen atmosphere or oxygen, both at a controlled flow rate. The microbalance continuously monitors the weight of the sample. Both the balance and the furnace are linked to the control unit, which simultaneously controls the temperature and records the sample mass. Another method is to keep the sample at a controlled temperature and to measure the change of weight over time.

The experimental data is usually presented as a plot of mass versus temperature or, in the second case, mass over time. Another useful way of presenting the data is to plot the first derivative, i.e. the change of weight over the change of time. This is especially useful to determine the exact temperature, where a particulate transition or weight loss occurs.

3.3.4 Differential scanning calorimetry

In differential scanning calorimetry (DSC) the thermal properties of polymers are measured as a function of temperature or as a function of time at a constant temperature. The heat flow into or from a sample chamber compared to a reference chamber is measured as a function of temperature or time. DSC gives much information about molecular ordering including the glass transition temperature (T_g),

the melting temperature (T_m), heat of fusion, or entropy of fusion (T_c). A DSC curve plots the energy absorbed or emitted as a function of time or temperature (figure 3.9)

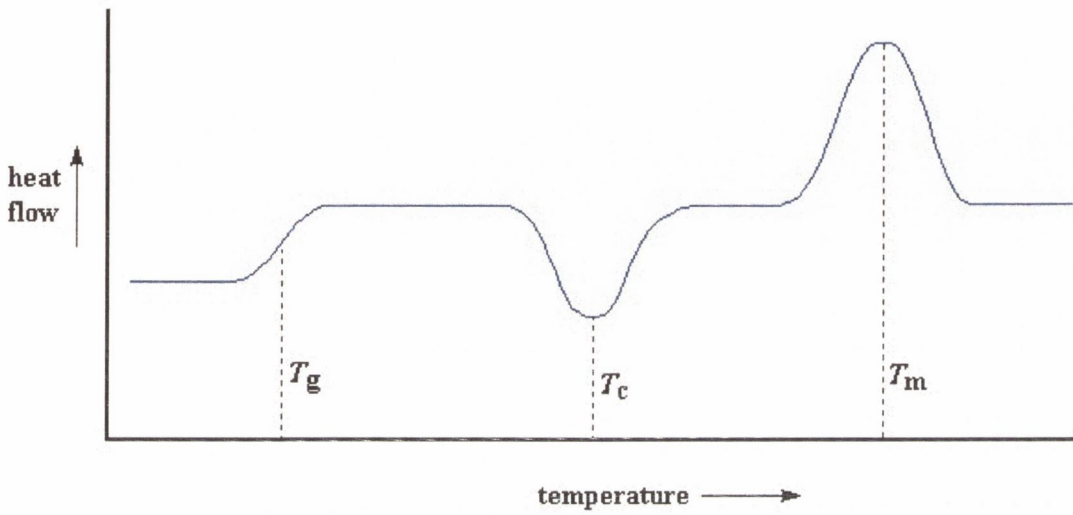


Figure 3.9 DSC plot

3.3.5 Dynamic mechanical analysis

Polymers are viscoelastic materials. In DMA measurements a load is applied to the polymer and the response is analysed for the viscous and the elastic part of the polymer. An oscillatory stress is applied to the specimen in the bending or tensile mode of deformation and the lag of the resulting oscillatory strain is measured²⁹. The sample is clamped into a frame and the applied sinusoidally varying stress of frequency ω can be represented as

$$\sigma_t = \sigma_0 \sin(\omega t + \delta)$$

where σ_0 is the maximum stress amplitude and the stress proceeds the strain by an angle δ . The strain is given by

$$\varepsilon_t = \varepsilon_0 \sin(\omega t)$$

where ϵ_0 is the maximum strain amplitude. These quantities are related by

$$\sigma_t = E_\omega^* \epsilon(t)$$

where E_ω^* is the dynamic modulus and

$$E_\omega^* = E'_\omega + iE''_\omega$$

E'_ω and E''_ω are the dynamic storage modulus and the dynamic loss modulus, respectively. For a viscoelastic polymer E' characterises the ability of the polymer to store energy (elastic behaviour), while E'' reveals the tendency of the material to dissipate energy (viscous behaviour)³⁰. The phase angle δ is then calculated from

$$\tan \delta = \frac{E''}{E'}$$

Normally E' , E'' and $\tan \delta$ are plotted against temperature or time (Figure 3.10)

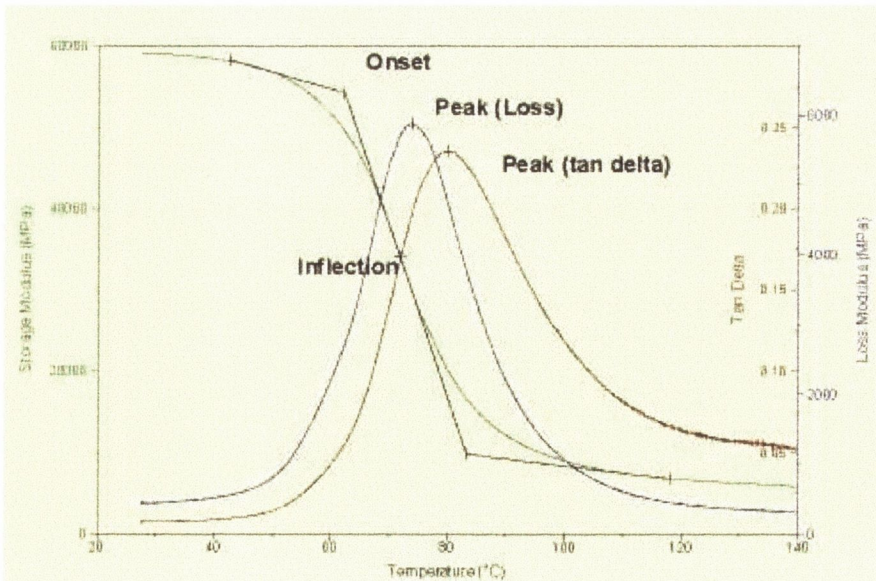


Figure 3.10 DMA plot

3.3.6 Transmission Electron Microscopy

Transmission Electron Microscopy (TEM) provides detailed pictures of carbon nanotubes and related materials, such as polyhedra or turbostratic graphite. As optical microscopy is limited by the wavelength of visible light, TEM can provide pictures of nanometric resolution. High resolution TEM can, in our case, show the individual shells of polyhedra and multi walled nanotubes.

TEM samples are imaged by passing an electron beam through the sample. This beam then hits a fluorescent viewing screen behind the window. The TEM used was a Hitachi 7000 and is shown in the picture below. The electron source or cathode is at the top, just above the specimen holder.

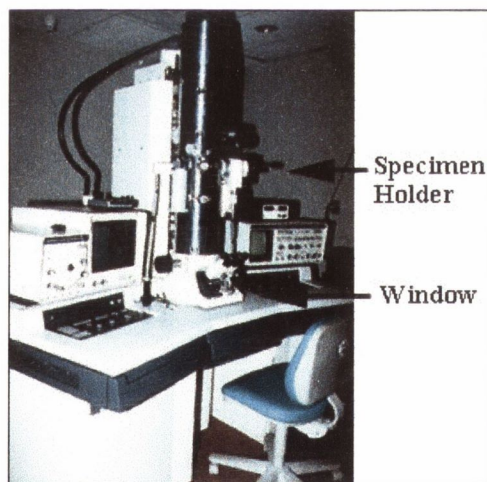


Figure 3.11 Hitachi 7000 TEM

It is a heated tungsten filament surrounded by a control grid. The cathode and control grid are at a negative potential equal to the desired accelerating voltage, usually 100kV in this study. The opposite electrode of the electron gun is the anode, which has the form of a disk with a hole. Electrons leave the cathode, accelerate

toward the anode, and pass through the central aperture at a constant energy. The specimen, mounted on a copper grid, is held in a small holder in a movable specimen. The electron beam passes through the specimen and forms an image on the fluorescent screen.

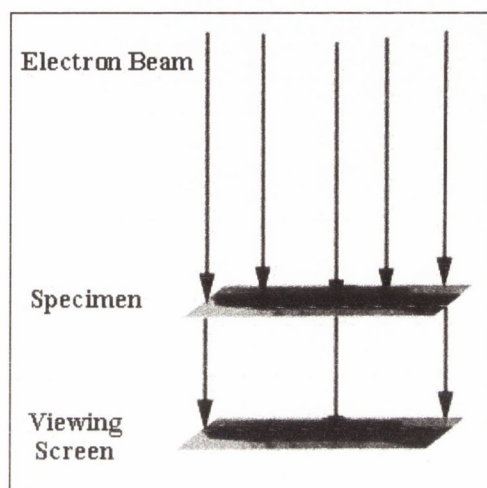


Figure 3.12 Schematic of TEM

Some images were taken after a CCD has been added to the system, which has the advantage of being more sensitive, thus images of higher magnification or resolution can be obtained.

To take images of the nanotube soot, the soot was dispersed in the solvent using a high power ultrasonic tip. A drop of this solution was put on a standard holey carbon TEM grid as shown in figure 3.13.



Figure 3.13 TEM grid, diameter 3mm

These grids are made from copper coated with a holey carbon film. After the solvent evaporates the nanotube soot is left on the holey carbon film and can be examined in the TEM.

3.3.7 Scanning Electron Microscopy SEM

The scanning electron microscope, designed for directly studying the surfaces of solid objects, uses a beam of focused electrons as an electron probe that is scanned in a regular manner over the specimen. The electron source which generates the beam is similar to the one described for the transmission electron microscope. This beam is scanned across the surface of the specimen and generates the emission of backscattered electrons. A schematic is shown in figure 3.14.

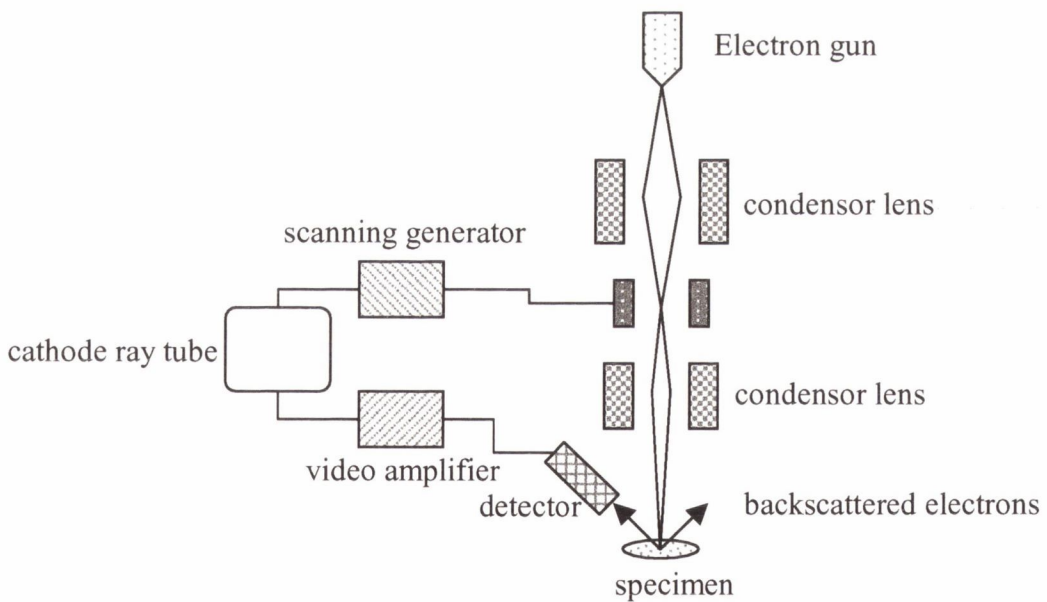


Figure 3.14 Schematic of SEM

These are collected and passed to a scintillator, which produces light when bombarded with electrons. The light is passed to a photomultiplier tube, where it is converted back to an electric signal with an effective gain of 10,000 times or more. The resultant amplified current is used to modulate the brightness of a cathode-ray display (or television) tube that is scanned in synchronism with the probe beam in the microscope column. Thus a picture of the scanned specimen is built on the screen.

3.3.8 Electron Paramagnetic Resonance spectroscopy

Electron paramagnetic resonance (EPR) was used to characterise nanotube soot produced with a Krätschmer generator. During this research this technique also was used to determine the purity of the nanotubes, e.g. the mass fraction of nanotubes in the soot. The spectrometer used was a Bruker EPR system.

According to quantum mechanics an electron must be in one of two possible spins, usually referred to as 'spin up' and 'spin down' or '+ $\frac{1}{2}$ ' and '- $\frac{1}{2}$ '. EPR measures the microwave absorption of the unpaired spins. These might result from free, conducting electrons or defect states. Different to other spectroscopic techniques, in EPR the frequency stays constant, but the applied magnetic field is swept.

The unpaired electrons, because of their spin, behave like tiny magnets. When materials containing such electrons are put in a strong stationary magnetic field, the magnetic axes of the unpaired electrons, or elementary magnets, partially align themselves with the strong external field, and they precess in the field. Resonance is the absorption of energy from the weak alternating magnetic field of the microwave

when its frequency corresponds to the natural frequency of precession of the elementary magnets. When stationary field strength is varied and the microwave frequency is kept constant, the measurement of radiation absorbed as a function of the changing variable gives an electron paramagnetic resonance spectrum. Such a spectrum is used to identify paramagnetic substances and to investigate the nature of chemical bonds within molecules by identifying unpaired electrons and their interaction with the immediate surroundings.

3.4 Mechanical Measurements

The techniques mentioned above were mainly used for characterisation of the produced nanotube materials. The composites made from these materials were then mechanically tested with one of the following techniques.

3.4.1 Nanoindentation

Nanoindentation is a technique widely use for the study of mechanical properties of thin films and coatings. Figure 3.15 shows the principle function of a nanoindenter.

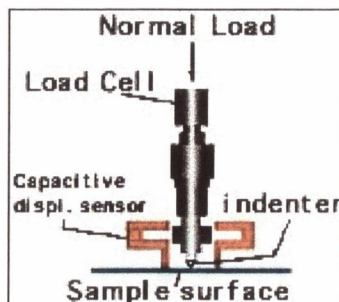


Figure 3.15 Schematic of nanoindenter

The measuring head consists out of the load cell, the indenter tip, a capacitive displacement sensor and a sapphire reference ring. The reference ring rests on the sample surface, and the indenter tip is driven into the sample. The applied load is measured by the load cell and the displacement with the capacitive sensor.

In contradiction to micro indentation, in nanoindentation the size of the indent is too small to be resolved by optical microscopy. It usually involves the constant recording of the load and the displacement of the indenter. Each test is a complete loading and unloading cycle. The data is usually visualised in a load vs. displacement plot (see figure 3.16).

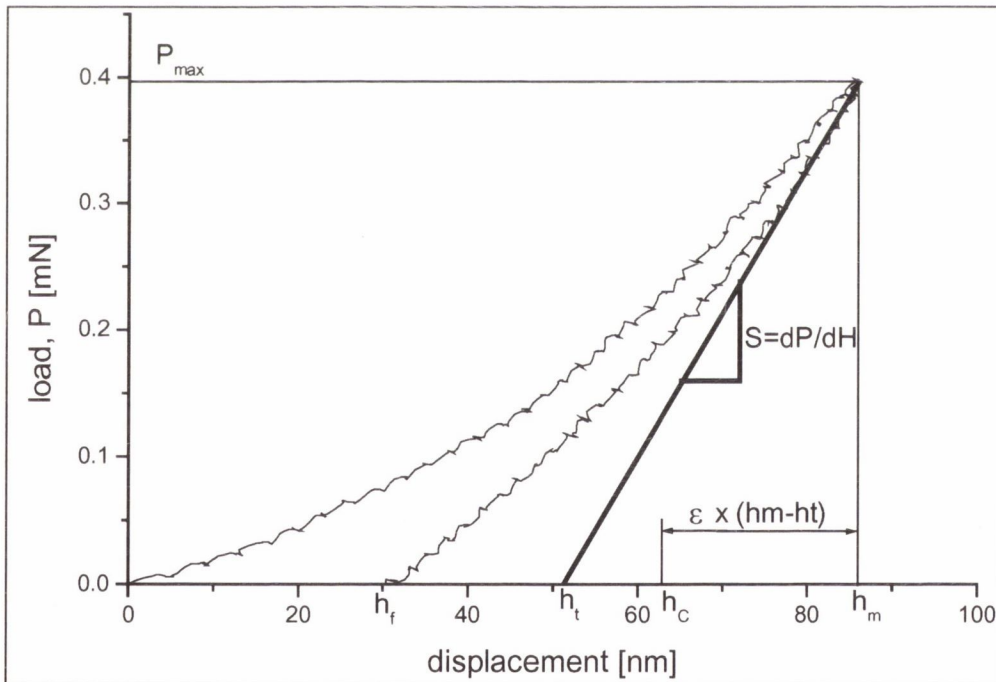


Figure 3.16 Load vs. displacement plot

A simple linear fit through the upper 1/3 of the unloading data intersects the depth axis at h_t . The stiffness, S , is given by the slope of this line. The contact depth, h_c , is then calculated as

$$h_c = h_m - \varepsilon(h_m - h_t)$$

where ε depends on the investigated material³¹. In practise, a more meticulous approach is used where a power law function is used to describe the upper 80% of the unloading data.

$$P = P_{\max} \left(\frac{h - h_o}{h_m - h_o} \right)^m$$

where the constants m and h_o are determined by a least squares fitting procedure.

The contact stiffness S ($=1/C$) is given by the derivative at peak load

$$S = \left(\frac{dP}{dh_{\max}} \right) = mP_{\max} \left[\frac{(h_m - h_o)^{m-1}}{(h_m - h_o)^m} \right] = mP_{\max} (h_m - h_o)^{-1}$$

and the tangent depth, h_c , is thus given by

$$h_t = h_m - \frac{P_m}{S}$$

The contact depth, h_c , is then

$$h_c = h_m - \varepsilon(h_m - h_t)$$

where ε now depends on the power law exponent, m . Such an exponent can be summarised for different indenter geometries:

Table 3.17 Constants depending on indenter geometry

indenter geometry	m (power law exponent)	ε
flat	1	1
paraboloid	1.5	0.75
conical	2	0.72

The reduced modulus, E_r , is given by

$$E_r = \frac{\sqrt{\pi}}{2} \frac{S}{\sqrt{A_c}} = \frac{\sqrt{\pi}}{2} \frac{1}{C} \frac{1}{\sqrt{A_c}}$$

which can be calculated having derived S and A_c (using the area function) from the indenter curve. The Young's modulus, E , can then be obtained from

$$\frac{1}{E_r} = \frac{1-\nu^2}{E} + \frac{1-\nu_i^2}{E_i}$$

The hardness is determined from the maximum load, P_{\max} , divided by the projected area after unloading

$$H = \frac{P_{\max}}{A_{PC}}$$

and will be discussed in more detail in chapter 6.

- ¹ J. N. Coleman, S. A. Curran, A. B. Dalton, A. P. Davey, W. J. Blau, B. McCarthy, and R. C. Barklie, *Physical Review B*, **58**, 7492 (1998)
- ² J. N. Coleman, S. A. Curran, A. B. Dalton, A. P. Davey, B. McCarthy, W. J. Blau, and R. C. Barklie, *Synth. Met.*, **102**, 1174 (1999)
- ³ J. N. Coleman, D. F. O'Brien, M. I. H. Panhuis, A. B. Dalton, B. McCarthy, R. C. Barklie, and W. J. Blau, *Synth. Met.*, **121**, 1229 (2001)
- ⁴ S. A. Curran, P. M. Ajayan, W. J. Blau, D. L. Carroll, J. N. Coleman, A. B. Dalton, A. P. Davey, A. Drury, B. McCarthy, S. Maier, and A. Strevens, *Advanced Materials*, **10**, 1091 (1998)
- ⁵ A. B. Dalton, H. J. Byrne, J. N. Coleman, S. A. Curran, A. P. Davey, B. McCarthy, and W. J. Blau, *Synth. Met.*, **102**, 1176 (1999)
- ⁶ A. B. Dalton, J. N. Coleman, M. i. h. Panhuis, B. McCarthy, A. Drury, W. J. Blau, B. Paci, J.-M. Nunzi, and H. J. Byrne, *Journal of Photochemistry and Photobiology A: Chemistry*, **144**, 31 (2001)
- ⁷ P. Fournet, J. N. Coleman, B. Lahr, A. Drury, W. J. Blau, D. F. O'Brien, and H. H. Horhold, *J. Appl. Phys.*, **90**, 969 (2001)
- ⁸ B. E. Kilbride, J. N. Coleman, D. F. O'Brien, and W. J. Blau, *Synth. Met.*, **121**, 1227 (2001)
- ⁹ B. McCarthy, J. N. Coleman, S. A. Curran, A. B. Dalton, A. P. Davey, Z. Konya, A. Fonseca, J. B. Nagy, and W. J. Blau, *J. Mater. Sci. Lett.*, **19**, 2239 (2000)
- ¹⁰ R. H. Friend and D. A. Tirrell, *Curr. Opin. Solid State Mat. Sci.*, **1**, 759 (1996)
- ¹¹ A. J. Heeger, *Angew. Chem.-Int. Edit.*, **40**, 2591 (2001)
- ¹² R. H. Friend, R. W. Gymer, A. B. Holmes, J. H. Burroughes, R. N. Marks, C. Taliani, D. D. C. Bradley, D. A. Dos Santos, J. L. Bredas, M. Logdlund, and W. R. Salaneck, *Nature*, **397**, 121 (1999)
- ¹³ C. J. Brabec, N. S. Sariciftci, and J. C. Hummelen, *Adv. Funct. Mater.*, **11**, 15 (2001)
- ¹⁴ K. F. Voss, D. Braun, and A. J. Heeger, *Synth. Met.*, **41**, 1185 (1991)
- ¹⁵ N. Tessler and R. H. Friend, *Synth. Met.*, **102**, 1122 (1999)
- ¹⁶ W. Helfrich and W. G. Schneider, *Physical Review Letters*, **14**, 229 (1965)
- ¹⁷ S. Kim, J. Jackiw, E. Robinson, K. S. Schanze, J. R. Reynolds, J. Baur, M. F. Rubner, and D. Boils, *Macromolecules*, **31**, 964 (1998)
- ¹⁸ H. Okawa, T. Wada, and H. Sasabe, *Synth. Met.*, **84**, 265 (1997)
- ¹⁹ R. H. Friend, G. J. Denton, J. J. M. Halls, N. T. Harrison, A. B. Holmes, A. Kohler, A. Lux, S. C. Moratti, K. Pichler, N. Tessler, and K. Towns, *Synth. Met.*, **84**, 463 (1997)

- ²⁰ M. Rehahn, A. D. Schluter, and G. Wegner, *Makromolekulare Chemie-Macromolecular Chemistry and Physics*, **191**, 1991 (1990)
- ²¹ R. A. Wessling, *Journal of Polymer Science, Polymer Symposium*, 55 (1986)
- ²² S. J. Chung, J. I. Jin, and K. K. Kim, *Adv. Mater.*, **9**, 551 (1997)
- ²³ S. Maier, *PhD Thesis*, Trinity College (2000)
- ²⁴ A. Drury, S. Maier, A. P. Davey, A. B. Dalton, J. N. Coleman, H. J. Byrne, and W. J. Blau, *Synth. Met.*, **119**, 151 (2001)
- ²⁵ H. G. O. Becker, W. Berger, G. Domschke, E. Fanghaenel, J. Faust, M. Fischer, F. Gentz, K. Gewalt, R. Gluch, R. Mayer, K. Müller, D. Pavel, H. Schmidt, K. Schollberg, K. Schwetlick, and E. Seiler, *Organikum*, Deutscher Verlag der Wissenschaften (1992), 19th Ed.
- ²⁶ J. March, *Advanced Organic Chemistry*, (1992), 4th Ed.
- ²⁷ S. Maier, *Diplom Thesis*, Fresenius Akademie (1997)
- ²⁸ Mettler Toledo, Collected Applications TA, *Pharmaceuticals*, (1997)
- ²⁹ J. I. Kroschwitz, *Polymers: polymer characterization and analysis*, Wiley Interscience (1990), 1st Ed.
- ³⁰ T. Hatakeyama and F. X. Quinn, *Thermal Analysis*, John Wiley & Sons (1999), 2nd Ed.
- ³¹ CSEM Application Bulletin, *Nano Hardness Tester*, (2000)

Chapter 4

Nanotube Production

Chapter 4 examines nanotube production in detail. Production parameters were investigated to produce the best yield in the shortest time. The soot generated was analysed, using a variety of techniques including electron microscopy.

4.1 Nanotube production

The production method used was the arc-discharge production method using a Krätschmer-Huffman generator. In such a generator, a current is applied between two graphite electrodes, so that a plasma forms. Due to the electrical potential between the two electrodes the anode is sublimed, while a deposit is formed on the cathode. The formation mechanism for the nanotubes and the other graphitic production by-products depend on the environment in the generator, the applied current, and the voltage drop between the electrodes.

The development of an evaluation method for the nanotube-percentage in the soot is described later. However, at the time this research began no such method was available. The only method available to describe the quality, purity and dimensions of the nanotubes was by visual examination, thus by electron microscopy. Random pictures of the as-produced soot were taken, and analysed for the content.

Figures 4.1 a) to d) show a typical sample of a soot particle produced with the Krätschmer generator, where an area with a very high nanotube content is highlighted.

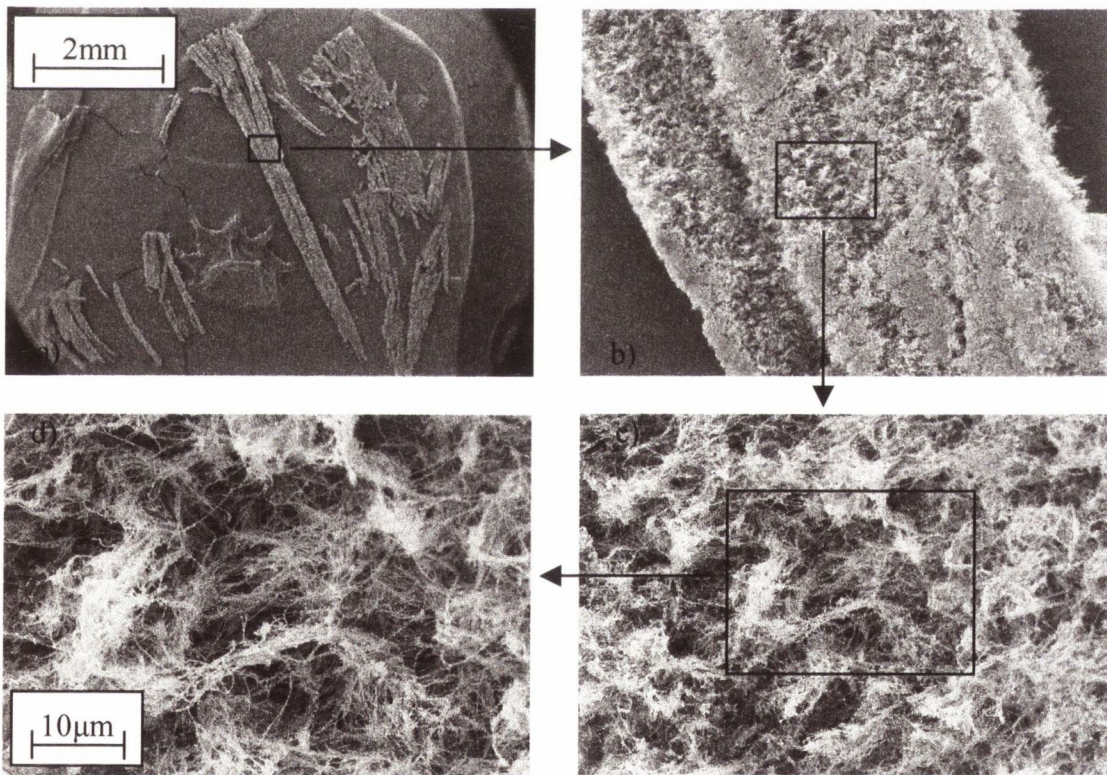


Figure 4.1 a) to d) SEM images of nanotube soot

4.1.1 Variation of the voltage

In addition to pressure and current density, the voltage is one of the important variables in fullerene production. At voltages below 22.5V a plasma will not be built, the anode will not be sublimed; hence no nanotubes will form on the cathode. A current will run through the electrodes, but a deposit is not developed. To obtain a voltage drop across the electrodes of 23.3V and more, the electrodes have to be moved to close together, so that no plasma sheath will built between them¹.

A range of nanotube samples (runs) were produced with average voltages between 22.6 to 23.0Volts. The produced nanotube material was analysed using SEM and TEM imaging of the raw soot. Since this was done after the completion of each run, there are other more subjective measurements of the quality of each run in situ during production. A good indication of the quality is the stability of the plasma². This is apparent to the operator by visual and aural inspection. Even if these are not scientific values, which can be measured quantitatively, it still gives an indication of the quality of each run. During production of fullerene materials, the generator vibrates and a 'buzzing' noise is audible at very distinct frequencies. Furthermore, the intensity of the plasma between the electrodes can be seen in a small window at the side of the generator. Depending on the voltage and the current the light changes from a low intensity, yellow colour to an intense yellow to a bright, almost white light.

For the SEM characterisation of the nanotube material, the raw soot was put onto a SEM sample holder. No purification or any other kind of treatment was carried out. Then the samples were coated with a thin gold film, to achieve the necessary conductivity of the sample. For the visualisation of the nanotubes produced at

various voltages images were taken at sample areas with very high purities, i.e. with almost no impurities. When nanotubes are produced using the Krätschmer generator, some impurities, so-called by products are produced as well, namely amorphous carbon, turbostratic graphite, and polyhedra (“Bucky onions”). When the soot is analysed for purity, this means the ratio of nanotubes to all other by products.

Figure 4.2 shows an SEM of nanotube material produced at 22.6V. This picture mainly shows nanotubes, but some impurities can be seen as well. However, it is not always possible to determine what kind of impurity can be seen on those pictures. At such a relative low voltage, the nanotube production is quite long. An average run took around 1.5 hours and consumed approximately 8cm of the anode. The optimisation of this production method aims to produce the highest purity possible in the shortest time possible.

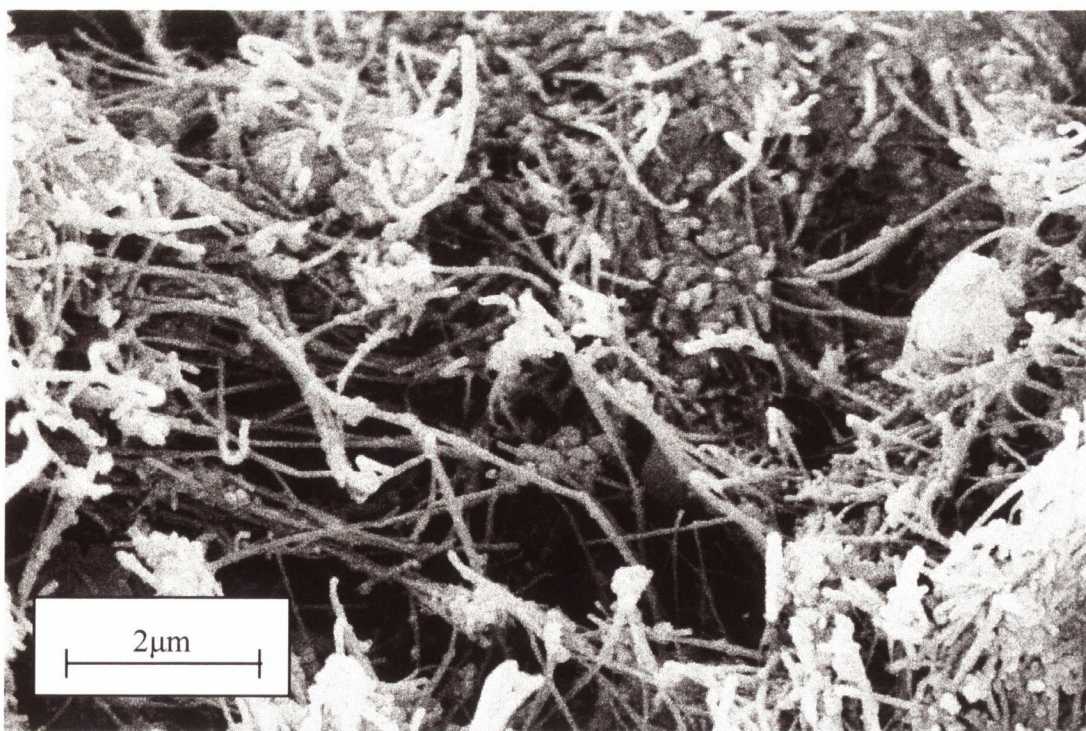


Figure 4.2 SEM image of nanotube soot produced at 22.6V

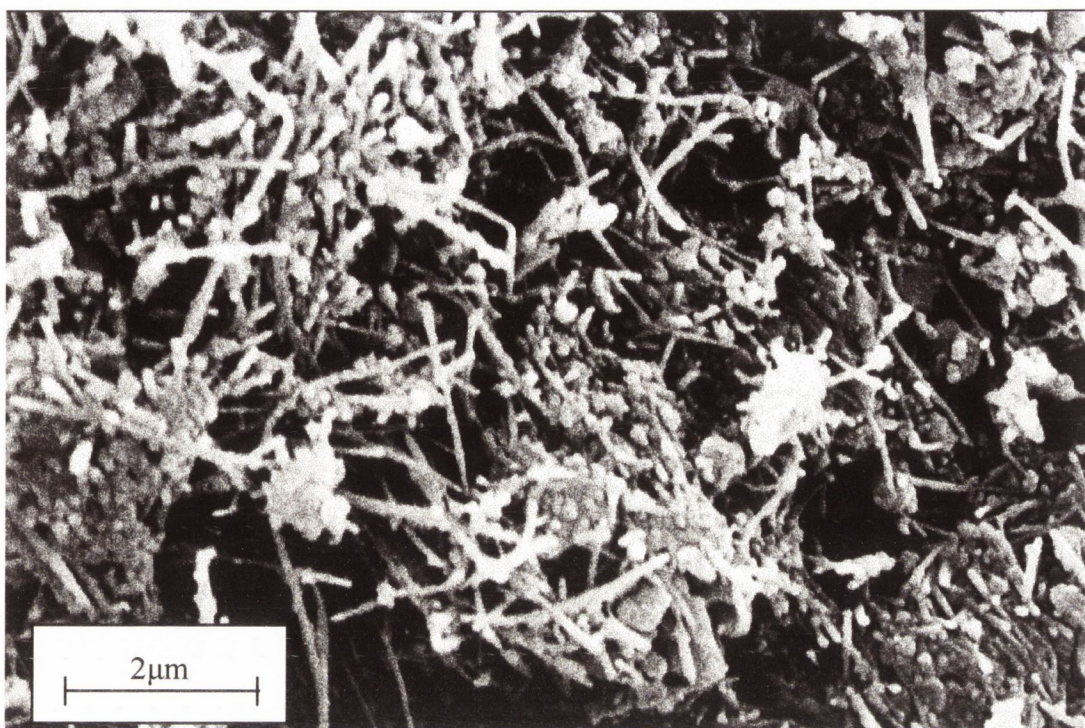


Figure 4.3 SEM image of nanotube soot produced at 22.7V

Figure 4.3 shows nanotube material produced at 22.7V. This SEM, like the pictures taken at all voltages, is taken at a random position on the sample. All pictures show representative areas of the produced soot. It shows no significant difference to the sample produced at 22.6V. It shows the same purity and the nanotubes have the same average tube length. The run took slightly less time (approx. 1hr 20min) than the one produced at 22.6V.

For the next run the average voltage was again increased by 0.1V. Figure 4.4 shows a sample produced at 22.8V. Once again the run took less time to finish (approx. 1hr), even though the voltage becomes less stable the higher the voltage is. This was even more noticeable at the runs produced at 22.9 and 23.0V.

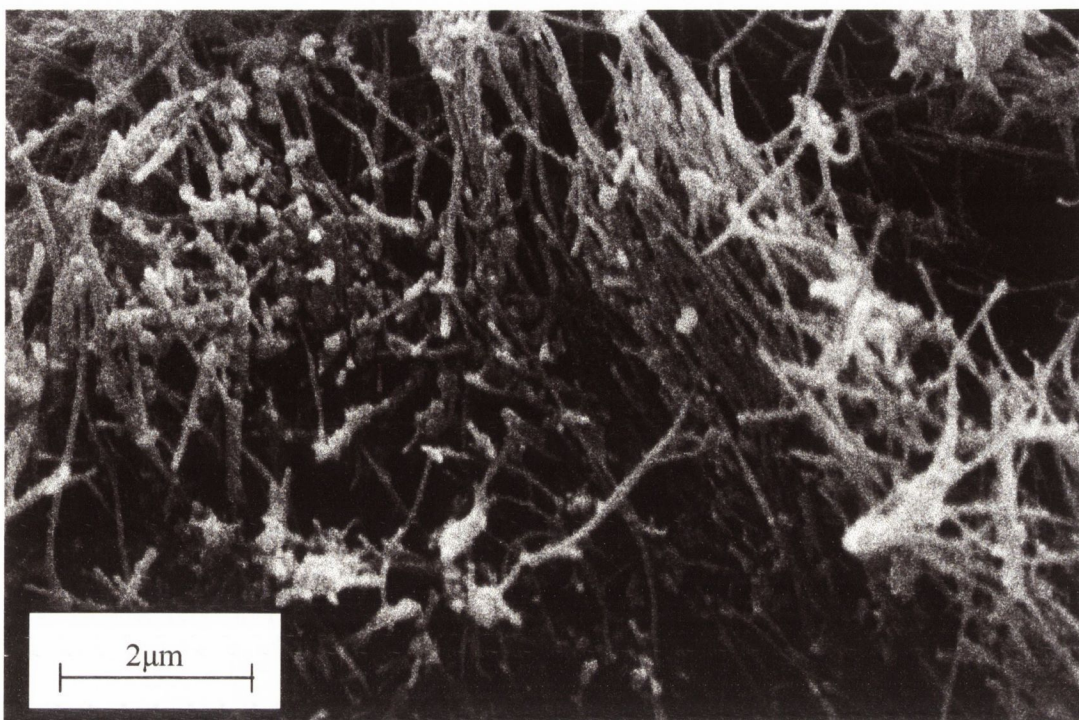


Figure 4.4 SEM image of nanotube soot produced at 22.8V

The next two figures show nanotubes produced at 22.9 and 23.0V respectively. As shown in the previous pictures, there is no noticeable change in the purity of the nanotubes. The average length of the nanotubes did not change either. However, with increasing voltage the time it took to consume about 8cm of the cathode decreased. An average run at 23.0V only took 45min, compared to around 1.5hrs at 22.6V.

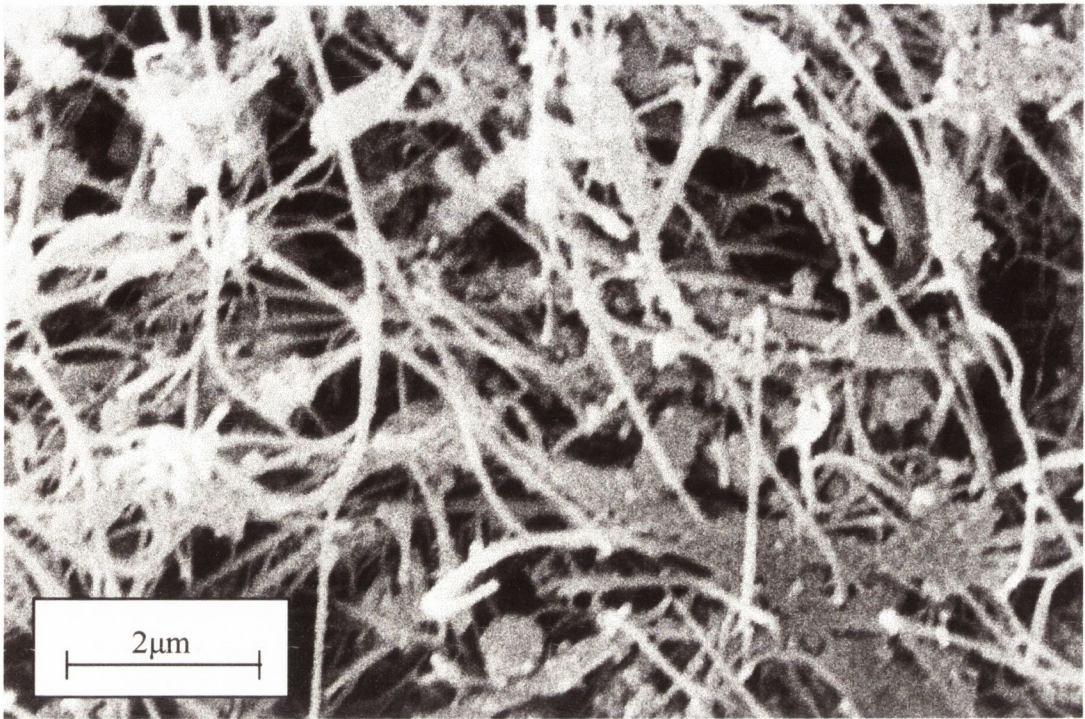


Figure 4.5 SEM image of nanotube soot produced at 22.9V

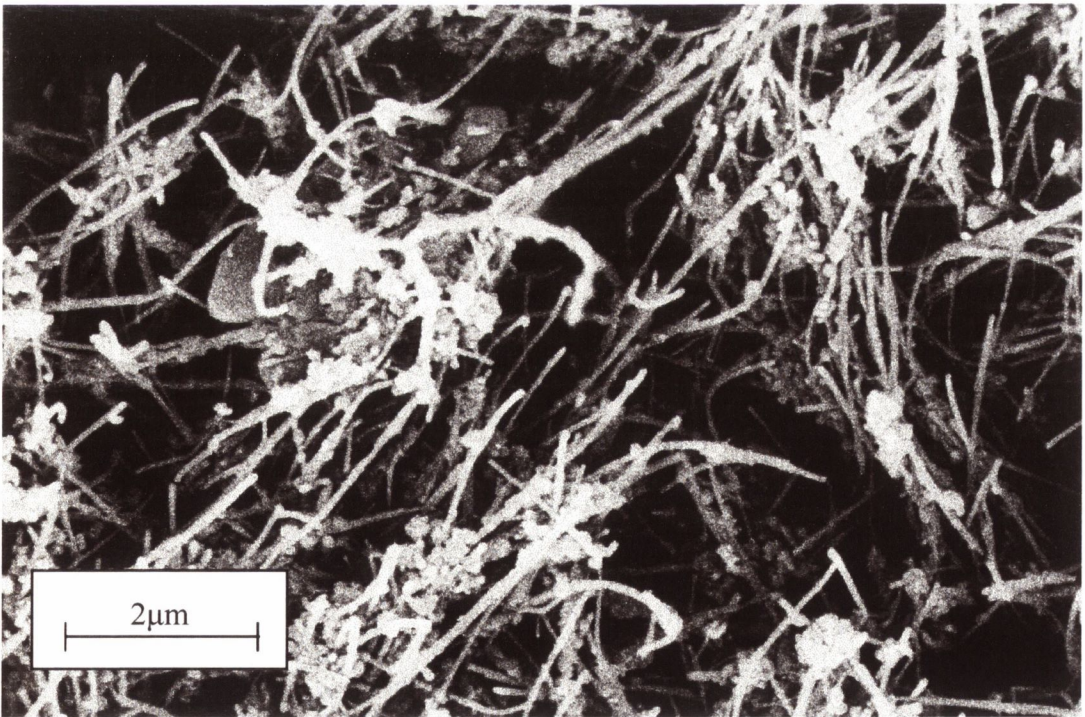


Figure 4.6 SEM image of nanotube soot produced at 23.0V

The samples were also analysed using TEM imaging. The samples were dispersed in ethanol with the high power ultrasonic tip, and then a drop of this solution was dropped onto the TEM sample grid. Figures 4.7 and 4.8 show samples produced at 22.9 and 23.0V respectively.

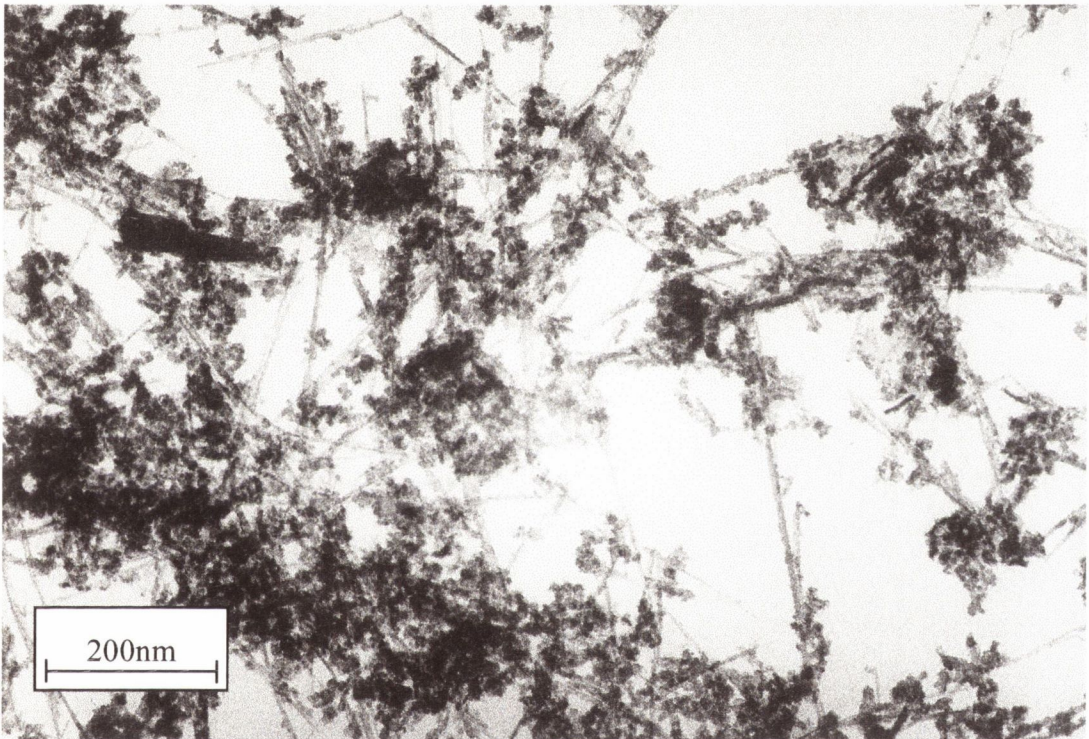


Figure 4.7 TEM picture of soot produced at 22.9V

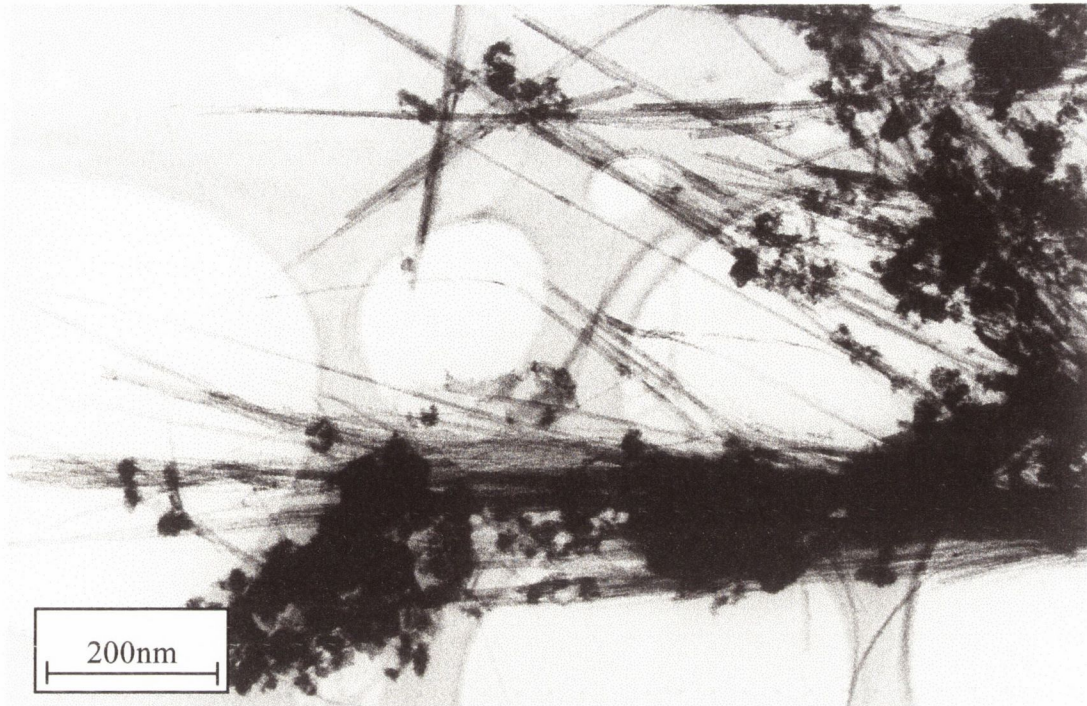


Figure 4.8 TEM picture of soot produced at 23.0V

As it can be seen from these images, the nanotubes form aggregates with the by products from the production method, hence these TEM pictures do not provide evidence for any changes in quality or purity.

Different TEM samples were prepared with sodium dodecyl sulphate (SDS) as a surfactant. Here it was possible to observe individual nanotubes. Figure 4.9 shows a picture of the nanotubes produced at 22.8V, dispersed with 1weight% SDS in toluene.

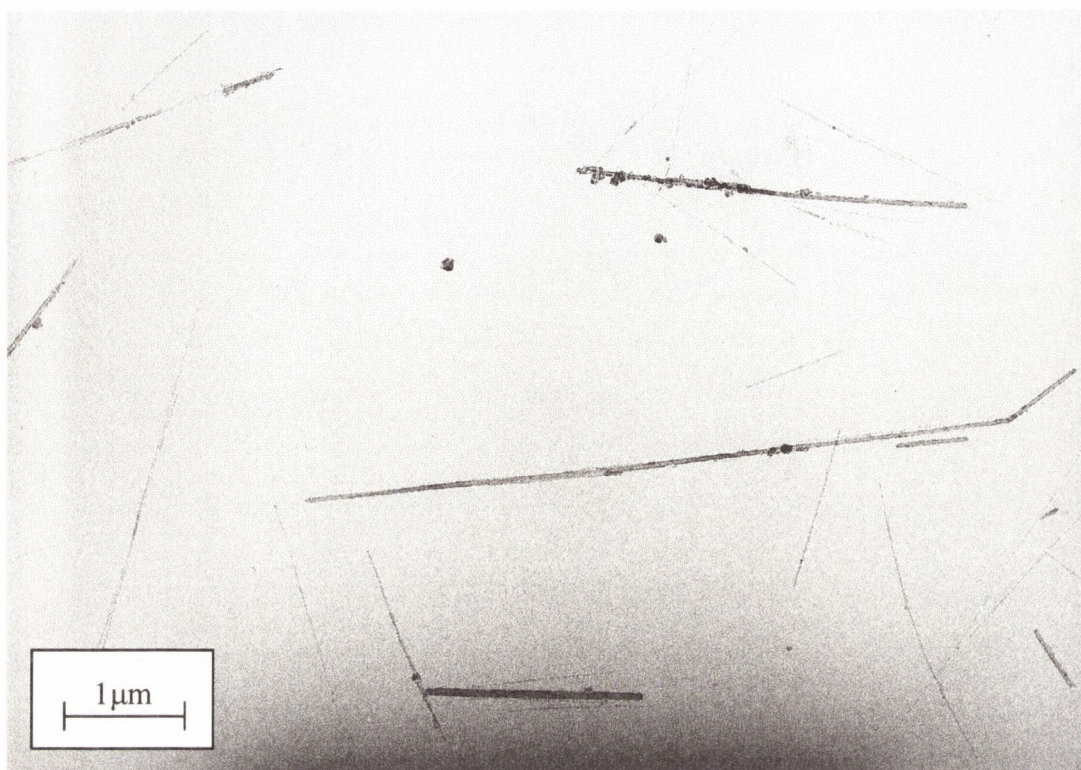


Figure 4.9 TEM picture of soot produced at 23.0V

However, SDS interacts differently with nanotubes and graphitic particles. In fact TEM pictures show that SDS micelles serve to disperse nanotubes well, while interacting less extensively with the graphitic impurities³. Therefore, an unrepresentative picture of nanotube purity is observed.

4.1.2 Variation of the pressure

As shown in the SEMs variation of the voltage did not affect the quality of the nanotube material produced, but the time to produce nanotubes decreased with higher voltage. Hence, all future runs were made at 23.0V. Now the pressure in the generator chamber was varied. At first nanotubes were produced at a pressure of

300Torr, which was then raised in steps of 25Torr to a final value of 450Torr.

Again, the material was analysed with SEM to find the best quality and purity.

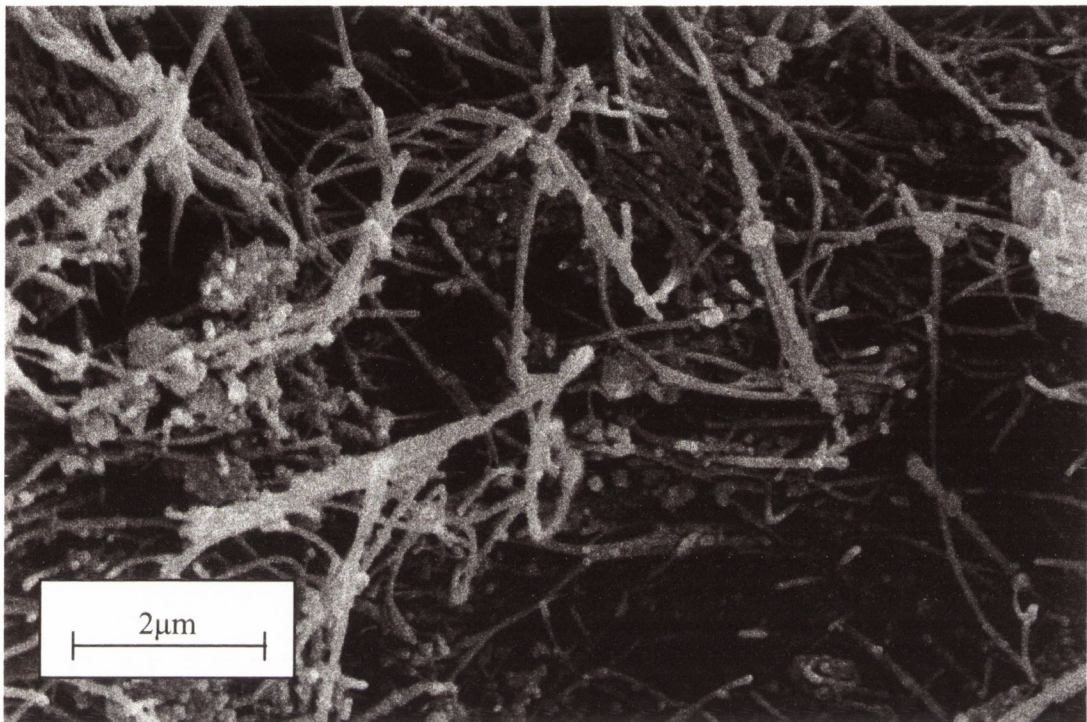


Figure 4.10 SEM image of nanotube soot produced at 300Torr

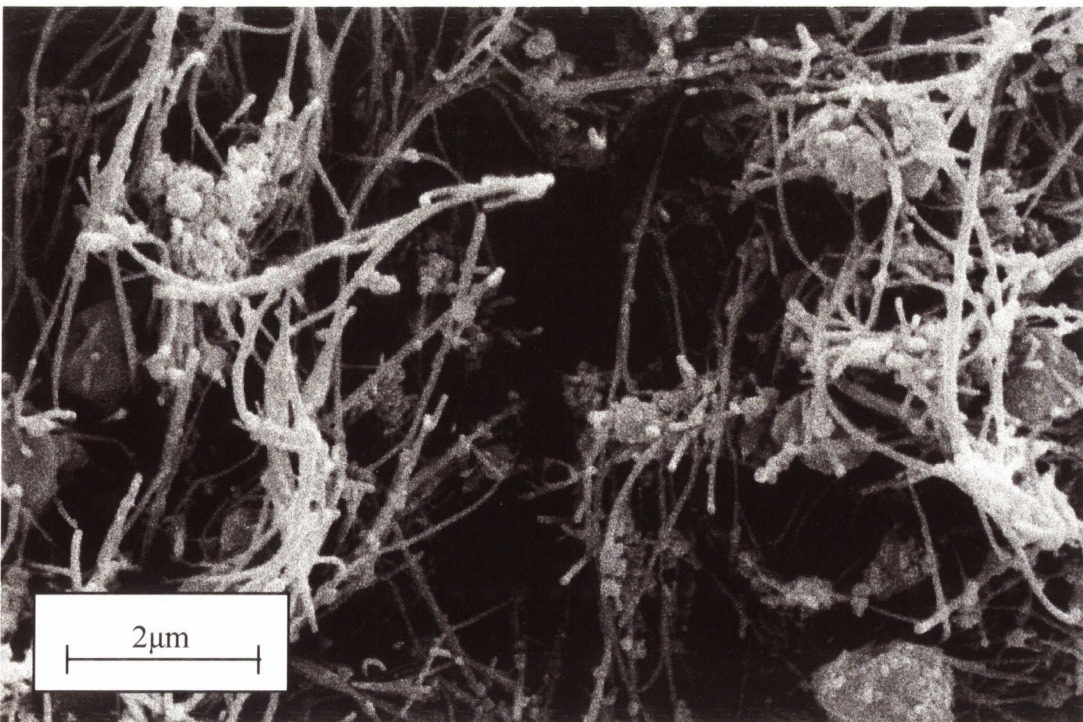


Figure 4.11 SEM image of nanotube soot produced at 350Torr

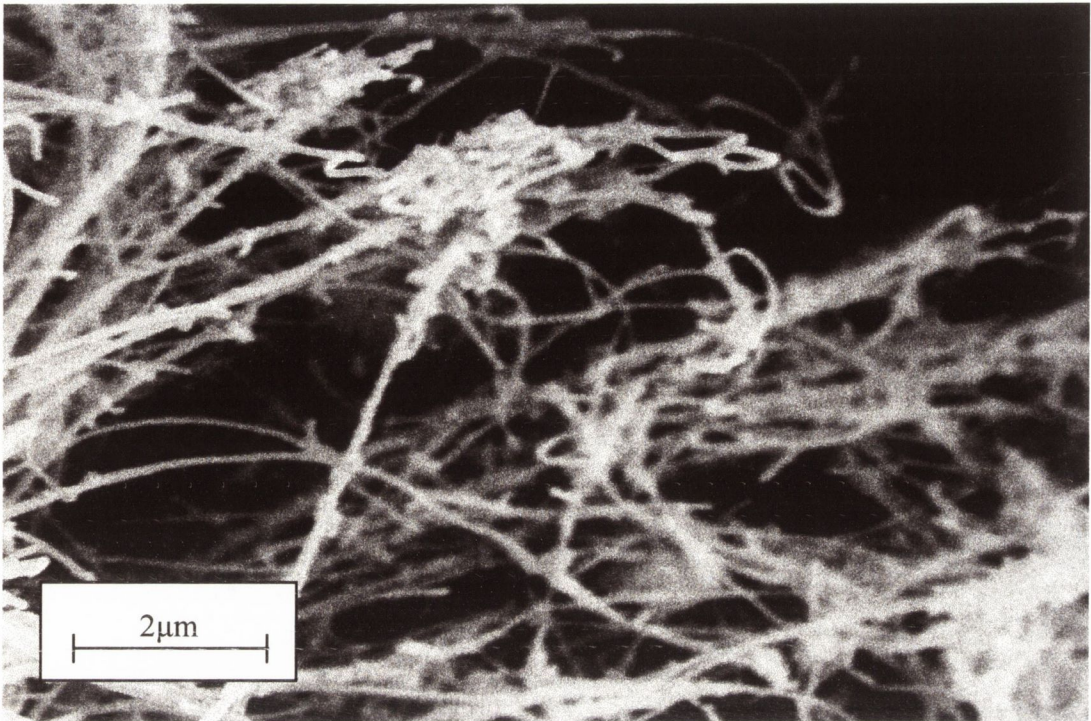


Figure 4.12 SEM image of nanotube soot produced at 400Torr

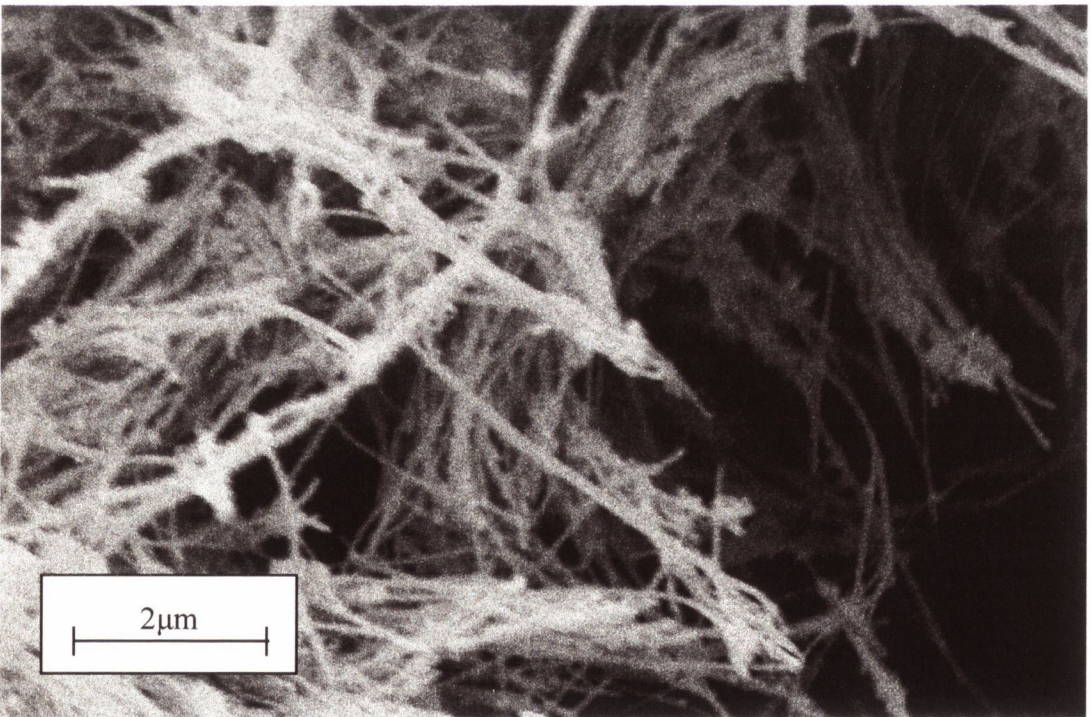


Figure 4.13 SEM image of nanotube soot produced at 450Torr

Only minor differences in quality and purity were found. The nanotube content in comparison to the by products such as turbostratic graphite was constant. However, in nanotube samples produced at higher pressures the nanotubes seem to be longer. This might be due to the fact that at higher pressures the plasma is more stable⁴. This can be seen by the fact that a smaller variation of the voltage between the electrodes is noticeable, as well as at the constant vibration and ‘buzzing’ of the entire generator while producing the nanotubes.

4.1.3 Variation of the current density

Finally, nanotubes were produced at different current densities. The current density J is calculated by the following equation

$$J = \frac{I}{A_e}$$

where I is the current and A_e is the area of the cross section of the electrodes.

As all nanotubes were produced using the same electrodes with a constant diameter, the current density is proportional to the current and therefore will be only referred to as current.

Having found the optimal voltage and pressure, all nanotubes were then produced with a voltage of approximately 23V and at a pressure of 400Torr. The current was changed from 34A to 40A in steps of 1A, and two more runs at 32A and 45A.

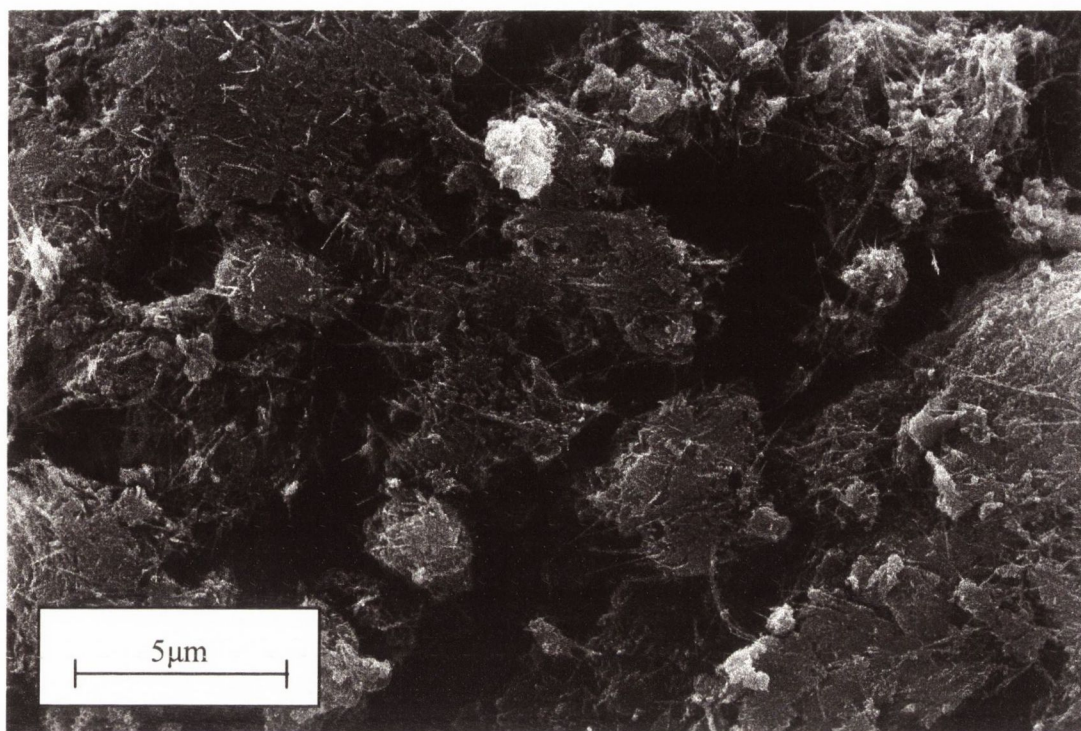


Figure 4.14 SEM image of nanotube soot produced at 32A

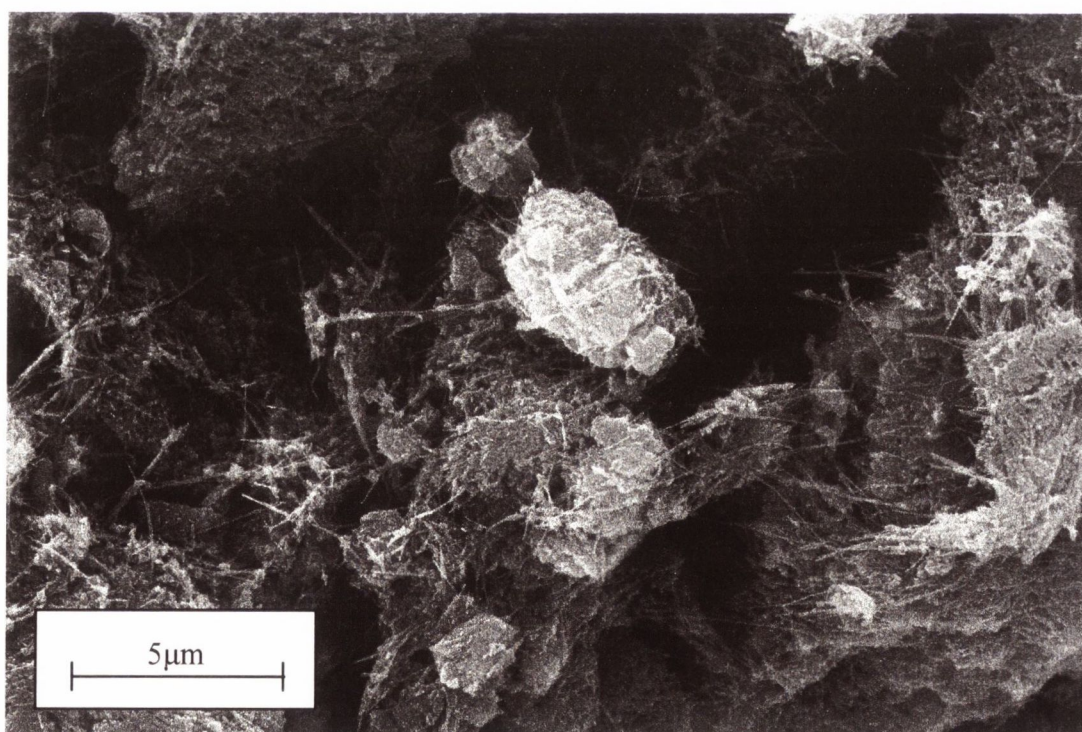


Figure 4.15 SEM image of nanotube soot produced at 34A

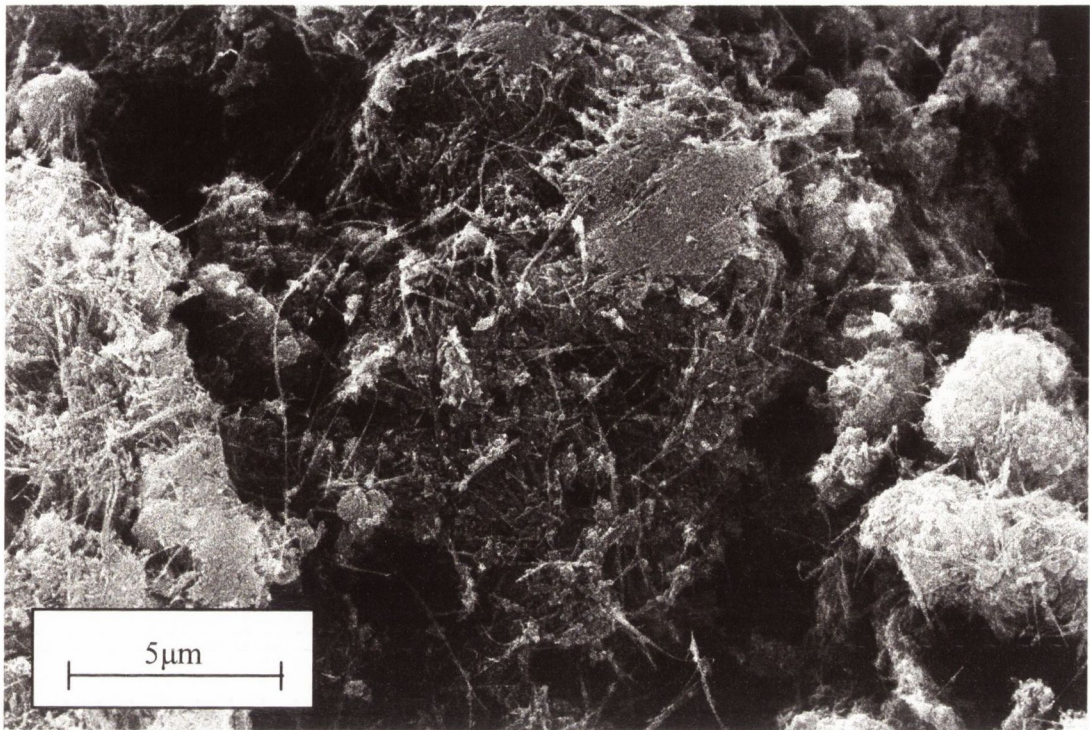


Figure 4.16 SEM image of nanotube soot produced at 36A

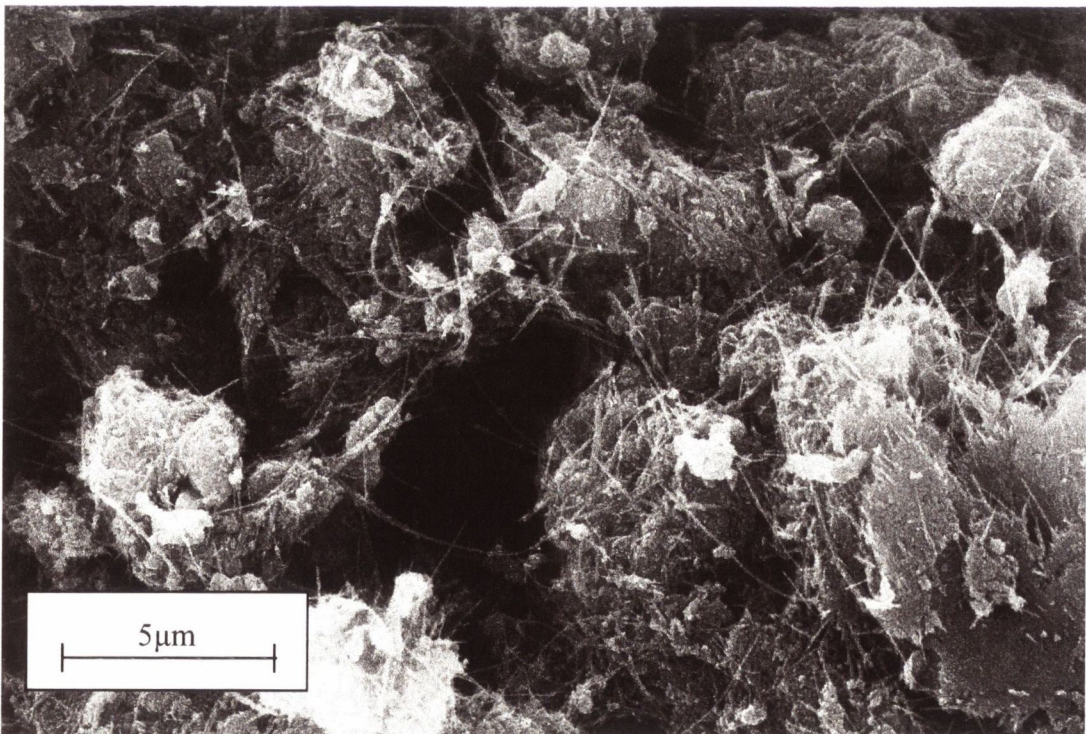


Figure 4.17 SEM image of nanotube soot produced at 38A

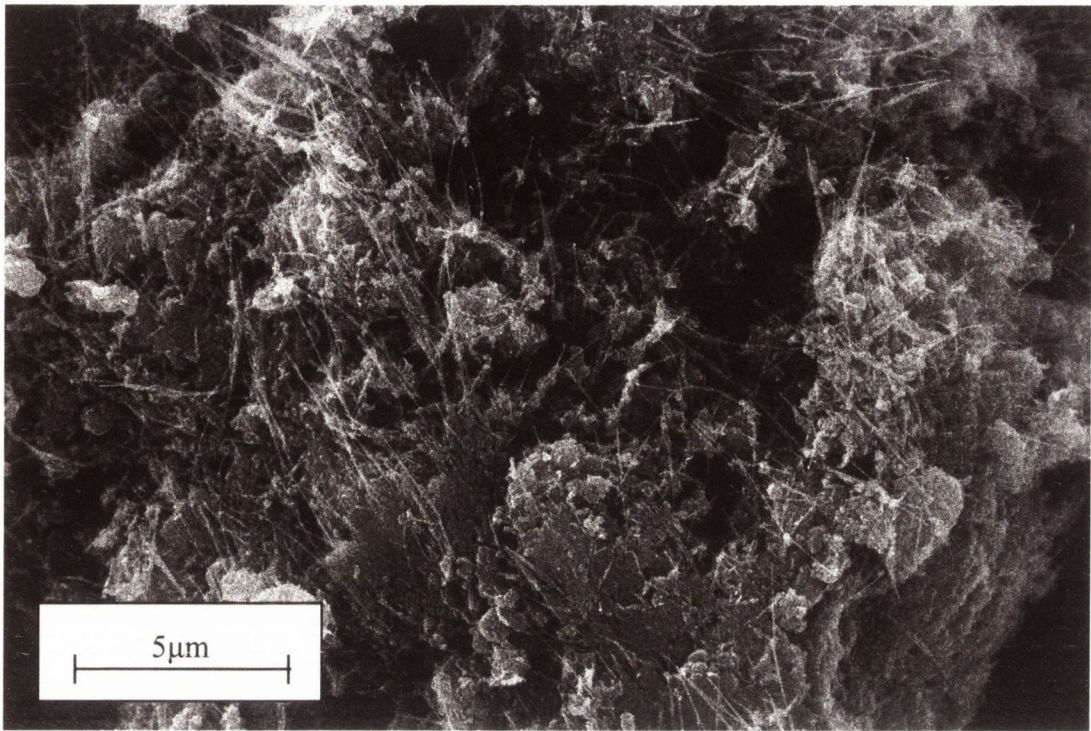


Figure 4.18 SEM image of nanotube soot produced at 39A

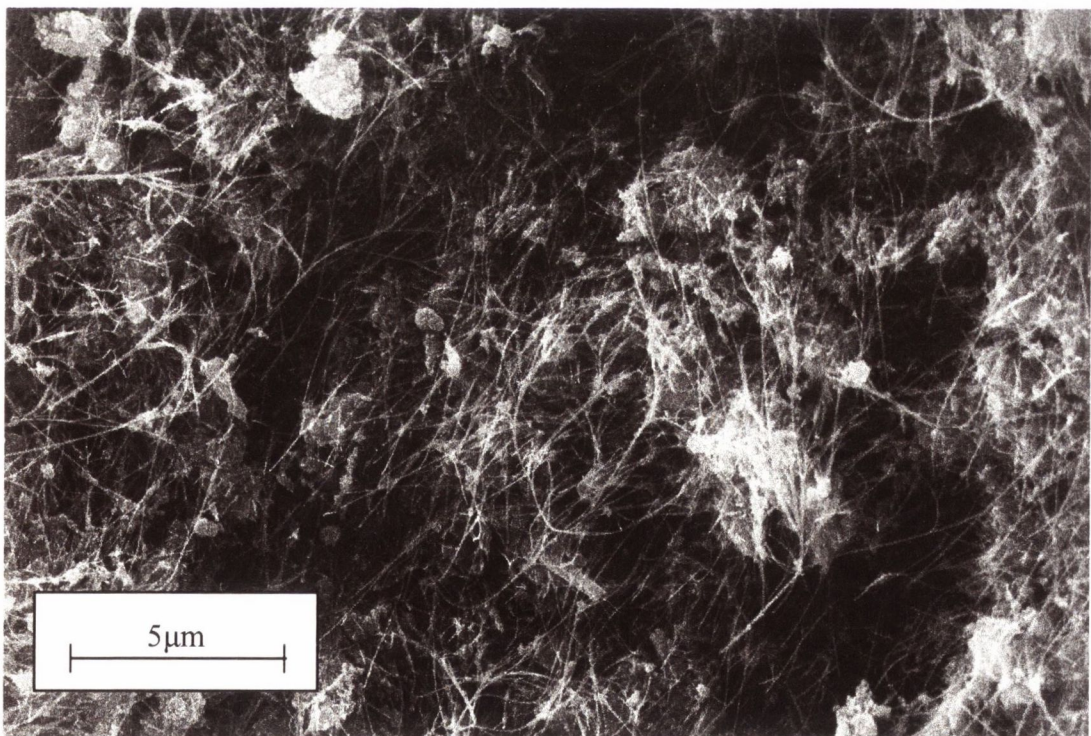


Figure 4.19 SEM image of nanotube soot produced at 40A

These pictures show that with increasing current the average length of the nanotubes increases as well. Furthermore, the ratio of graphitic particles to nanotubes appears to be the same throughout the lower currents, but above 39A there are more nanotubes in the soot.

The nanotubes produced from 36A to 40A have been analysed using EPR. The EPR signal can be deconvoluted into two distinct peaks for multiwalled nanotubes and turbostratic graphite, respectively. The area under those peaks (A_{MWNT} , A_{TSG}) is representative of the amount of those materials in the sample. The ratio of the two areas is a direct measure of the purity of the nanotube soot and is shown in table 4.20

Table 4.20 EPR results

I [A]	A_{MWNT}/A_{TSG}
36	0.469
37	0.497
38	0.538
39	0.625
40	0.753

Those results confirm the information gained from analysing the SEM pictures.

At even higher currents the amount of by products increases. As figure 4.21 shows, the nanotubes have a very high average length, but the nanotube content over all has decreased.

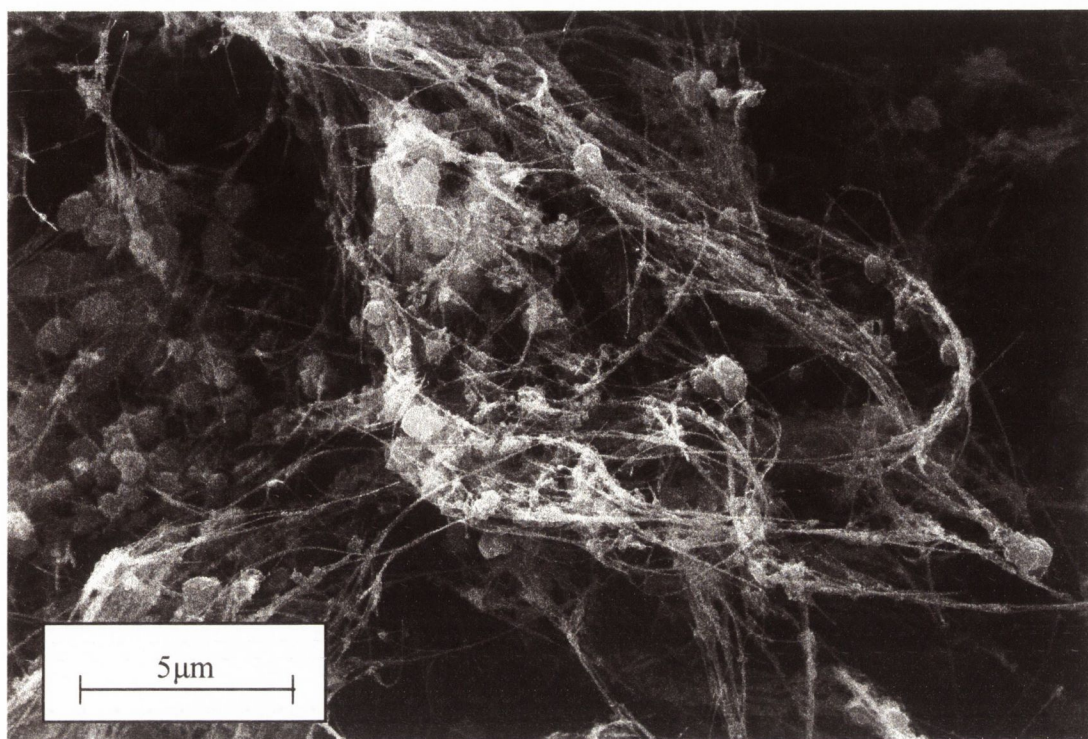


Figure 4.21 SEM image of nanotube soot produced at 45A

4.2 Results and discussion

The main interest was to optimise the arc discharge production method by examining

- Purity of the nanotubes produced
- Length of the nanotubes produced
- Length of time for each run

The influence of different voltages, pressures and currents in the arc discharge nanotube production method was investigated.

The change of the voltages in the reaction chamber did not affect the purity or the length distribution in the samples as seen in the SEMs. However, by slightly increasing the voltage the run time decreases. The variation of the helium pressure

in the reaction chamber showed, that at slightly higher pressures the plasma was more stable, hence the nanotubes produced are slightly longer. In addition, the pressure did not have any influence on the purity of the nanotubes produced.

The biggest influence on the quality of the nanotubes produced was the current density, at which the nanotubes are produced. By increasing current, the nanotubes became much longer. Since a high aspect ratio of nanotubes is very important for this research, the nanotube production method was optimised to produce the best nanotube material by arc discharge production method using the Krätschmer generator. The nanotubes produced for the composites described in chapter 5 and 6 have been made at a pressure of 450Torr, a voltage of 23.0V and a current of 40A. The nanotubes produced at these parameters had an average diameter of 10nm to 40nm and an average length of about 0.5 μ m to 1 μ m.

- ¹ A. Maiti, C. J. Brabec, C. Roland, and J. Bernholc, *Physical Review B*, **52**, 14850 (1995)
- ² S. Iijima, *Mater. Sci. Eng. B-Solid State Mater. Adv. Technol.*, **19**, 172 (1993)
- ³ G. S. Düsberg, *private communication*
- ⁴ H. Zhang, D. Wang, X. Xue, B. Chen, and S. Paeng, *Physics D: Applied Physics*, **30**, L1 (1997)

Chapter 5

Thermal Characterisation

This chapter deals with the characterisation of the thermal properties of PmPV, nanotube materials, and composites.

5.1 Thermogravimetric Analysis of PmPV

Thermal characterisation is an important tool in polymer characterisation. Especially if the polymers are not purchased from a commercial supplier, but polymerised in small batches by different research groups. One of the tests done with every batch of the PmPV synthesised by our group is thermogravimetric analysis (TGA). Usually TGAs are performed in an inert atmosphere, e.g. in nitrogen. Since this would prevent the oxidisation of the polymers, only a part of the important information can be obtained in an inert atmosphere. Figure 5.1 shows two different TGAs with the same PmPV polymer, one in air and the second in nitrogen.

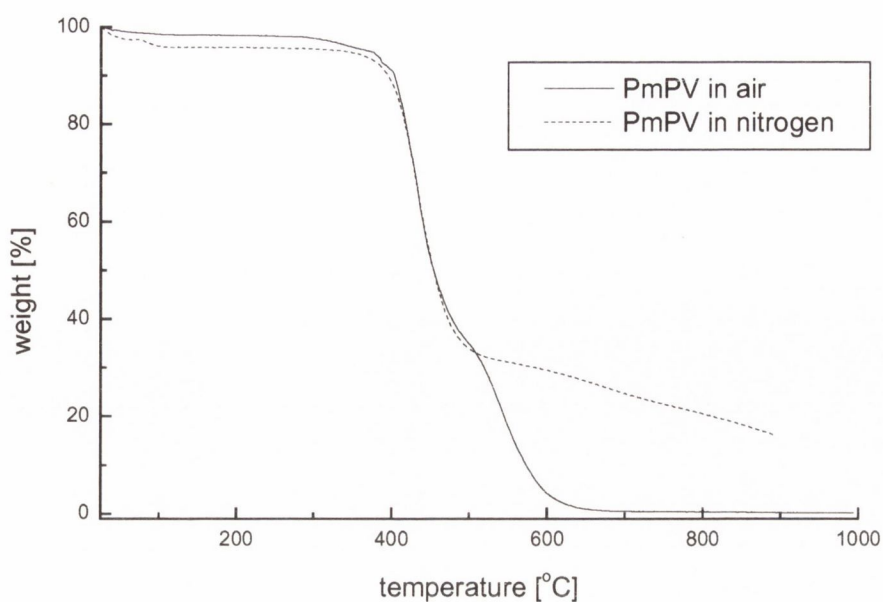


Figure 5.1 Comparison of TGA in air and in nitrogen

Since the oxidation of the nanotube material, as shown later in this chapter, occurs at much higher temperatures, all TGAs were performed in air.

After the first batches of PmPVs were analysed, after the measurement was finished, some residue could be observed in the crucible. Figure 5.2 shows a TGA of one of these batches.

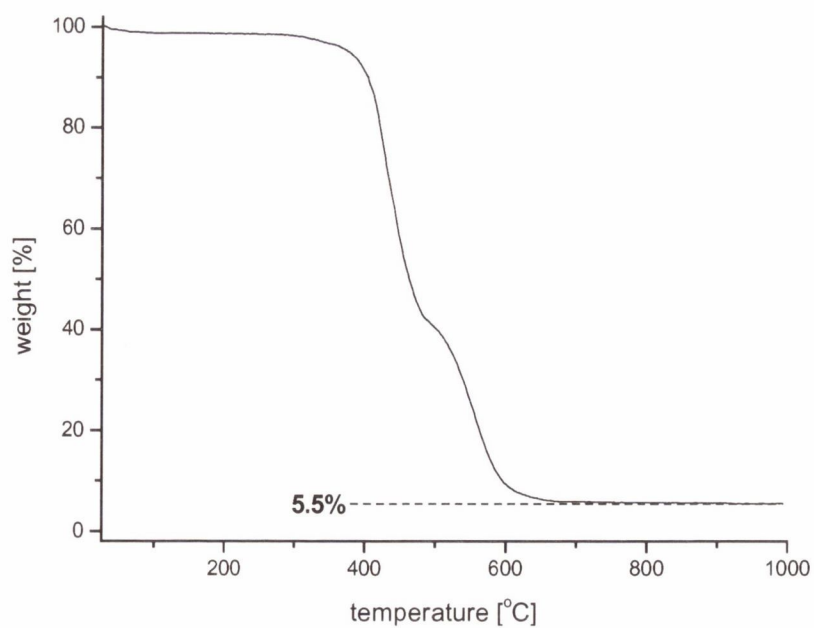


Figure 5.2 TGA of PmPV with impurities

As organic compounds usually oxidise in temperatures below 1000°C the residue was analysed with elemental analysis. This was done using the energy dispersive X-ray analysis which is attached to the SEM. Table 5.3 shows the results of the elemental analysis of the residue.

Table 5.3 Elemental analysis of the residue

element	average weight [%]	standard deviation	element	average weight [%]	standard deviation
Mg	9.92	2.41	Cr	0.66	0.32
Al	0.24	0.36	Fe	1.73	0.87
Si	21.23	3.94	Ni	0.27	0.31
P	25.33	6.76	Cu	0.87	0.23
K	1.86	0.72	Zn	2.11	0.48
Ca	4.81	0.41	C	20.79	10.26
Ti	0.29	0.10	O	9.90	3.34

All of these impurities could be traced back to the polymerisation reaction of the PmPV. Among other reasons these were due to the use of certain filters (Si), or the usage of non-deionised water (Mg, K, Ca). The polymerisation was repeated with different filters and deionised water, and afterwards the TGA revealed that no more residue was left over.

To compare different polymerisation routes and different batches polymerised by the same route, TGAs were recorded. Figure 5.4 shows the TGA plots of different PmPVs, polymerised at different temperatures.

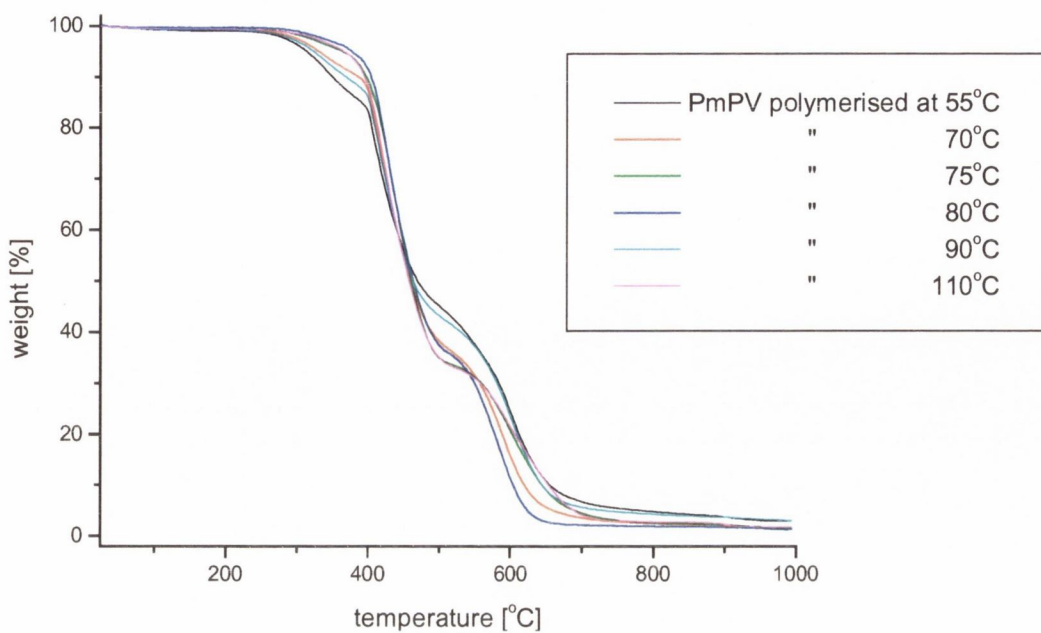


Figure 5.4 TGA of PmPV polymerised at different temperatures

More information can be obtained from a plot of the first derivatives as shown in figure 5.5.

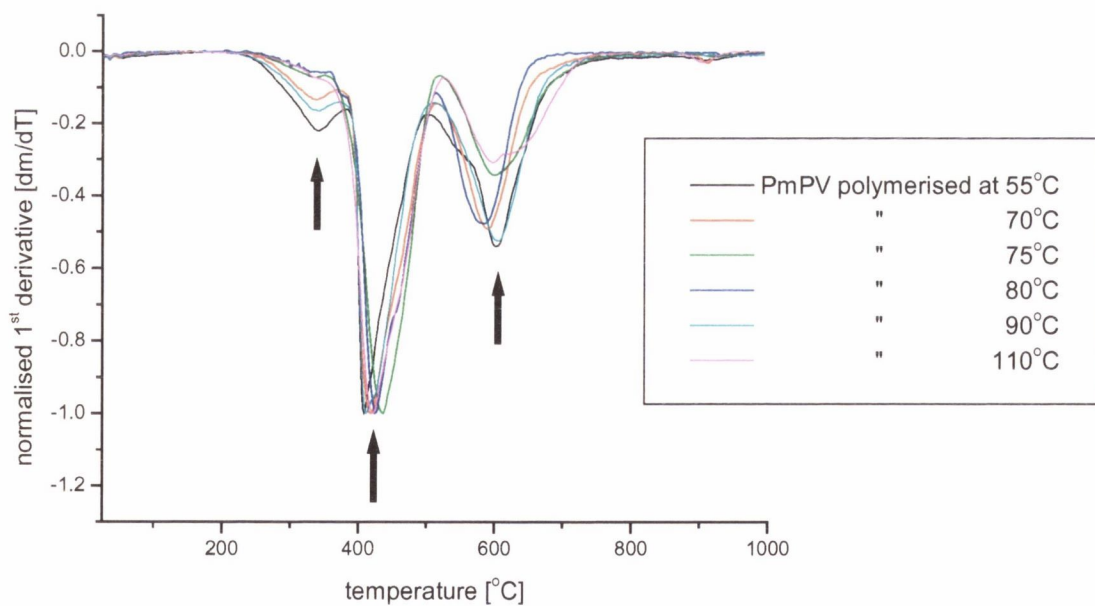


Figure 5.5 First derivatives ($\Delta m/\Delta T$)

This plot shows the change of the slope of the first plot. Here it becomes clear that three different transitions (indicated with three arrows) occur. These three different transitions can be associated with the oxidation of three different segments of the PmPV molecules. The first oxidation is the oxidation of the OC_8H_{17} side arms of the polymer, the second with the oxidation of the benzene rings, and the last one with the oxidation of the polymer backbone. Figure 5.6 shows the TGA of another batch of PmPV. Even though it was polymerised the same way as the PmPV shown above, it shows distinct differences in its thermal properties.

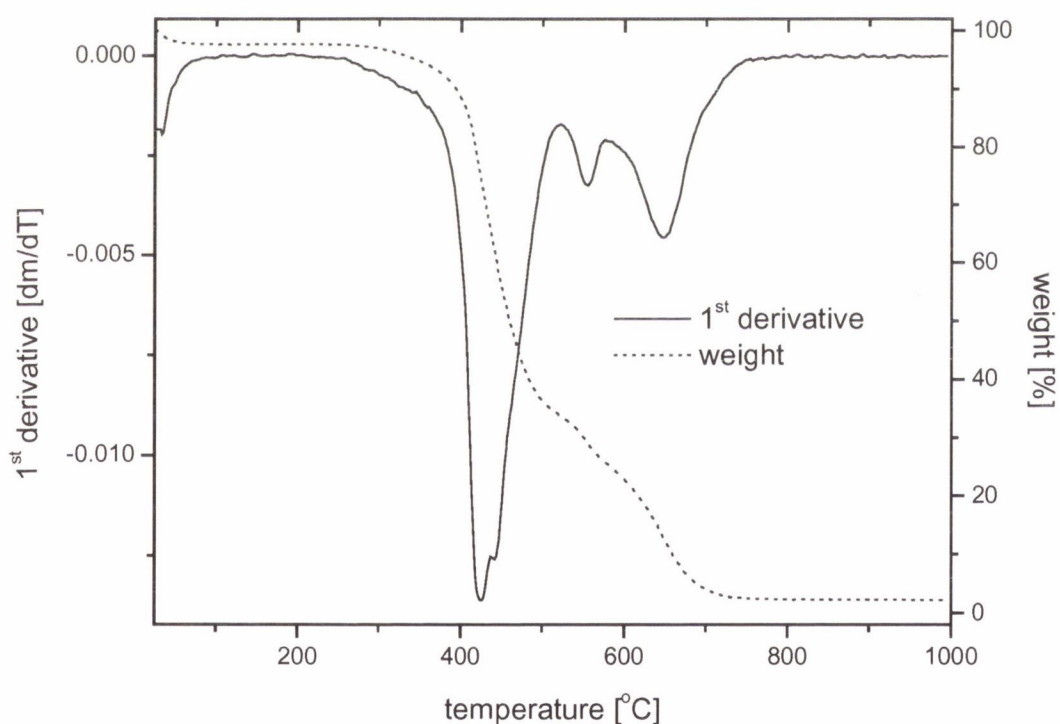


Figure 5.6 TGA and 1st derivative of a different PmPV batch

This was one of the first batches polymerised by our group. The differences, which can be seen especially in the plot of the 1st derivative, give reason to believe that

there are significant alterations in the polymeric structure of this batch. This batch also did not show any interactions with the nanotubes and was not used for the preparation of the composites described later.

5.2 Thermogravimetric Analysis of nanotube material

All the nanotube soot produced has been thermally characterised. Figure 5.7 shows the TGA and first derivative of nanotube soot produced at 37A. Figure 5.8 shows the TGA and first derivative of pure graphite taken from a graphite electrode which is used for the arc discharge production of nanotubes.

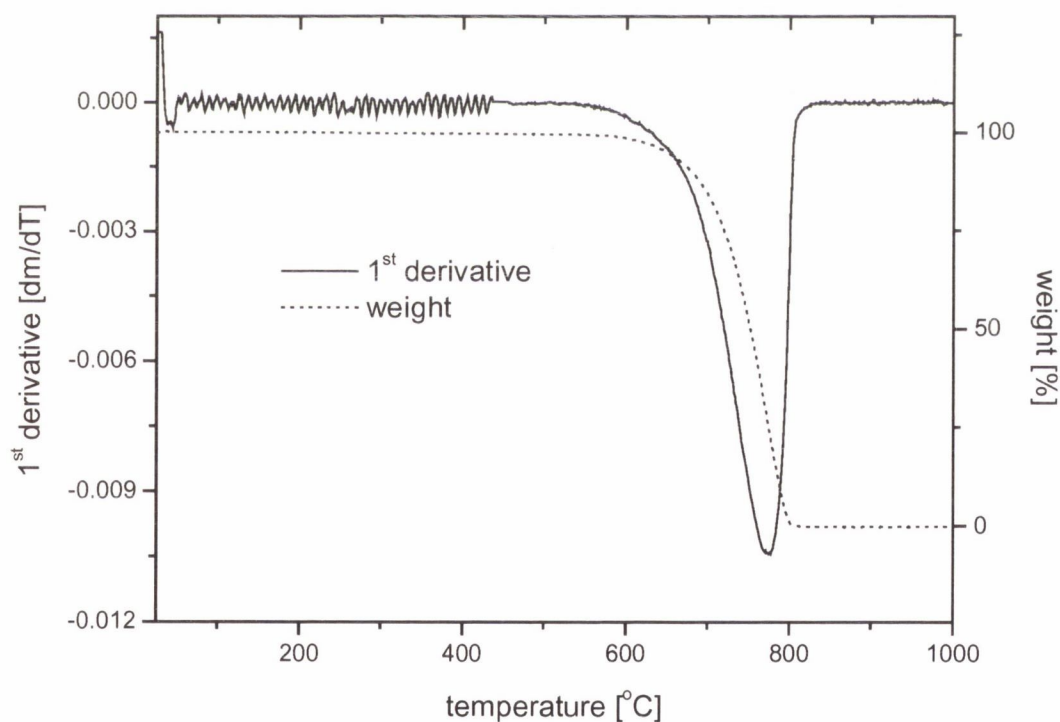


Figure 5.7 TGA graph of nanotube soot (produced at 37A)

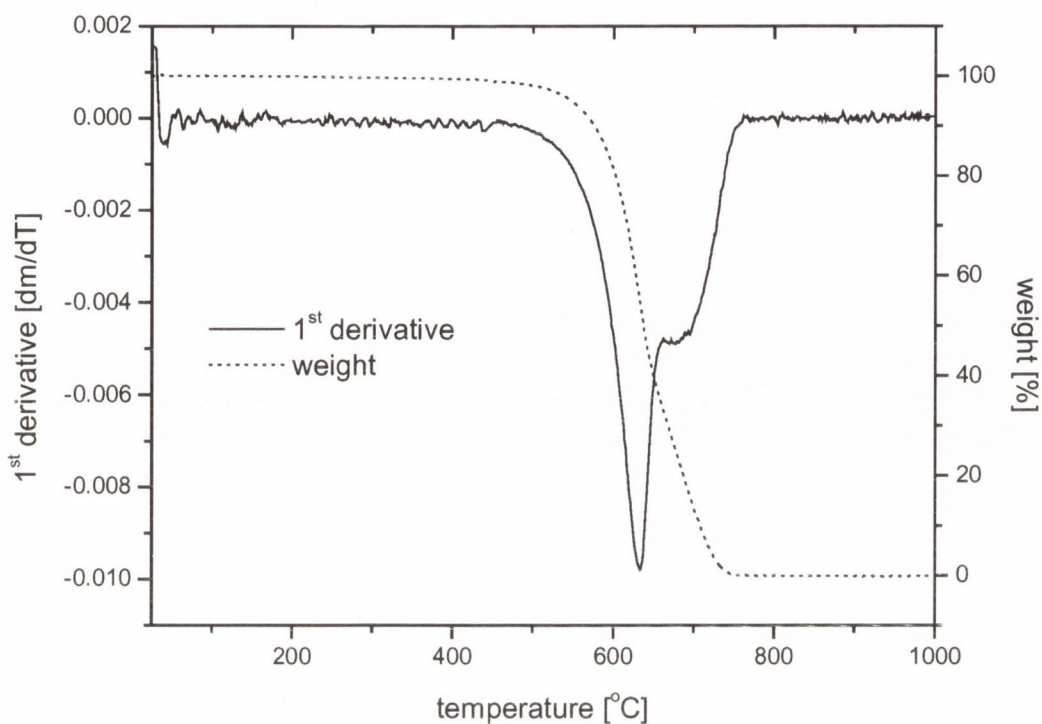


Figure 5.8 TGA graph of pristine graphite

While the maximum peak of the first derivative for graphite is at 635°C, the first peak for the nanotube material is at 775°C. As the onset of the oxidation has shifted by 140K, this indicates that all of the graphite has been converted, either into nanotubes or into polyhedra.

Nanotubes produced using different parameters did not show significant differences to the sample shown above using this method of thermal characterisation.

5.3 Thermogravimetric Analysis of composites

As mentioned before, PmPV solubilises nanotubes only, and none of its by products, hence nanotube composites have been prepared and thermally characterised. The

PmPV polymer was dissolved in toluene with a concentration of 20g/l and sonicated for two hours. Then the desired amount of the raw nanotubes were added and the sample was sonicated with a high power ultrasonic tip for two minutes. After that the sample was placed in the ultrasonic bath for two hours. This solution was left settling for 24 hours and the nanotube/PPV solution was decanted from the precipitate. The solution was poured onto a Teflon sheet and placed in an oven to evaporate the solvent.

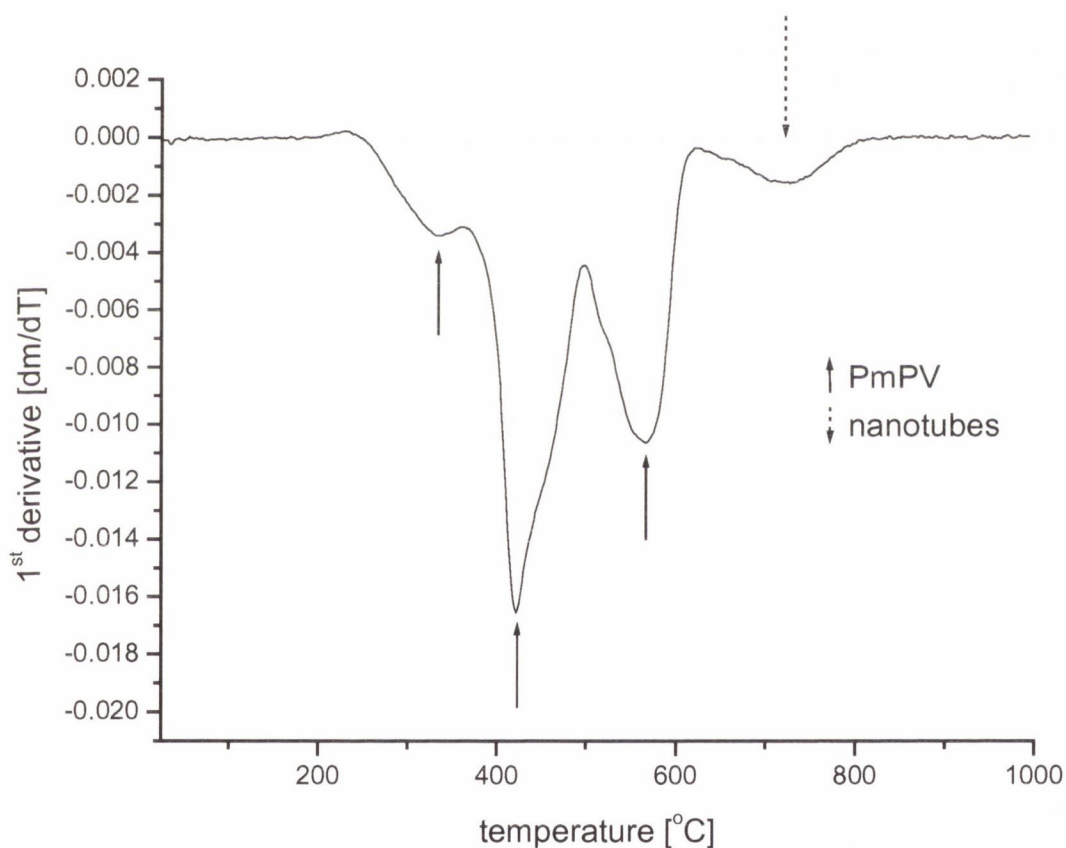


Figure 5.9 1st derivative of nanotube PmPV composite

The plot of the 1st derivative clearly shows four distinct peaks. The first three can be associated with the oxidation polymer and the fourth peak is from the later occurring namely oxidation of the nanotubes.

Figure 5.10 shows the TGA of the same measurement.

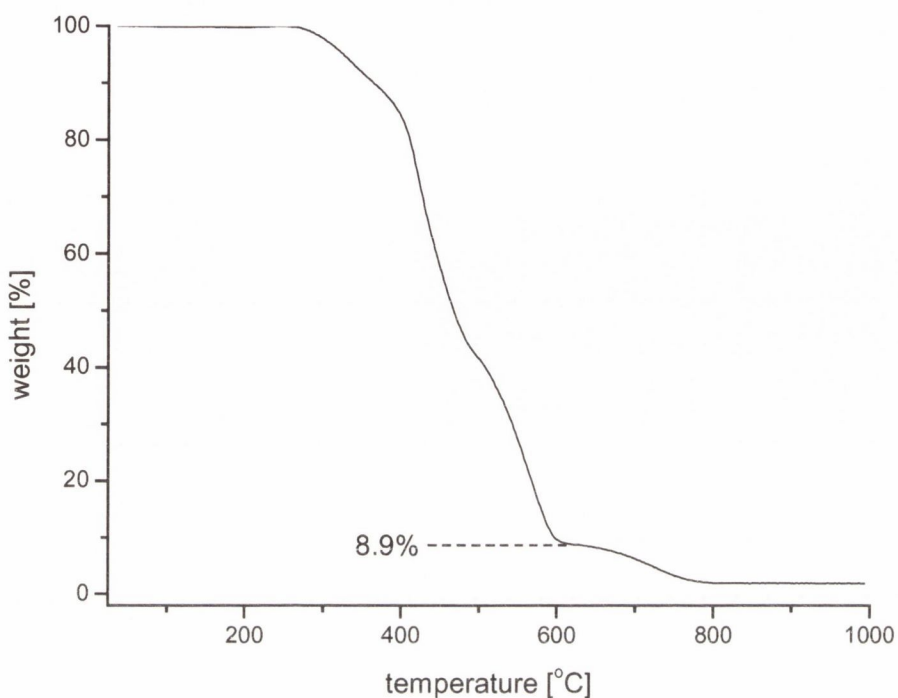


Figure 5.10 TGA graph of nanotube PmPV composite

This graph shows a distinct shoulder, where the polymeric material is fully oxidised, but not the nanotubes. It has been shown previously¹ that this shoulder represents the nanotubes only and not the by products. This shoulder indicates the real nanotube content in the composite.

Figure 5.11 shows TGAs of three different composites. The nanotube soot contents which were added are 20%, 33%, and 50%. After the separation of the nanotubes from the by products, the TGA reveals that there are 7%, 11.5%, and 15% of nanotubes left in the composite. This number now can be used to calculate the real nanotube content in the soot.

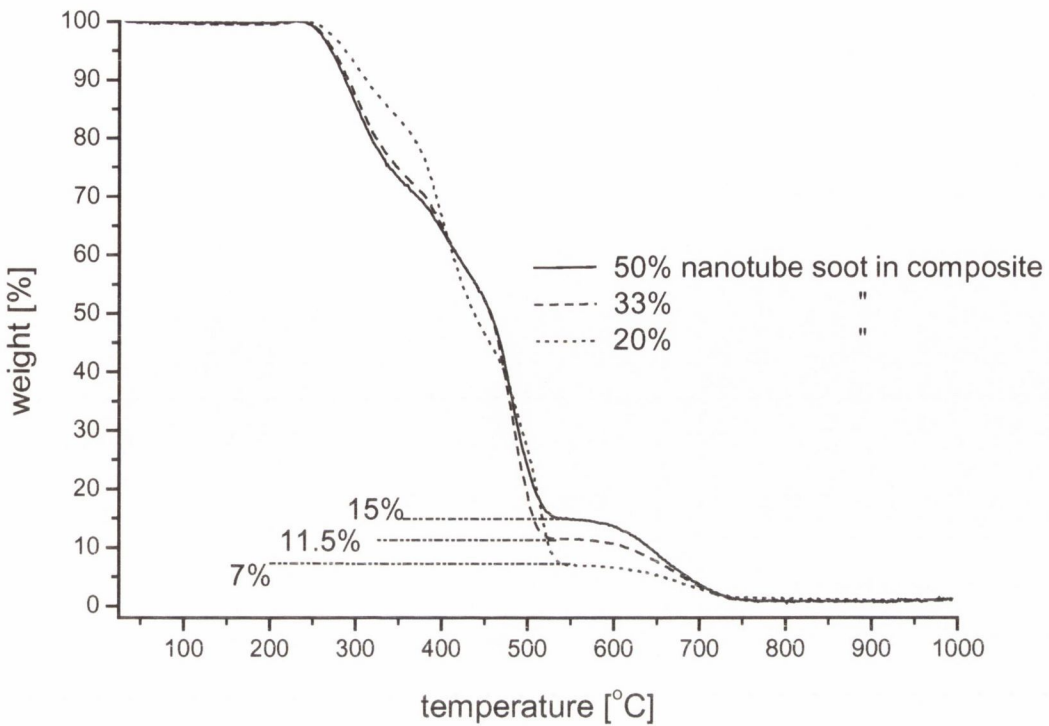


Figure 5.11 TGA graph of nanotube PmPV composites

The way to calculate the nanotube yield in the soot (NT_Y) from the percentage of soot before separation (NT_S) and the amount of soot in the composite (NT_C), which is measured with the TGA, is given in the following equation

$$NT_Y = \frac{100 * NT_C}{NT_S}$$

With the percentages shown in figure 5.11 this gives an average yield of 33.2% of nanotubes in the produced soot. This was the first quantitative method developed to measure the nanotube yield in the soot.

Further studies revealed², that some nanotubes fall out together with the precipitate, and thus are separated from the composite when the solution is decanted from the sediment. Thus the calculated numbers shown above are the lower limits of the

nanotube yield, as those nanotubes fallen out are not taken into count. Hence, the calculated yield is smaller than the real yield, the real nanotube content is higher.

5.4 Differential Scanning Calorimetry of composites

The polymers and composite were also characterised using differential scanning calorimetry (DSC). This technique gives valuable information about molecular thermal properties including the glass transition temperature T_g or the melting temperature T_m . Figure 5.12 shows a DSC plot of the pure PMMA.

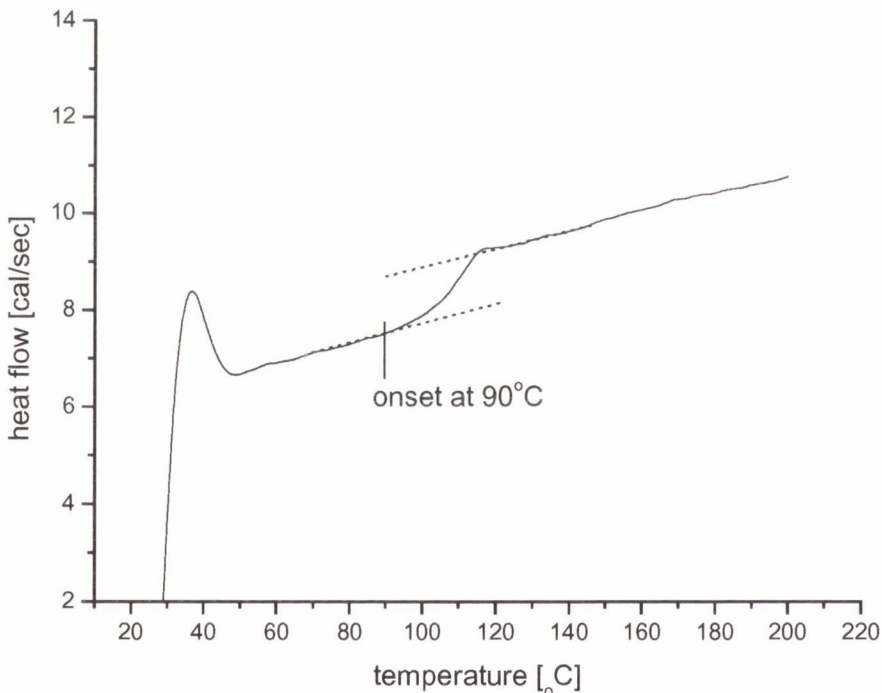


Figure 5.12 DSC of PMMA

The shoulder in the graph shows the glass transition of the PMMA. The onset of the phase transition is at a temperature of 90°C.

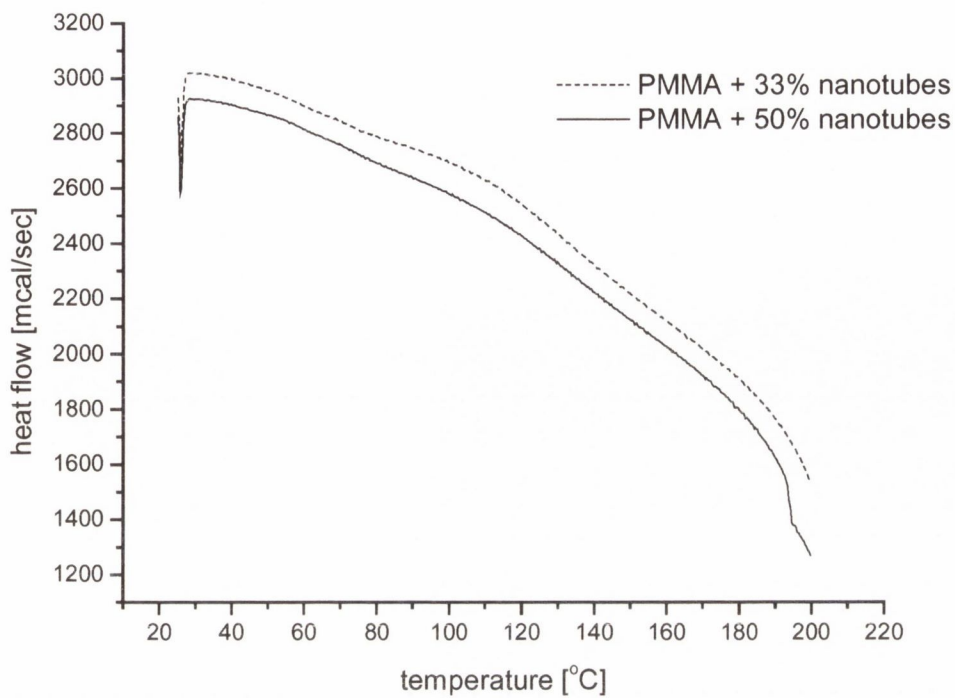


Figure 5.13 DSC of PMMA composites

Figure 5.13 shows DSC for two different PMMA nanotube composites. Only composite samples of approx. 4mg could be examined. This is due to the spatial distribution of films, which means that only a relatively small sample mass can be readily loaded into the DSC pan. This lowers the resolution of the DSC substantially. Even though there are no clear transitions such as those seen in the pure PMMA sample, shoulders are also apparent in those graphs, where the onset temperature seems to be slightly lower than 90°C. This would suggest that possibly the nanotubes act as plasticiser.

DSC curves for PS and PS composites are shown in figure 5.14 and 5.15.

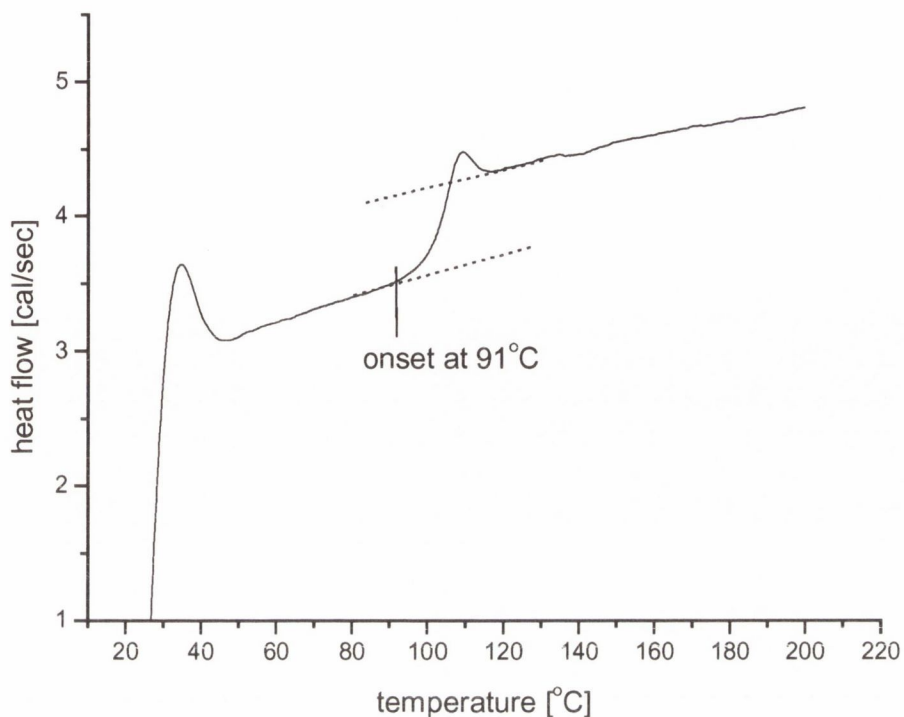


Figure 5.14 DSC of PS

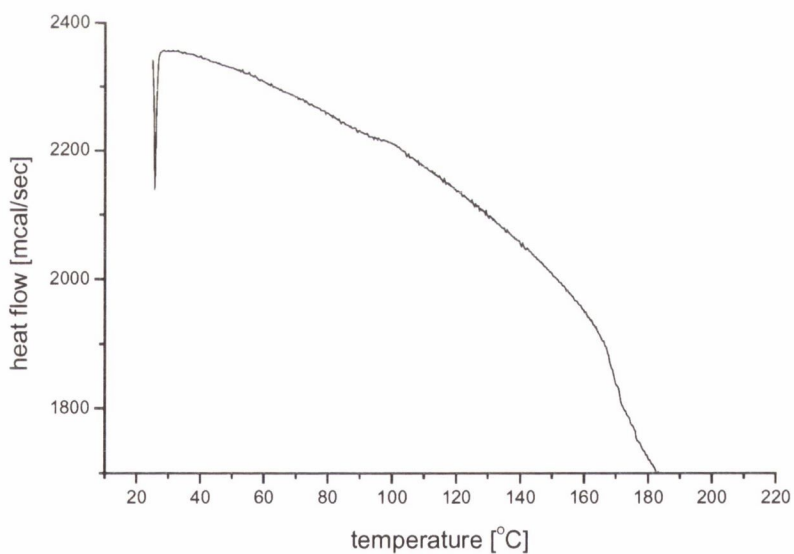


Figure 5.15 DSC of PS composite with 50 % nanotubes

As the same problems appeared with the preparation of the composite samples as described for the PMMA, this needs further investigation. There was no significant change in the glass transition temperature observed.

The glass transition of PmPV³ is at around 0°C and as it was not possible to measure sub ambient temperatures with the equipment used, no DSC curves for PmPV and its composites have been recorded.

5.5 Dynamic Mechanical Analysis of composites

The films analysed with the dynamic mechanical analysis (DMA) were dropcast onto a Teflon sheet and peeled off after drying. The film thickness has to be known in order to measure the mechanical and thermal properties using DMA. Film thickness measurements were performed using Fourier transform infrared spectroscopy (FT-IR). Two sample strips were sandwiched between two sodium chloride (NaCl) plates, separated by a gap which approximately equals the sample thickness. The interference fringes produced by the two NaCl plates therefore correspond to the film thickness. Figure 5.16 shows the interference pattern for the PmPV composite with 50% nanotubes.

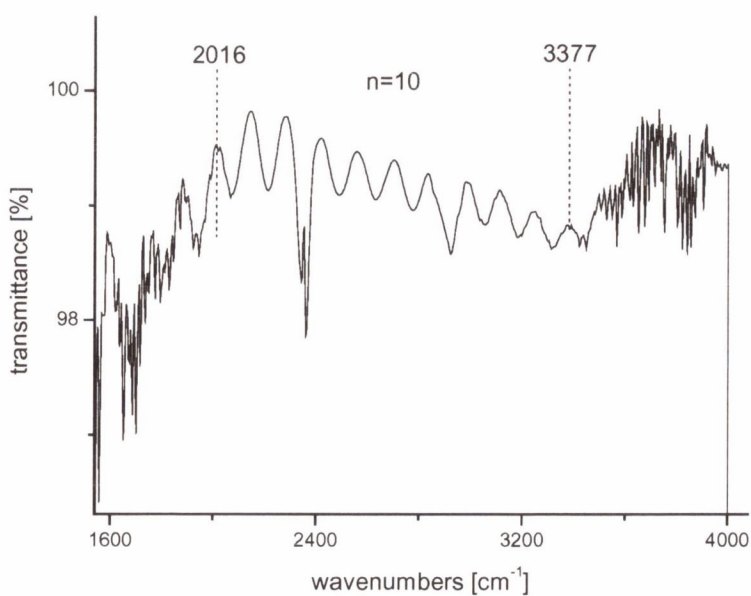


Figure 5.16 FT-IR interference pattern for PmPV composite with 50% nanotubes

The following formula shows how the separation of the two NaCl and thus the film thickness is calculated:

$$b = \frac{n}{2(\nu_1 - \nu_2)}$$

where b is the thickness of the cell in cm, n is the number of fringes between ν_1 and ν_2 , and ν_1 and ν_2 are the respective wavenumbers chosen for the limits of the range in which well defined fringes can be counted⁴. Using this formula, the sample shown above gives a film thickness of

$$b = \frac{10}{2(3377 - 2016)\text{cm}^{-1}} = 0.00367\text{cm} = 36.7\mu\text{m}$$

As described in chapter 3, DMA measures the storage modulus and the loss modulus as a function of temperature. The storage modulus of a polymer usually remains stable until its glass transition temperature is reached. At the glass transition temperature it decreases and this gives rise to a maximum in the loss modulus. $\text{Tan}\delta$, which is the ratio of the two moduli, has also a peak at this temperature.

The DMA plot for the PmPV composite with 50% nanotubes is shown in figure 5.17.

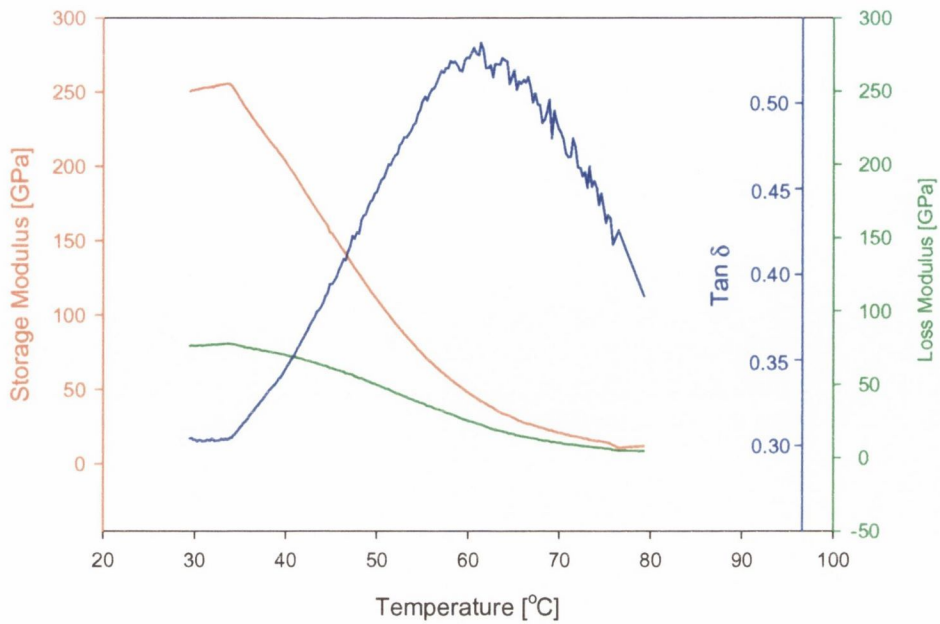


Figure 5.17 DMA of PmPV composite with 50% nanotubes

Both moduli, the storage modulus and the loss modulus, show a decrease from the beginning. This indicates an insufficient response of the film to the measurement, meaning that the mechanical properties of the sample are probably too weak to be recorded. Usually the $\tan\delta$ peak indicates the glass transition temperature. However, it is known that the glass transition temperature of PmPV is at 0°C ³ and therefore the data is misleading. It is possible that the $\tan\delta$ peak is due to an experimental artefact. Thicker films could possibly produce better results. The fact that the DMA machine is limited to moduli measurements above 10GPa, adds further to the difficulties in these measurements, as this means that in most cases the measurements stop before $\tan\delta$ has reached a maximum.

5.6 Results and discussion

The polymers and polymer composites have been analysed using DSC, DMA, and TGA. The DSC measured the glass transition temperature for PMMA, PS and composites of both polymers. For the PMMA the glass transition shifted slightly, which may be explained with the nanotubes functioning as a plasticiser. However there is no observable change in the glass transition temperature for PS.

DMA measurements could not confirm the DSC measurements, as all produced films were too thin to be measured accurately.

The TGA analysis of the initial polymerised PmPV samples revealed inorganic impurities in the polymer. These impurities have been identified using elemental analysis and this information has been used to improve the quality of PmPV. Procedures have since been adopted which have enabled the impurities to be eliminated during the polymerisation of the PmPV batches used for further composite studies.

TGA was performed on PmPV nanotube composites with different nanotube mass fractions. Work on this composite in Trinity have used PmPV treatment of carbon nanotubes as a method of carbon nanotube purification². It has been shown that the PmPV selectively binds to the nanotubes enabling impurities to be filtered out. Also this polymer treatment technique has been used to develop a method of measuring the nanotube content in the arc discharge produced soot. Prior to this a process of estimation was used, where the nanotube content was judged from TEM or SEM pictures. Hence, for the first time a quantitative method was available to determine the yield of nanotube production.

- ¹ S. A. Curran, P. M. Ajayan, W. J. Blau, D. L. Carroll, J. N. Coleman, A. B. Dalton, A. P. Davey, A. Drury, B. McCarthy, S. Maier, and A. Strevens, *Advanced Materials*, **10**, 1091 (1998)
- ² J. N. Coleman, A. B. Dalton, S. Curran, A. Rubio, A. P. Davey, A. Drury, B. McCarthy, B. Lahr, P. M. Ajayan, S. Roth, R. C. Barklie, and W. J. Blau, *Adv. Mater.*, **12**, 213 (2000)
- ³ S. Maier, *PhD Thesis*, Trinity College (2000)
- ⁴ R. T. Conley, *Infrared Spectroscopy*, Allyn and Bacon (1966), 1st Ed.

Chapter 6

Mechanical Properties of Composite Materials

Chapter 6 describes mechanical analysis of a range of polymer-nanotube composites. The focus is on the Young's moduli of the compounds. Additionally, the hardness of those materials used will be discussed.

6.1 Sample preparation

A range of different polymer-nanotube composites of different weight ratios has been investigated. These were mainly PmPV-nanotube composites but PMMA and PS composites were also tested. However due to the poor aggregation of nanotubes in PMMA and PS solutions, these samples first had to be 'coated' with PmPV.

The raw nanotube material has to be purified in order to separate the nanotubes from all by-products obtained during the arc-discharge production. This is done by a

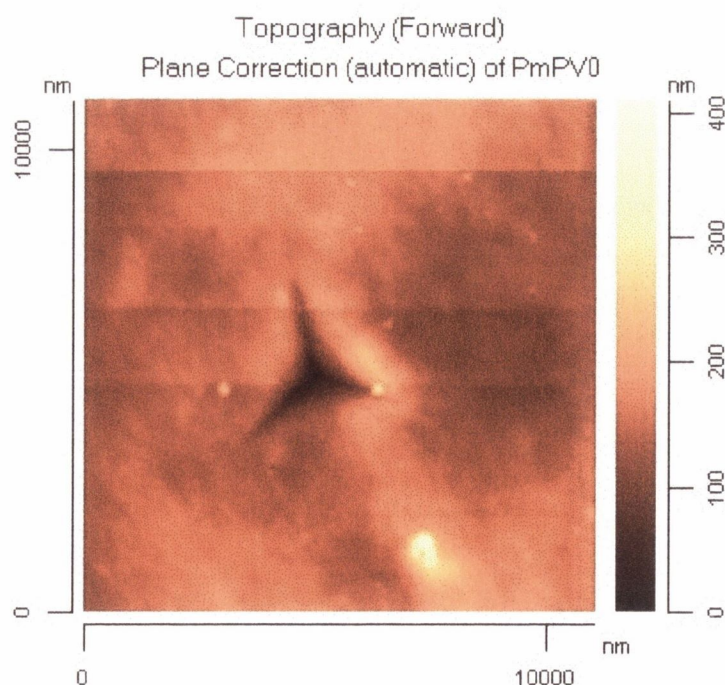
separation method employing PmPV. Therefore the PmPV was first dissolved in toluene followed by addition of the raw multi-walled carbon nanotube powder. To break up aggregation and to disperse the raw nanotube powder in the polymer solution the mixture was sonicated for 2 minutes with a high power ultrasonic tip. Afterwards the suspension was placed in a low power ultrasonic bath for several hours. Finally, the mixture was left standing for 24 hours. During this time, the turbostratic graphite and other by-products settled to the bottom while the nanotubes stayed in the polymer solution. Then the solution can be decanted to separate the sediment from the nanotube containing solution. In order to calculate the purity of the nanotubes produced using the arc-discharge method, it was assumed that all nanotubes remained in solution. However, this is not the case as some nanotubes precipitated but the amount can be neglected. The yield was found to be around 25 to 35% for this production procedure¹.

For the polymer-nanotube composite preparation, films of different material composition were prepared. The PmPV-nanotube films were simply drop-cast from PmPV-nanotube toluene solutions of different concentrations. As already mentioned, due to the poor solubility of nanotubes in PMMA and PS solution, the nanotubes for these samples were 'coated' with PmPV. Therefore a solution of 1:1 nanotubes and PmPV in toluene was prepared. In order to dissolve PMMA and PS in toluene, the mixtures were sonicated using the low power ultrasonic bath for two hours. To obtain composites of different material ratios, a certain volume of the PmPV-nanotube solution, corresponding to the required polymer-nanotube concentration, was added to the PMMA- or PS-toluene solution. These solutions were then again sonicated for two hours in the ultrasonic bath.

The films were drop cast on glass substrates. These substrates were pre-heated to 50°C for a faster evaporation of the solvent. In order to get the required film thickness needed for the Nano Hardness Test, multiple layers were added. After addition of each layer the samples were dried in a vacuum oven at 50°C for one hour.

6.2 Nanoindentation

In this chapter, the nanoindentational measurements of nanotube composite films are described. A range of measurements have been performed and evaluated to obtain hardness values and Young's moduli for several polymers, pure and with nanotubes. Figure 6.1 shows an Atomic Force Microscopy (AFM) image of a typical indentation on polymeric materials.



Picture 6.1 AFM micrograph of an indentation in PmPV

Using the AFM imaging tool the indentations can easily be visualised. This is necessary to check for instance, whether the various indentations on one sample have been sufficiently far from each other. Furthermore it can be used to analyse the edges of each indentation. Some materials, especially soft polymeric materials, tend to built a ‘pile-up’ at the edges of the contact area with the diamond tip. This effect can be seen on figure 6.2 at the point labelled with number “3”. This pile-up effects the real contact area compared to the projected area which is taken to calculate hardness and Young’s modulus. Thus it has to be checked to see whether it has to be taken into consideration or not. As the nanoindenter is fitted with an AFM microscope these pictures are easily acquired. Each material; has been checked for this effect.

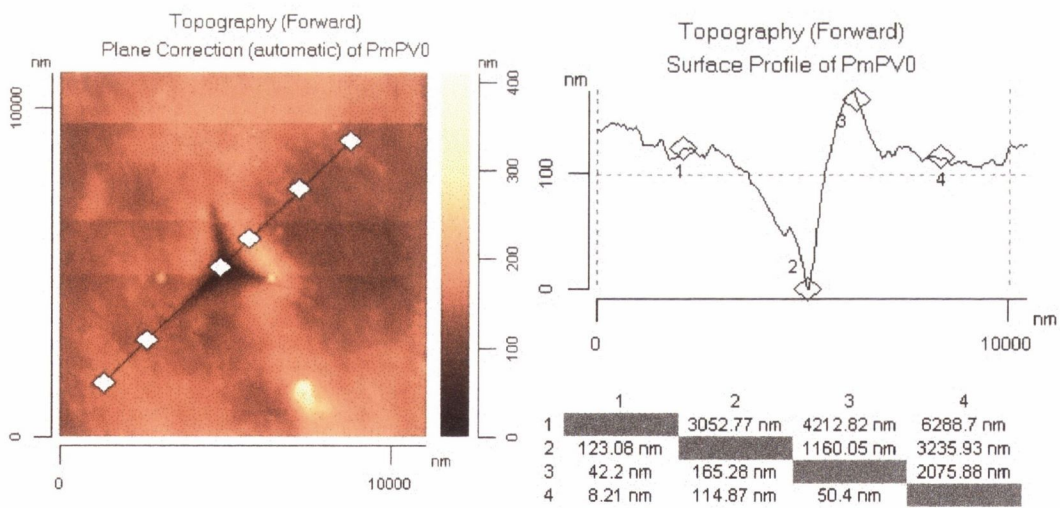


Figure 6.2 Topographic information from an AFM micrograph

6.2.1 Hardness

First nanoindentations were carried out on PmPV, PMMA and PS films. For the PmPV samples the nanotube content in was 0%, 20%, 33%, and 50%. All films were drop-casted onto glass substrates. Since such drop-casted films have only a thickness of around 1 micron, the applied load and the resulting indentational depth had to be kept as low as possible. Thus, the indentations were carried out near the lower limit of the resolution of the Nano Hardness Tester. This leads to a relative high standard deviation in all measurements.

Table 6.3 Hardness of PmPV-nanotube composite films

Sample	Meyer hardness [GPa]	Standard deviation	Vickers hardness [Vickers]	Standard deviation
PmPV	0.029	0.0024	2.70	0.22
PmPV 20	0.034	0.0003	3.18	0.02
PmPV 33	0.046	0.0090	4.22	0.84
PmPV 50	0.038	0.0039	3.51	0.36

For the measured PMMA composites the nanotube content of the samples was 0%, 20%, 33%, and 50%. As mentioned previously nanotubes do not disperse evenly enough to form homogeneous composites, the nanotubes had to be coated with PmPV. Therefore the nanotubes were, before they were mixed with the PMMA, dispersed in PmPV. The weight ratio of nanotubes:PmPV was 1:1. The hardness values obtained with those samples are given in table 6.4.

Table 6.4 Hardness of PMMA-nanotube composite films

Sample	Meyer hardness [GPa]	Standard deviation	Vickers hardness [Vickers]	Standard deviation
PMMA	0.1198	0.0126	11.11	1.17
PMMA 20	0.1793	0.0243	16.62	2.25
PMMA 33	0.0443	0.0048	4.10	0.45
PMMA 50	0.0604	0.0049	5.60	0.46

For PS composites the nanotube content was 20%, 33%, and 50%. Like in PMMA, nanotubes are not soluble in PS solutions. Here the nanotubes had to be PmPV-coated as well. The ratio of nanotubes:PmPV was 1:1 as well. Table 6.5 shows the Hardness of the different PS composites.

Table 6.5 Hardness of PS-nanotube composite films

Sample	Meyer hardness [GPa]	Standard deviation	Vickers hardness [Vickers]	Standard deviation
PS 20	0.16998	0.0212	15.75	1.96
PS 33	0.19397	0.0266	17.98	2.46
PS 50	0.13089	0.0146	12.13	1.35

As shown, there are only minor changes to the hardness of the tested materials. For most of polymer and polymer-composite applications the surface hardness itself is a less important figure. Far more important, especially if the polymer will undergo further treatment or coating, are the surface morphology and chemical structure of the polymer. As these are not affected by the addition of nanotubes, these composites are well suitable for all known application.

6.2.2 Young's modulus

Far more important for polymer applications are the mechanical properties of the composites. The most descriptive value for the strength of a material is the elastic or Young's modulus.

This modulus is also determined by measurements with the Nano Hardness Test as it was employed in the present work.

The elastic modulus can be obtained from the contact stiffness $S=dF/dh$ on any point of the unloading curve. According to theoretical calculations² following relations are valid:

$$E_r = 0.5(dF / dh) / (A_c / \pi)^{1/2}$$

$$1 / E_r = (1 - \nu_s^2) / E_s + (1 - \nu_i^2) / E_i$$

E_r is the so-called reduced modulus, which takes the elastic deformation of the indenter into account, too. F is the load, h is the according depth, A_c the area of the

indent. The Poisson ratio is ν , the indices s and I refer to the sample and the indenter material respectively.

Tables 6.6 to 6.9 show the Young's moduli of PmPV-, PMMA-, and PS-nanotube composites.

Table 6.6 Young's moduli of PmPV-nanotube composites

Sample	Young's modulus [GPa]	Standard deviation
PmPV	0.86	0.07
PmPV 20	0.95	0.17
PmPV 33	1.06	0.16
PmPV 50	1.17	0.07

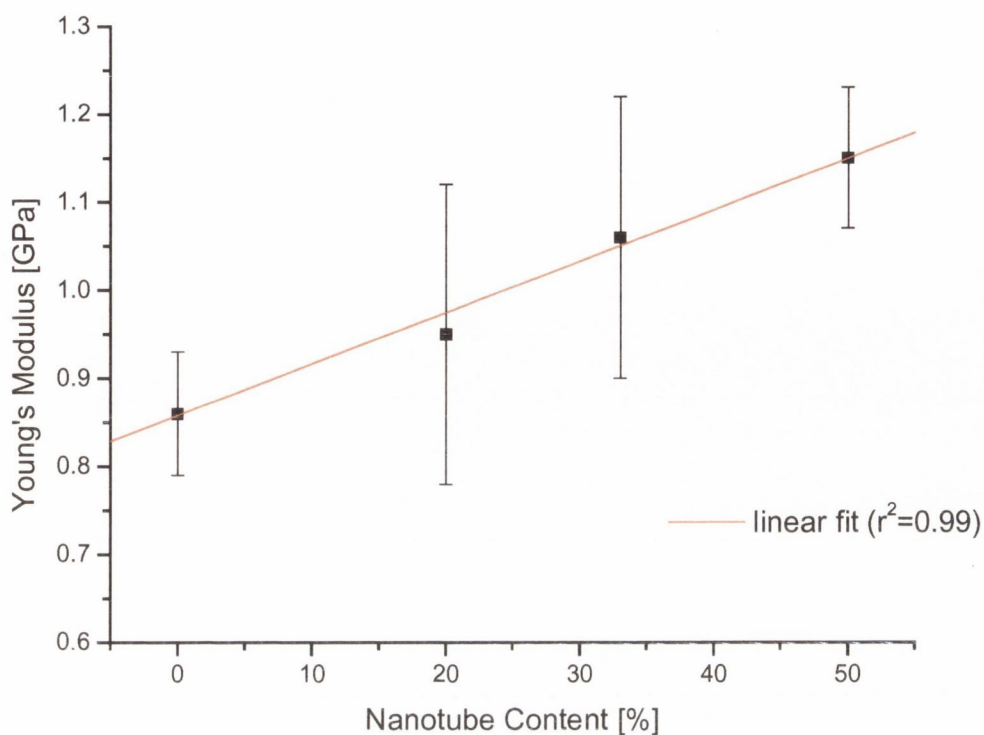


Figure 6.7 Young's moduli of PmPV-nanotube composites

Figure 6.7 shows the increase of the Young's modulus for PmPV-nanotube composites. This indicates that the PmPV-nanotube interactions, which are mentioned in previous chapters, are strong enough to not only hold nanotubes in solution and creating composites, but to transfer some of the applied load from the polymeric matrix to the fibre-like nanotube reinforcement.

Table 6.8 Young's moduli of PMMA-nanotube composites

Sample	Young's modulus [GPa]	Standard deviation
PMMA	3.62	0.18
PMMA 20	3.81	0.16
PMMA 33	1.98	0.11
PMMA 50	2.53	0.10

Table 6.9 Young's moduli of PS-nanotube composites

Sample	Young's modulus [GPa]	Standard deviation
PS 25	3.57	0.21
PS 50	3.38	0.36
PS 100	2.57	0.17

For both materials, PMMA and PS, the Young's modulus decreases when nanotubes are introduced into the system. This effect may not be related to the nanotubes alone, but to their PmPV coating. As mentioned before, the PmPV coating is required for a good dispersion of the nanotubes in PMMA and PS, as pure nanotubes

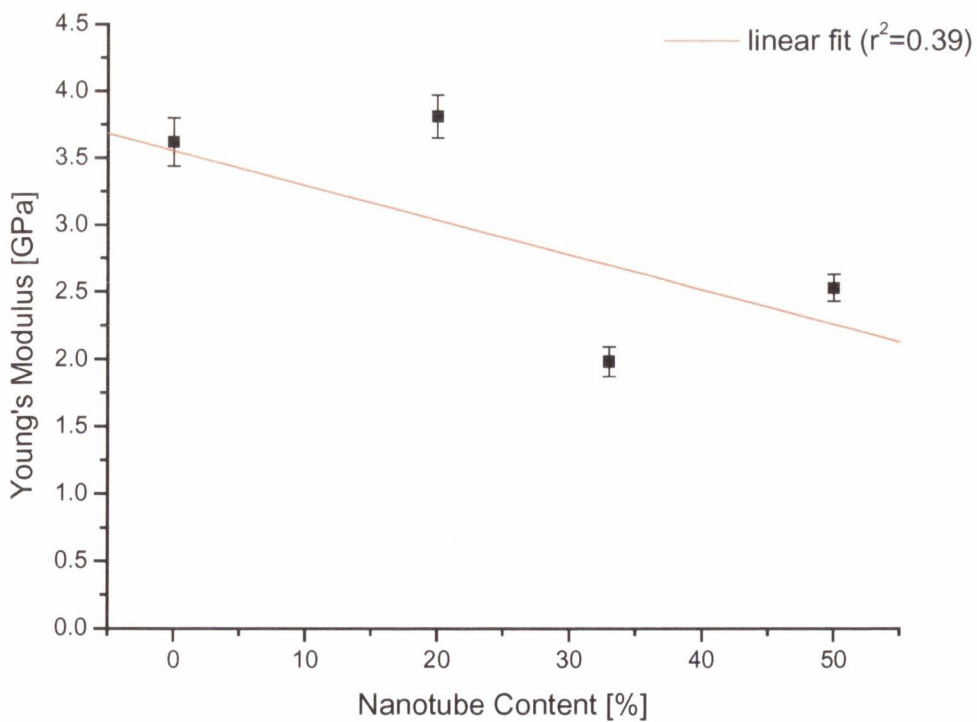


Figure 6.10 Young's moduli of PMMA-nanotube composites

tend to aggregate in these polymer solutions. Since both, PMMA and PS, have a much higher Young's modulus than PmPV, the introduction of PmPV in either PMMA or PS does not seem to increase the modulus of these composites. Figure 6.11 shows this decrease of the Young's modulus in PS-nanotube composites.

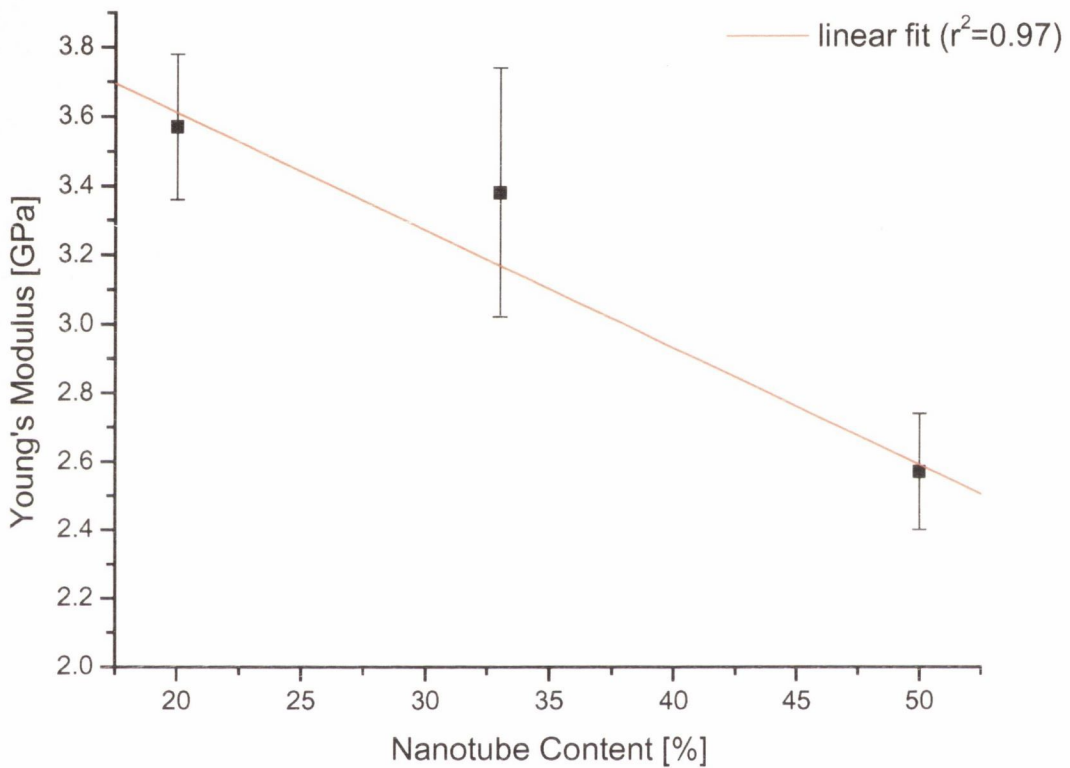


Figure 6.11 Young's moduli of PS-nanotube composites

Further measurements were made using a weaker PmPV-nanotube concentration. The samples were prepared as mentioned above, but this time with a PmPV:nanotube ratio of 1:5. Then this solution was added to the PMMA-solution. Figure 6.12 shows the Young's modulus of those films. Here the composites have a

significant higher Young's modulus than the first samples. However, there is no significant difference in Young's modulus if it is compared to the pure PMMA sample.

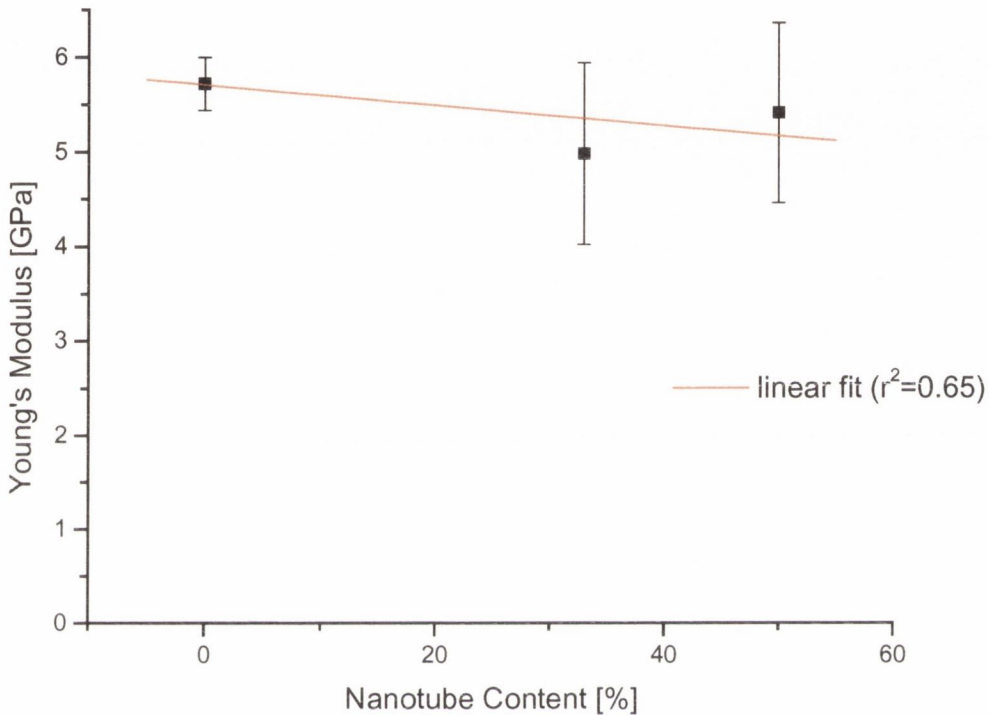


Figure 6.12 Young's moduli of PMMA-nanotube composites

6.3 Results and discussion

The nanohardness test has been employed to measure mechanical properties, such as hardness and Young's modulus, for different polymeric composites. Since it is not possible to disperse nanotubes in PS or PMMA solutions, PmPV was introduced to coat the nanotubes and to create a homogeneous composite. However, the introduction of nanotubes into these polymers resulted in a decrease in the mechanical properties. It is unclear if this is due to the lack of polymer-nanotube interaction, or simply because of the introduction of the much weaker PmPV.

It has been shown that adding nanotubes to pure PmPV increases the mechanical properties of this polymer. This shows that the interactions of the nanotubes with the PmPV polymer are strong enough to support a partial load transfer from the polymeric matrix to the fibre. The composite with the highest nanotube content, i.e. 50% soot by weight, has the highest Young's modulus of the investigated PmPV composites. However, the measured moduli appear to saturate in the region of this percentage. Further investigations are required in order to verify this trend.

It has therefore been shown that the nanohardness test can be used to measure the mechanical properties of polymers and polymer composites. These were among the first nanoindentational measurements for such soft materials and the positive industrial feedback received indicates the significance of these measurements.

- ¹ J. N. Coleman, A. B. Dalton, S. Curran, A. Rubio, A. P. Davey, A. Drury, B. McCarthy, B. Lahr, P. M. Ajayan, S. Roth, R. C. Barklie, and W. J. Blau, *Adv. Mater.*, **12**, 213 (2000)
- ² B. Wolf, *Crystal Research and Technology*, **35**, 377 (2000)

Chapter 7

Conclusions

This chapter will concisely review the main results of this thesis.

Carbon nanotubes and nanotube based composites have been developed and investigated for the purposes of mechanical reinforcement. Initially, the nanotube production method was optimised to give high quality suitable samples for mechanical improvement of the composites. Specifically what was required was the efficient production of nanotube samples of a high purity and a high aspect ratio.

The influence of different factors such as voltage, pressure and current in the arc discharge nanotube production method was investigated. Purity and length distribution in the samples was found to be voltage independent. However, by slightly increasing the voltage, the run time decreased. The variation of the helium pressure in the reaction chamber showed that, at slightly higher pressures, the plasma

was more stable, hence the nanotubes produced are slightly longer. In addition, the pressure did not have any influence on the purity of the nanotubes produced.

The biggest influence on the quality of the nanotubes produced was the current density at which the nanotubes were produced. By increasing current, the nanotubes produced were much longer. Since a high aspect ratio of nanotubes is very important for reinforcement purposes, the nanotube production method was optimised to produce the most suitable nanotube material for these studies.

TGA was performed on PmPV nanotube composites with different nanotube mass fractions. Work on this composite in Trinity has used PmPV based composites as a method of carbon nanotube purification. It has been shown that the PmPV selectively binds to the nanotubes enabling impurities to be filtered out. This has been used to develop a quantitative method of measuring the nanotube content in the arc discharge produced soot for the first time. Prior to this, a qualitative process was used, where the nanotube content was estimated from TEM or SEM pictures.

Thermal analysis of the initial polymerised PmPV samples revealed inorganic impurities in the polymer. These impurities have been identified using elemental analysis and this information has been used to improve the quality of PmPV. Procedures have since been adopted which have enabled the impurities to be eliminated during the polymerisation of the PmPV batches used for further composite studies.

The polymers and polymer composites have been analysed using DSC, DMA, and TGA. The DSC measured the glass transition temperature for PMMA, PS and composites of both polymers. For the PMMA, the glass transition shifted slightly,

which may be explained by the nanotubes functioning as a plasticiser. However there is no observable change in the glass transition temperature for PS.

The nanohardness test has been employed to measure mechanical properties, such as hardness and Young's modulus, for different polymeric composites. Blends of PMMA or PS and the PmPV based composite are used, since it is not possible to disperse nanotubes in PS or PMMA solutions. However, the introduction of nanotubes into these polymers resulted in a decrease in the mechanical properties. It is unclear if this is due to the lack of polymer-nanotube interaction, or simply because of the introduction of the much weaker PmPV.

Adding nanotubes to pure PmPV increases the mechanical properties of this polymer. This shows that the interactions of the nanotubes with the PmPV polymer are strong enough to support a partial load transfer from the polymeric matrix to the fibre. The composite with the highest nanotube content, i.e. 15% nanotubes in the composite, has the highest Young's modulus of the investigated PmPV composites. However, the measured moduli appears to saturate in the region of this percentage.

It has been shown that the nanohardness test can be used to measure the mechanical properties of polymers and polymer composites. These were among the first nanoindentational measurements for such soft materials and the positive industrial feedback received indicates the significance of these measurements.

Publications

“Determination of Mechanical Properties of Multi-Walled Carbon Nanotubes composites using nanoindentation”

B. Lahr, B. McCarthy, A. Drury, J. N. Coleman, and W. J. Blau
Applied Physics Letters, to be submitted

“Carbon Nanotubes, High-Strength Reinforcing Compounds for Composites”

B. Lahr and J. Sandler
Kunststoffe Plast Europe, 90, 42 (2000)

“A Microscopic and Spectroscopic Study of Interactions between Carbon Nanotubes and a Conjugated Polymer”

B. McCarthy, J.N. Coleman, R. Czerw, A.B. Dalton, M. in het Panhuis, A. Maiti, A. Drury, P. Bernier, J.B. Nagy, B. Lahr, H.J. Byrne, D.L. Carroll, W.J. Blau
Journal of Physical Chemistry B, accepted

“Optimisation of the Arc-Discharge Production of Multi-walled Carbon Nanotubes”

M. Cadek, R. Murphy, B. McCarthy, A. Drury, B. Lahr, R. C. Barklie,
M. in het Panhuis, J. N. Coleman, and W. J. Blau
Carbon, in press,

“Raman spectroscopy and conductivity measurements on polymer-multiwalled carbon nanotubes composites”

C. Stéphan, T. P. Nguyen, B. Lahr, W. J. Blau,
S. Lefrant, and O. Chauvet
Journal of Materials Research, Vol. 17, No.2, Feb. 2002

“Enhanced Brightness in Organic Light-emitting Diodes using a Carbon Nanotube Composite as an Electron-transport Layer”

P. Fournet, J. N. Coleman, B. Lahr, A. Drury, W. J. Blau,
D. F. O'Brien, and H. H. Horhold
Journal of Applied Physics, 90, 969 (2001)

“Phase Separation of Carbon Nanotubes and Turbostratic Graphite Using a Functional Organic Polymer”

J. N. Coleman, A. B. Dalton, S. Curran, A. Rubio, A. P. Davey, A. Drury, B. McCarthy, B. Lahr, P. M. Ajayan, S. Roth, R. C. Barklie, and W. J. Blau
Advanced Materials, 12, 213 (2000)

“Electron Paramagnetic Resonance as a Quantitative Tool for the Study of Multiwalled Carbon Nanotubes”

J. N. Coleman, D. F. O'Brien, A. B. Dalton, B. McCarthy, B. Lahr, R. C. Barklie, and W. J. Blau
Journal of Chemical Physics, 113, 9788 (2000)

“Measurement of Nanotube Content in Pyrolytically generated Carbon Soot”

J. N. Coleman, D. F. O'Brien, A. B. Dalton, B. McCarthy, B. Lahr, A. Drury, R. C. Barklie, and W. J. Blau,
Chemical Communication, 2001 (2000)